

OPTIMIZING THE EXCITED STATE PROCESSES OF CONJUGATED POLYMERS FOR IMPROVED
SENSORY RESPONSE

BY

AIMEE ROSE

B.S., CHEMISTRY
SAINT MICHAEL'S COLLEGE, COLCHESTER, VERMONT; 1996

SUBMITTED TO THE DEPARTMENT OF CHEMISTRY IN PARTIAL
FULFILLMENT OF THE REQUIREMENTS FOR THE DEGREE OF

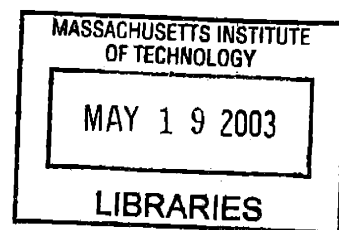
DOCTOR OF PHILOSOPHY IN CHEMISTRY

AT THE

MASSACHUSETTS INSTITUTE OF TECHNOLOGY

FEBRUARY 2003

ARCHIVES



© 2003 MASSACHUSETTS INSTITUTE OF TECHNOLOGY. ALL RIGHTS RESERVED.

THE AUTHOR HEREBY GRANTS TO MIT PERMISSION TO REPRODUCE AND TO DISTRIBUTE PUBLICLY PAPER
AND ELECTRONIC COPIES OF THIS THESIS DOCUMENT IN WHOLE OR IN PART.

SIGNATURE OF AUTHOR:

Aimee Rose

DEPARTMENT OF CHEMISTRY
OCTOBER 10, 2002

CERTIFIED BY:

Timothy M. Swager

TIMOTHY M. SWAGER
PROFESSOR OF CHEMISTRY
THESIS SUPERVISOR

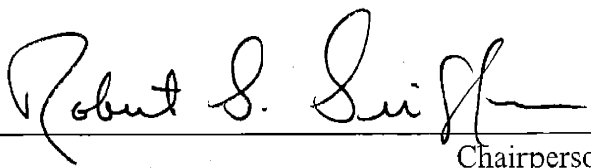
ACCEPTED BY:

Robert W. Field

ROBERT W. FIELD
CHAIRMAN, DEPARTMENTAL COMMITTEE ON GRADUATE STUDENTS

This doctoral thesis has been examined by a Committee of the Department of Chemistry as follows:

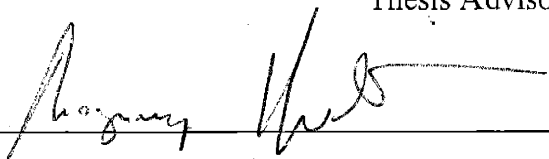
Professor Robert G. Griffin


Chairperson

Professor Timothy M. Swager

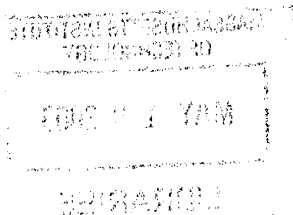
Thesis Advisor

Professor Vladimir Bulović



Professor Michael F. Rubner





Optimizing the Excited State Processes of Conjugated Polymers for Improved Sensory Response

by

AIMEE ROSE

Submitted to the Department of Chemistry on January 10, 2003
in partial fulfillment of the requirements for the Degree of
Doctor of Philosophy in Chemistry

ABSTRACT

Conjugated polymers exhibit useful and interesting electrical and optical properties. We exploit the wandering excitons produced after photoexcitation for chemosensory applications. By sampling many sites in a polymer film, the excitation has a greater chance to encounter an analyte, such as 2,4,6 trinitrotoluene (TNT), electrostatically poised to induce non-radiative decay. The result is attenuation of the fluorescence signal characteristic of these bright polymers. Because energy migration is responsible for the amplification of sensory response, we sought to augment this migration by integrating chromophores with long-lived excited states into the polymer backbone. The first chromophore we targeted, triphenylene, has a symmetrically-forbidden ground state transition, resulting in a long excited state lifetime. Chapter 2 describes the synthetic incorporation of triphenylene into conjugated polymer backbones, and Chapter 3 details the spectroscopic interrogation of these materials. We demonstrate that lifetime extension is universal to all triphenylene-containing polymers. The longer excited state lifetimes are then correlated with increased energy migration through polarization spectroscopy. In Chapter 4, we extend this paradigm for elongating energy migration in conjugated polymers to several other systems. Unique polymers with symmetric, aromatic chromophores are investigated. These materials allow us to look more rigorously at the variations of effective conjugation pathways and their implications before and after chromophore cyclization. The novel dibenzo[*g,p*]chrysene, triphenylene and thiophene-based systems afforded us a more complete understanding of the interplay of rigidification, symmetrization, lifetime, and energy migration in conjugated polymers. In the final chapter, we exploit another excited state process in conjugated polymers, stimulated emission, to provide additional amplification of sensory response. We demonstrate that lasing action in optically-pumped conjugated polymer thin film structures can be inhibited by exposure of samples to trace amounts of electron deficient aromatic analytes such as TNT. Analyte exposure introduces non-radiative pathways in the polymer, increasing the lasing threshold. Because lasing is a non-linear phenomenon, it provided two orders of magnitude greater sensitivity to TNT. In combination, we hope that the developments described in this thesis will serve to improve current demining technology in the near future.

Thesis Supervisor: Timothy M. Swager
Title: Professor of Chemistry

In minute reciprocation for unfettered and inexhaustible support,
I dedicate this thesis to my mother, Joyce Louis Rose.

Table of Contents

	page
Chapter 1: Harnessing energy migration in conjugated polymers for sensory applications: A brief introduction	7
1. Introduction	8
2. Excitons and energy migration in conjugated polymers	8
2.1. Exciton formation	8
2.2. Energy migration in solution	10
2.3. Energy migration in thin films	10
3. Amplifying sensory response with conjugated polymers	12
3.1. Solution studies	12
3.2. Solid-state studies	13
4. Directions to be detailed	15
5. References	16
Chapter 2: Modifying conjugated polymer photophysics: synthesis of triphenylene-based poly(p-phenyleneethylenes)	18
1. Introduction	19
2. Results and discussion	23
2.1. Triphenylene monomer and polymer synthesis	23
2.2. Model polymer synthesis	28
3. Conclusions	30
4. References	30
5. Experimental Section	33
Chapter 3: Combining excited state lifetime measurements and polarization spectroscopy in tracking energy migration	40
1. Introduction	41
2. Results and Discussion	41
2.1. Experimental	41
2.2. Monomer spectroscopy	43
2.3. Polymer spectroscopy	45
2.4. Chain length selection and spectroscopy	49
2.5. Polarization spectroscopy	50
2.6. Chain length selection and spectroscopy	57
3. Conclusions	59
4. References	59
Appendix 1- TPPE spectra	61
Appendix 2- PPE spectra	65

Chapter 1

Harnessing energy migration in conjugated polymer for sensory applications:

A brief introduction.

1. Introduction

Many general review articles concerning the photophysics of conjugated polymers (CPs), authored by experts in the field, have appeared in the literature.^{1, 2a} This introduction will not attempt to rival them but will focus on prior art using CPs to amplify sensory response. Therefore, we concentrate here on precedents set in the Swager group to provide the motivation and aims behind this thesis of work. First, we will briefly describe the energy migration in CPs and some key experiments characterizing this migration. We will then relate how this property has been applied to our end, generating materials more sensitive to analytes such as 2,4,6 trinitrotoluene (TNT). We conclude by detailing the approaches we adopted in this thesis to further advance chemosensory CP materials.

2. Excitons and energy migration in conjugated polymers

2.1. Exciton formation

Controversy swarmed the nature of the primary photoexcitation in CPs for many years.² Research aimed at distinguishing an electron-hole pair, i.e. excitonic, from a free-carrier model in order to advance device applications (Fig. 1) of CPs. Intensive spectroscopic characterization of excited states in CPs was necessary before experts reached a consensus; in the absence of intense radiation fields and impurities, the exciton is the primary species created after photon absorption. This excitation is then transmitted energetically down the polymer chain (Fig 2). The transmission is fast and efficient, in most cases preceding the highly allowed emission that returns the CP to the ground state.

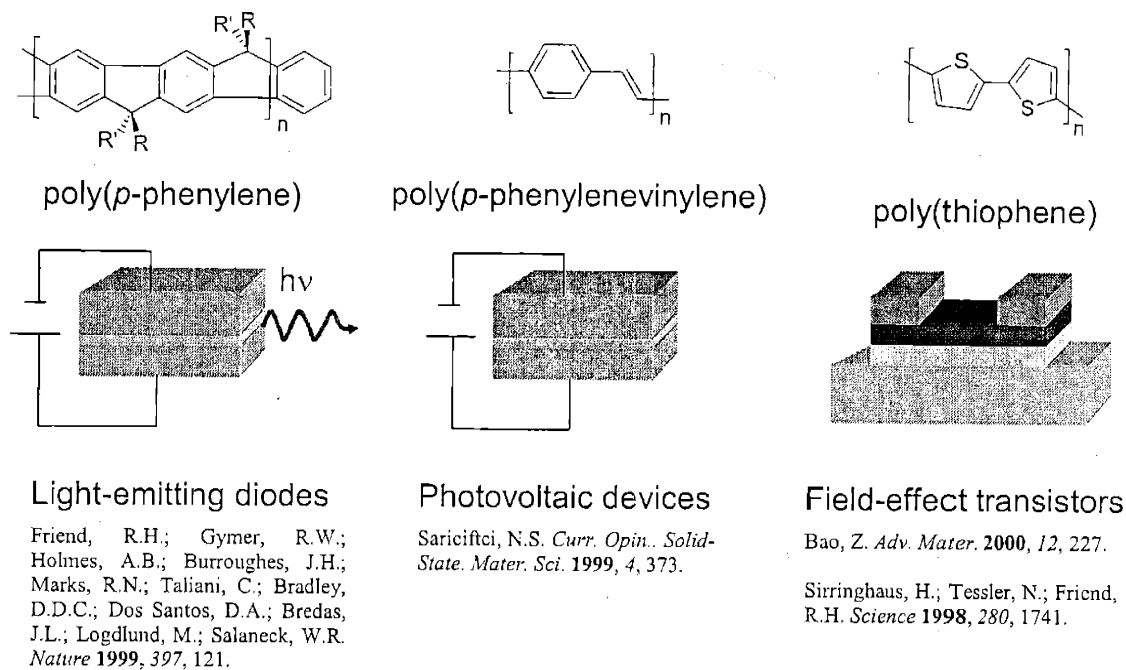


Figure 1. Some conjugated polymers and corresponding devices in which they have been incorporated.

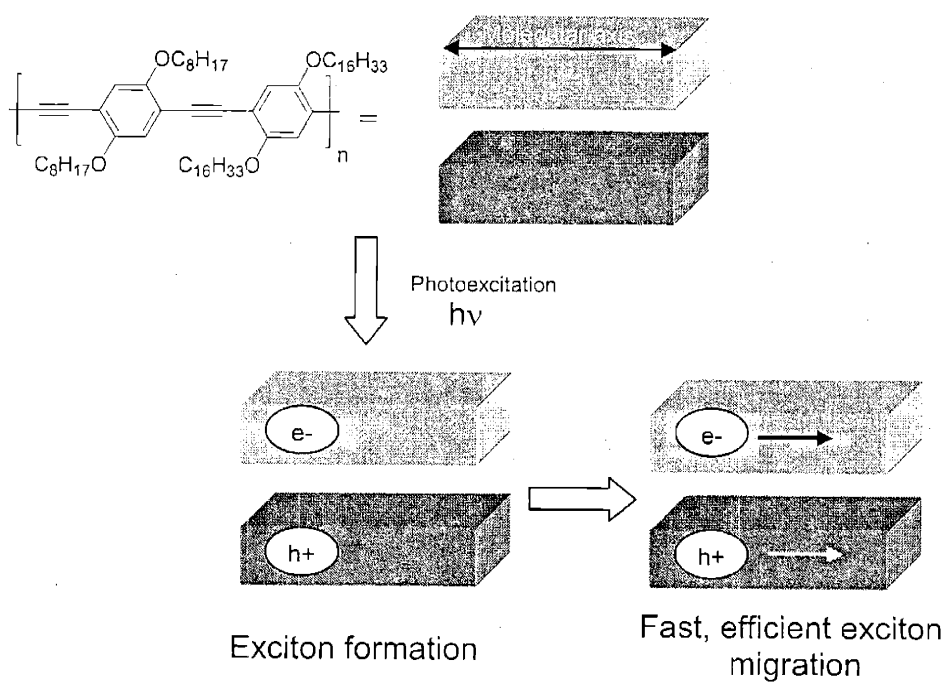


Figure 2. Simplified pictorial of energy migration in a conjugated polymer.

Therefore, photoluminescence principally occurs from segments of longer conjugation length, i.e. lower energy, imparting conjugated polymers with a large observed Stokes shift. This inhomogeneous broadening has been probed extensively through site-selective fluorescence techniques³ indicating that in most CPs the inherent Stokes shift is small compared to that induced by energy migration.

2.2 Energy migration in solution

Energy transfer allows the excitation in a CP to sample many sites along the polymer chain before radiative recombination occurs. This has been quantified in poly(*p*-phenylene ethylene)s (PPEs) by coupling the polymer endgroups with energy-accepting chromophores (Fig. 3).⁴ Only the energy-trapping endgroups fluoresce after exciting the main chain, indicating that excitations are quantitatively transferred to these traps before radiative recombination occurs. Studies of the effect of increasing chain length on energy migration determined that excitons can migrate in excess of 100 nm in solution. Beyond this length, the main chain begins to contribute to the fluorescence signal as its emission profile is observed.

2.3 Energy migration in thin films

Solid-state studies have also been performed on similar systems. Exploiting Langmuir-Blodgett film deposition techniques, individual monolayers were deposited atop silica substrates (Fig. 4).⁵ Number of layers was varied but in all cases, a small amount of an energy accepting dye was adsorbed to the surface of the striated films.

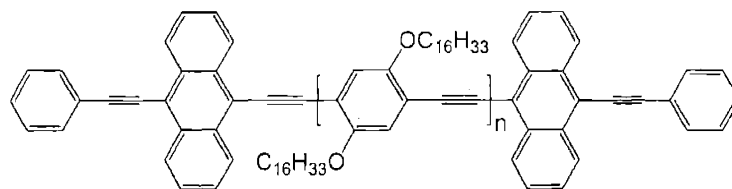
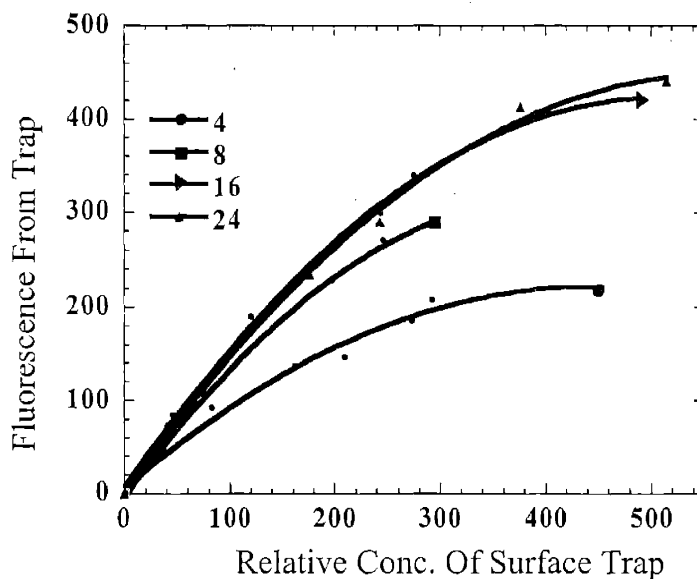
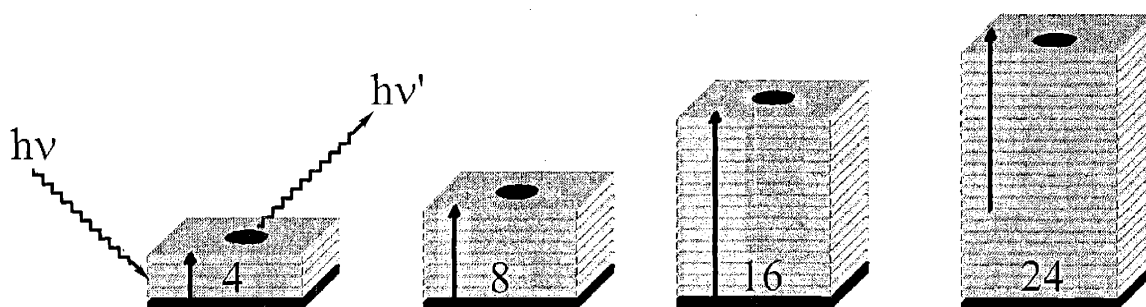


Figure 3. Fluorescent PPE with energy-accepting endgroups shown in gray. Upon excitation of the main chain, emission is mainly observed at 524 nm, the emission maxima of the endgroups.



Levitsky, I.A.; Kim, J.; Swager, T.M. *J. Am. Chem. Soc.* 1999, 121, 1466-1472.

Figure 4. Z-directional energy transfer limit in PPEs. Fluorescence intensity of the surface dye after excitation of the underlying layer does not increase in films with more than 16 layers, delineating an energy transfer limit.

Emission intensity from this acceptor was compared among films with 2 to 36 monolayers when the underlying polymer layers were photoexcited. A maximum in emission intensity from dye traps was observed in films with 16 monolayers. Additional monolayers did not contribute further to dye emission intensity, indicating that energy is drawn from only the closest 16 layers. Therefore, adding more monolayers only wastes material and input photons. These experiments helped quantify the energy transfer efficiencies we were trying to improve in successive generations of CPs.

3. Amplifying sensory response with conjugated polymers

3.1. Solution studies

In our laboratory, we have used this migration to amplify sensory response (Fig 5). In a traditional fluorescent chemosensor, an analyte interacts with the excited state of a chromophore to induce a measurable response. Conjugating these chromophores within

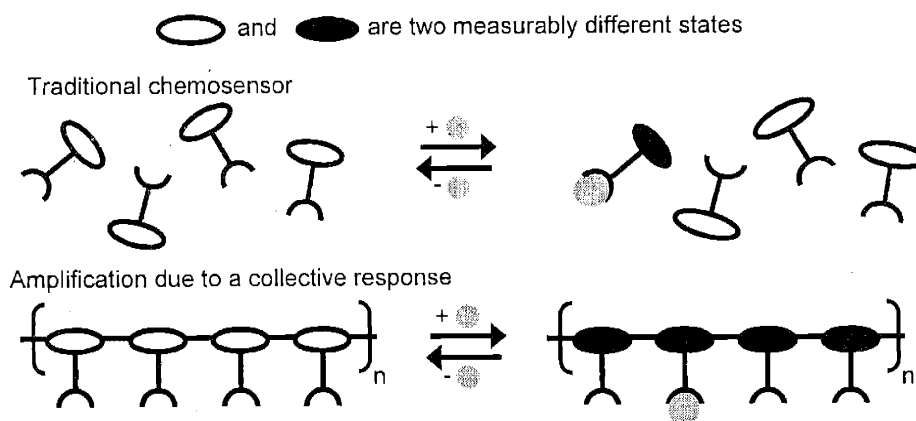


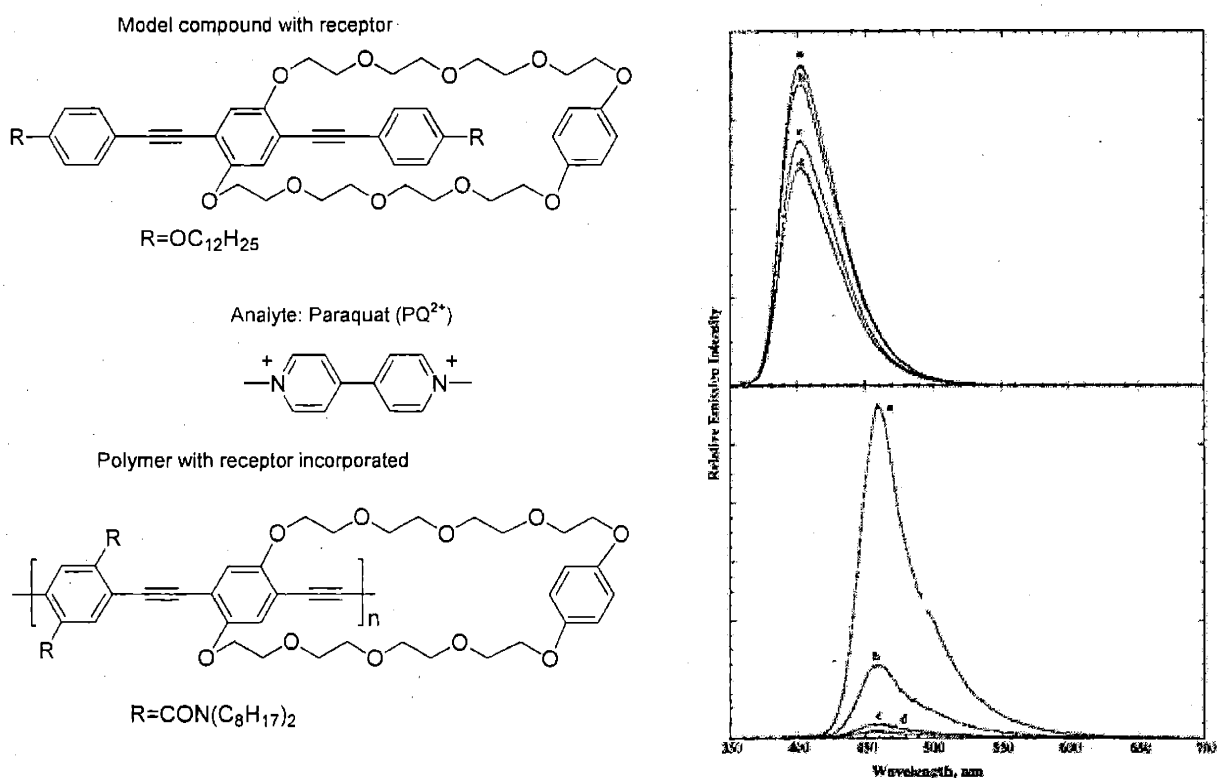
Figure 5. Enhancement of sensory response due to energy migration.

a polymer backbone amplifies the fluorescence response since wandering excitations have an increased probability of reaching the interaction site via energy migration. Initial

experiments probing this effect were performed in solution on systems with well-defined binding constants for fluorescence quenchers and precise molecular weights (chain lengths).⁶ Fluorescence quenching in a model monomeric compound was compared to that of the conjugated polymer. In this case, polymerization augmented fluorescence quenching by almost two orders of magnitude.

3.2. Solid-state studies

A natural succession to this discovery was to reproduce these effects in the solid



Zhou, Q.; Swager, T. M. *J. Am. Chem. Soc.* 1995, 117, 7017-8.

Figure 6. Emission spectra of monomer (top) and polymer (bottom) as a function of added PQ²⁺. The curves are labeled to indicate the amount of PQ²⁺ added: (a) [PQ²⁺] = 0, (b) [PQ²⁺] = 3.56 × 10⁻⁵ M, (c) [PQ²⁺] = 2.10 × 10⁻⁴ M, (d) [PQ²⁺] = 3.45 × 10⁻⁴ M.

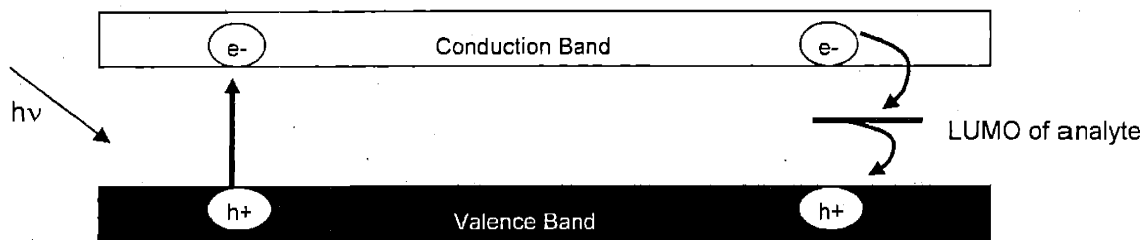
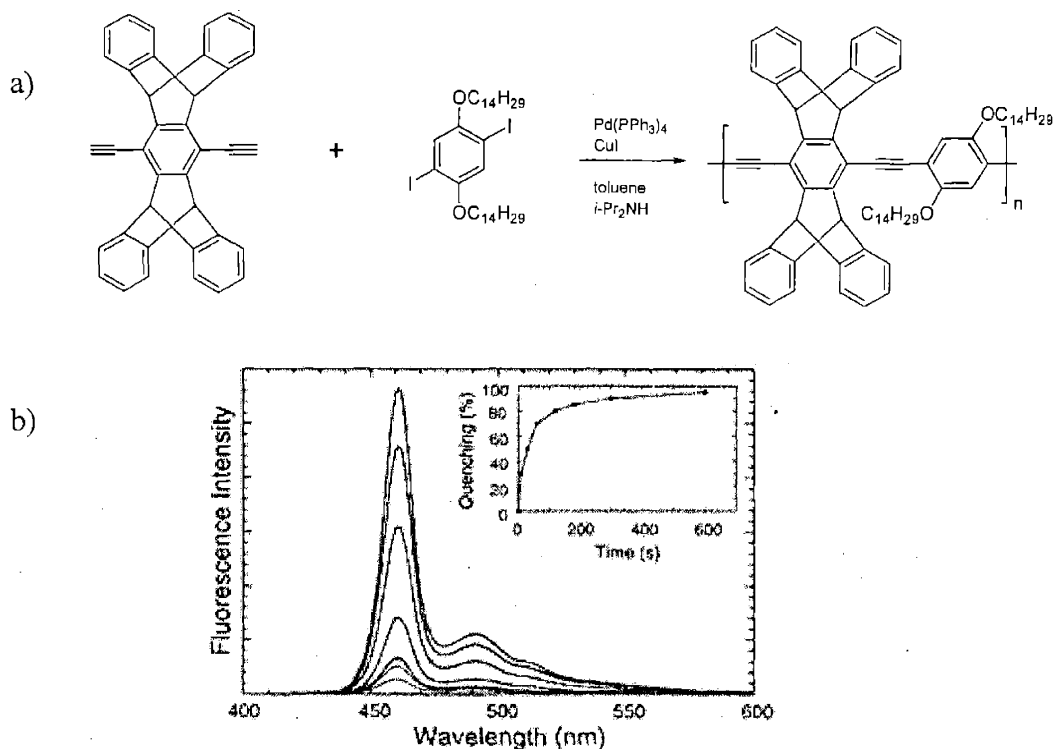


Figure 7. Fluorescence quenching mechanism in CPs. Photoexcitation at energy $h\nu$ creates an excited state. An electron transfer event from the excited state of the PPE to the LUMO of TNT is then energetically favorable. Such an event provides a non-radiative decay pathway for the exciton.

state in the interest of creating a robust sensing device. Though a different analyte, TNT, was targeted, the quenching mechanism is similar. In both cases, electron-deficient species interact with electron-rich PPE backbones to induce non-radiative decay. This most likely occurs through a photoinduced electron transfer event from the excited state of the CPs to the LUMO of the analyte (Fig 7). In the absence of the target compound, the exciton would recombine radiatively, emitting bright fluorescence. In its presence, we observe signal significant attenuation.

Self-quenching through packing effects is also known to lower the quantum yield of CPs in the solid state. Unique iptycene-based systems were fabricated to prevent aggregation and self-quenching (Fig. 8). The rigid scaffold also allows efficient analyte intercalation to minimize unquenched background fluorescence.⁷ As a result, these materials retain their fluorescence in thin films and demonstrated reversible fluorescence attenuation upon exposure to TNT.



Yang, J.; Swager, T.M. *J. Am. Chem. Soc.*, 1998, 120, 11864.

Yang, J.; Swager, T.M. *J. Am. Chem. Soc.*, 1998, 120, 5321.

Figure 8. a) First generation of CPs demonstrating extreme sensitivity to TNT. b) The time-dependent fluorescence intensity of PPE shown in (a) in a 25-Å film upon exposure to TNT vapor (room temperature) at 0, 10, 30, 60, 120, 180, 300, and 600 s (top to bottom), and the fluorescence quenching (%) as a function of time (inset).

4. Directions to be detailed

The global humanitarian devastation caused by TNT-containing landmines combined with exciting initial results prompted design improvements to further amplify sensory responses. This thesis details approaches to this end. We strived to understand excited state dynamics and energy transfer mechanisms underlying observed amplification so that we might invoke calculated improvements through rational synthetic design of new CPs. Unique synthetic modifications allowed us to elongate the excited state lifetime of PPEs in the interest of extending the energy migration that augments

sensory response. Interrogation of their photophysical properties allowed us to assess the enhancement achieved. To further advance these efforts, we exploited the nonlinear optical properties of our highly fluorescent CPs. As attractive candidates for laser gain media, our CPs have demonstrated the lowest amplified spontaneous emission (ASE) thresholds to date.⁸ By ‘turning off’ the otherwise accessible lasing peak, we can couple the nonlinear quench to the amplification already demonstrated by CPs. The combination of these advancements provides sensitivities to TNT that are currently being explored for commercial development by Nomadics, Inc. The intent is to produce devices from these materials and methods that will uncover buried landmines, saving life and limb.

¹ (a) Kraft, A.; Grimsdale, A. C.; Holmes, A. B. *Angew. Chem. Int. Ed.* **1998**, *37*, 402. (b) Greenham, N. C.; Friend, R. H. *Solid State Phys.* **1995**, *49*, 149.

² (a) Heeger, A. J. *Angew. Chem. Int. Ed.* **2001**, *40*, 2591. (b) Yan, M.; Rothberg, L. J.; Papadimitrakopoulos, F.; Galvin, M. E.; Miller, T. M. *Phys. Rev. Lett.* **1994**, *72*, 1104. (c) Bassler, H.; Brandl, V., Deussen, M., Gobel, E. O.; Kersting, R.; Kurz, H.; Lemmer, U.; Mahrt, R. F.; Ochse, A. *Pure Appl. Chem.* **1995**, *67*, 377. (d) Friend, R. H.; Bradley, D. D. C.; Townsend, P. D. *J. Phys. D-Appl. Phys.* **1987**, *20*, 1367.

³ Bassler, H.; Schweitzer, B. *Acc. Chem. Res.* **1999**, *32*, 173.

⁴ Swager, T. M.; Gil, C. J.; Wrighton, M. S. *J. Phys. Chem.* **1995**, *99*, 4886.

⁵ Levitsky, I. A.; Kim, J. S.; Swager, T. M. *J. Am. Chem. Soc.* **1999**, *121*, 1466.

⁶ (a) Zhou, Q.; Swager, T. M. *J. Am. Chem. Soc.* **1995**, *117*, 7017.

(b) Zhou, Q.; Swager, T.M. *J. Am. Chem. Soc.*, **1995**, *117*, 12593.

⁷ (a) Yang, J.; Swager, T. M. *J. Am. Chem. Soc.* **1998**, *120*, 11864. (b) Yang, J.; Swager, T. M. *J. Am. Chem. Soc.* **1998**, *120*, 5321.

⁸ Scherf, U.; Riechel, S.; Lemmer, U.; Mahrt, R. F. *Curr. Opin. Solid State Mat. Sci.* **2001**, *5*, 143.

Chapter 2

Modifying Conjugated Polymer Photophysics ~ Synthesis of Triphenylene-based Poly(p-phenyleneethylenes).

Portions of this chapter have appeared in print:

Rose, A.; Lugmair, C. G.; Swager, T. M. *J. Am. Chem. Soc.* **2001**, *123*, 11298-11299.

1. Introduction

The ability to synthetically manipulate the electronic and photonic properties of conjugated polymers (CPs) is often touted when the characteristics of these materials are discussed. However, most synthetic modification of these properties has previously focused only on changing their HOMO-LUMO levels. Two main approaches^{1,2} are usually adopted. Grafting different sidechains onto a particular polymer backbone represents one technique, as the sidechains affect HOMO-LUMO levels primarily through their relative donation or withdrawal of electron density from the main chain. Side-chain variation can also govern the effective conjugation length by influencing polymer conformation in solution. Because conformation is transferable to solid state films,³ it has important implications for device applications. A second approach, in which the main chain constituents are varied, can have a more pronounced effect on excitonic energies. Heteroatom incorporation and copolymerization can shift HOMO and LUMO levels significantly. Materials resulting from these conventional variations exhibit a spectrum of absorption and emission maxima, allowing one to choose tunable output colors and to match the energy levels of materials for either charge or energy transfer. Device applications abound for components with controllable energy levels. Thus, CPs have been incorporated into light-emitting diodes,⁴ photovoltaics⁵ and field-effect transistors,⁶ fueling even more intensive investigations in this field.

We chose an alternate approach to synthetically manipulate the photophysics of CPs with the goal of providing the highest amplification in our sensory schemes.⁷ Rather than shifting HOMO-LUMO levels, we sought to adopt synthetic strategies which

enhance the energy migration in CPs. This would allow the excitation a greater average diffusion length and a higher probability of encountering a receptor occupied by an analyte. Additionally, because energy migration is exploited in most of the other device applications of CPs, advancements achieved in this area are of broad relevance and utility.

A thorough understanding of the mechanisms underlying energy migration in CPs is necessary to design its enhancement. The high efficiency of energy transfer in most conjugated systems^{8,9} relative to systems with pendant chromophores^{10,11} suggests that strongly coupled electronic intrachain (Dexter-type) processes may increase transport in these systems over that provided solely by the dipole-dipole (Förster-type)¹² processes that govern weakly interacting chromophores. Discrepancies between the two mechanisms allow one to determine which reigns over CPs ubiquitous energy migration.

As derived by Dexter,¹³ the dipole-dipole approximation yield a transition probability (k_{et}):

$$k_{ET} = 1/\tau_d (R_o/r)^6$$

where τ_d is the pure radiative lifetime for the donor excitation. R_o can range from 50 to 100 and is the theoretical transfer distance beyond which energy transfer does not occur. Therefore, a poorly allowed transition, as manifest in a long radiative lifetime, should discourage purely Coulombic energy transfer.

Electron exchange effects contributing to energy transfer described by Dexter¹³, accounts for shorter range processes which result from direct wavefunction overlap of interacting molecules. In this case, the transition probability is described by:

$$k_{et} = K * J * \exp(2R_{da} / L)$$

where K is related to specific orbital interactions, J is the spectral overlap, R_{da} is donor-acceptor distance and L is van der Waal radii distance between donor and acceptor. This is often termed electron exchange or the collisional mechanism since molecules must be almost within van der Waal radii of each other to undergo this process. In the specific case of CPs, the chromophores are chemically bonded and energy migration proceeds quickly and efficiently to areas of longer conjugation length. Therefore, one might expect the Dexter mechanism to place a large contribution into the overall efficiency of energy migration.

In contrast to Coulombic energy transfer, the rate of electron exchange energy transfer is independent of the oscillator strengths of D^* to D and A to A^* transitions. We exploited the oscillator strength independence of the Dexter mechanism to determine if it indeed governs energy migration in isolated CPs in solution. To increase Coulombic energy transfer, one would target shorter radiative lifetimes as indicated by its rate

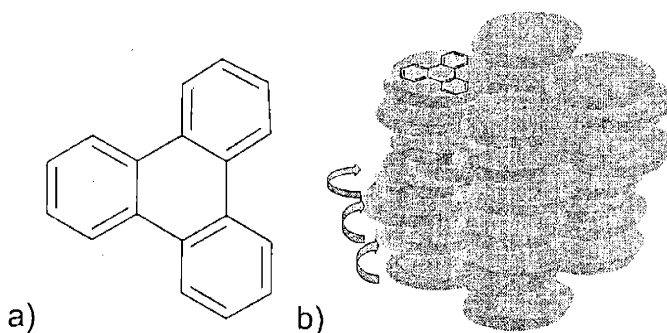


Figure 1. a) Chemical structure of triphenylene. b) Columnar stacking of triphenylenes allows for intermolecular charge and energy transport in liquid crystals.

equation. However, because the electron exchange mechanism does not depend on oscillator strength, longer lifetimes affected by disallowed transitions should increase

energy transfer by providing more time for the excitation to migrate before radiative decay. Therefore, we sought to systematically reduce the oscillator strength in CPs and determine the effects on energy migration.

Poly(phenylene ethylenes) (PPEs) are appropriate backbones for this study due to their relatively rigid geometry and their ability to effectively transfer energy over long distances.¹⁴ To modify the lifetimes and hence oscillator strength of these systems, we chose to incorporate triphenylene chromophores (Fig 1a) into the polymer backbone. This fused 3 aromatic ring system has a well-known¹⁵ symmetrically forbidden S_1 - S_0 transition resulting in a long-lived excited state. Upon functionalization and polymerization, clearly the triphenylene wavefunction¹⁶ will be perturbed, and the stringent symmetry responsible for its optical properties will be broken. However, molecular modeling indicates that the ground state wavefunction is localized mainly within the rings, and we

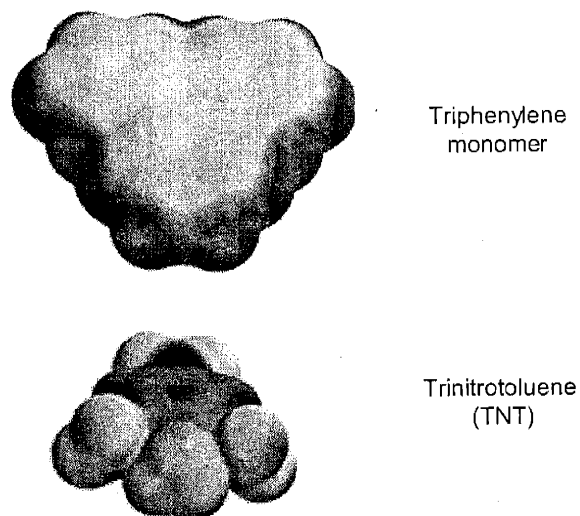


Figure 2. Electrostatic map of triphenylene interacting with TNT. Dark shades indicate electron poor regions and light shades indicate electron rich areas.

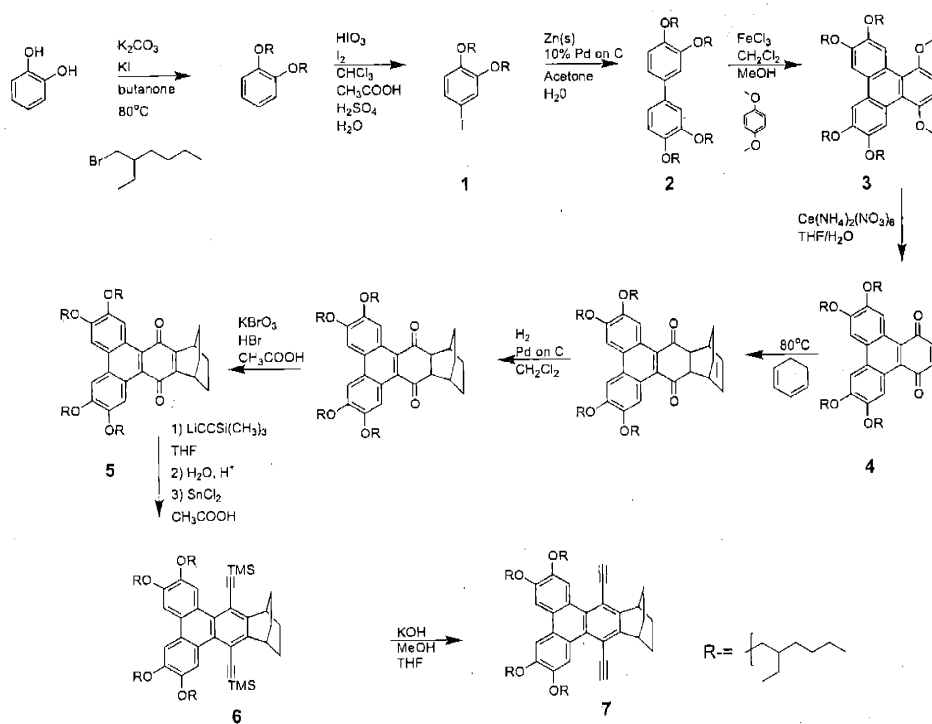
considered that this strongly aromatic structure should retain some of its individual identity, extending the excited state lifetimes in poly(triphenylene ethynylenes) (TPPEs). In addition to their desired electronic properties, triphenylene-based materials also have a tendency to form π -stacked discotic liquid crystalline phases that facilitate charge and energy transport (Fig. 1b).^{17,18} Resulting materials should therefore be healthy candidates for energy transfer studies in all respects except their reduced transition dipoles, the target of our interrogation. Our previous success with 2,4,6 trinitrotoluene (TNT) detection provided a benchmark by which to assess the success of our design principles in enhancing sensory response. The transduction mechanism is fluorescence quenching induced by an electron transfer event from an electron-rich polymer chain to electron-deficient TNT. The electrostatics of the triphenylene ring (Fig 2), as modeled by Dr. Vance Williams, allows TNT to induce a similar quench in fluorescence.

2. Results and discussion

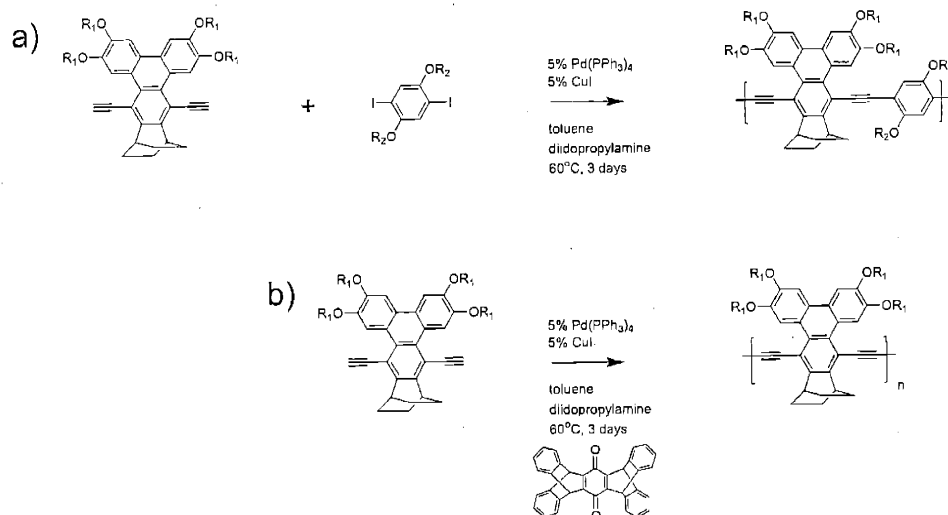
2.1. Triphenylene monomer and polymer synthesis

Both chemical^{19,20} and electrochemical²¹ methods to symmetrically substituted triphenylene have existed for many years. Most are straightforward and high-yielding. Asymmetric routes have only surfaced more recently²² as interest in triphenylenes as liquid crystals has grown. We drew on these more challenging routes because incorporation of triphenylene into a PPE backbone required an asymmetric monomer.

A novel route to such a monomer was pioneered by Dr Claus G. Lugmair, a postdoctoral associate in our laboratory from 1997-1999. He heroically synthesized monomers with a variety of sidechains to insure optimal packing and high quantum



Scheme 1. Triphenylene monomer synthesis.



Scheme 2. Polymerization conditions used to synthesize TPPEs. (a) Sonigashira-Hagihara polymerization. (b) The catalyst is intentionally oxidized by the quinone to homocouple the monomer.

efficiencies persistent in the solid state. Fluorescence quenching in the solid state due to π -stacking was overcome by including branched bulky sidechains and a bicyclooctane ring to keep the polymer chains sufficiently separated. A thorough study of energy transfer mechanisms demands investigation of several copolymers to accurately assign trends in photophysical behavior to triphenylene incorporation rather than deviations among individual polymers. It was therefore necessary to scale up the monomer synthesis to provide quantities sufficient for several copolymerizations. This warranted modification of Dr. Lugmair's original synthesis to eliminate the column chromatography that becomes impractical on a larger scale. The resulting synthesis is depicted in Scheme 1.

The triphenylene monomer is synthesized with an overall yield of 12%. Iodination of 1,2 dialkoxybenzene with periodic acid and iodine²³ afford 3,4-dialkoxyiodobenzene (1) and subsequent zinc/palladium (0) coupling²⁴ generates 3,3',4,4'-tetraalkoxybiphenyl (2) in high yields. Iron (III) trichloride and *p*-dimethoxybenzene afford cyclization to the triphenylene (3). Selective oxidation of the methoxy groups with cerium ammonium nitrate forms the quinone (4). A Diels-Alder [4+2] cycloaddition in neat cyclohexadiene incorporates the bicyclooctane moiety. The isolated double bond is hydrogenated and subsequent oxidation with potassium bromate generates the quinone (5). Lithiated trimethylsilane acetylide adds to the quinone carbonyls and subsequent dehydroxylation with tin dichloride reconstitutes the triphenylene ring system (7). Deprotection with base gives the diethynyl monomer which is copolymerized with diiodo-functionalized monomers using Sonigashira-Hagihara palladium cross coupling²⁵ (Scheme 2a) with the exception of Polymers 17, 19 and 17a for which an oxidative coupling method is used (Scheme 2b).²⁶

Chart 1. Triphenylene-based PPEs (TPPEs) synthesized.

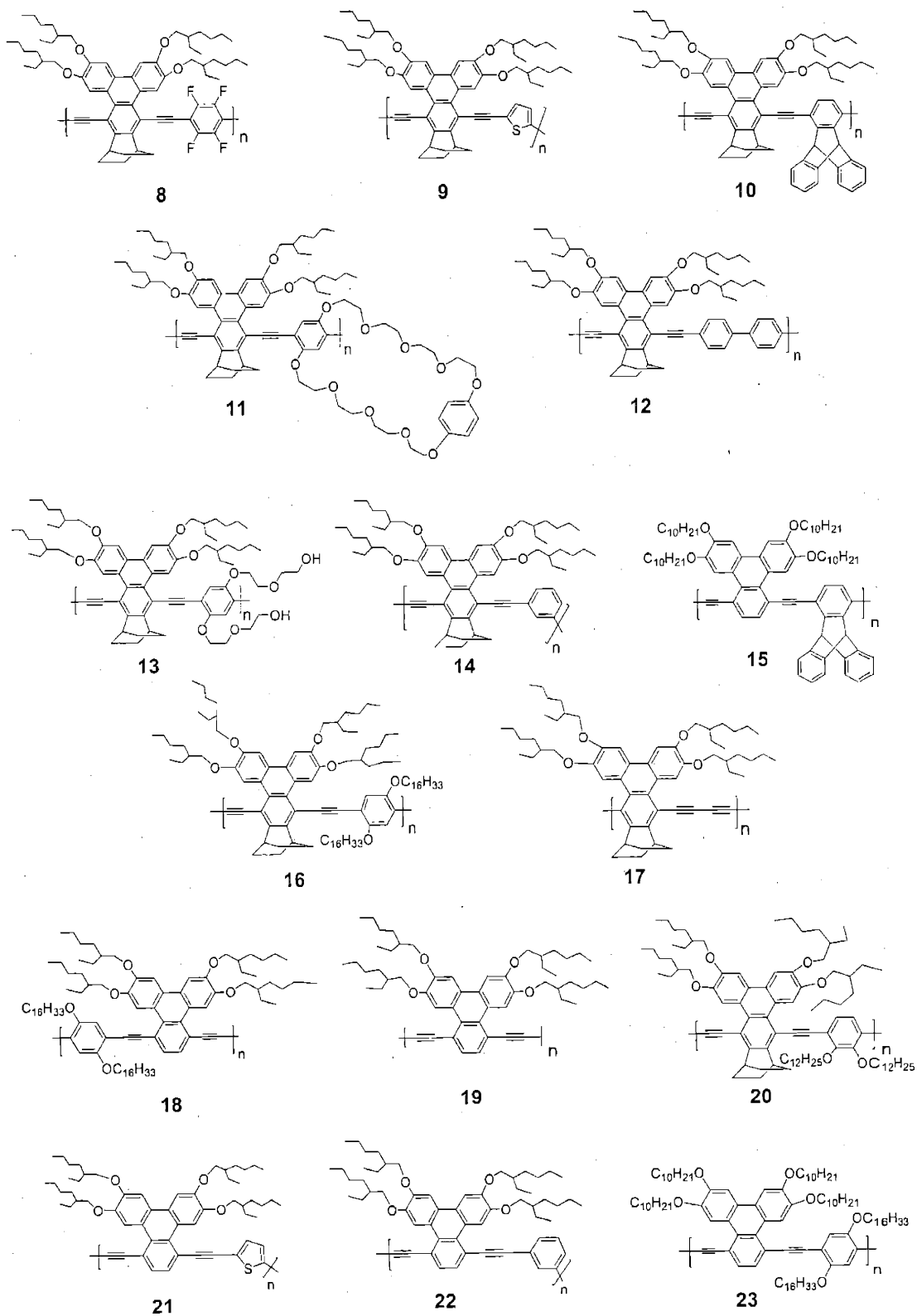
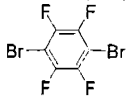
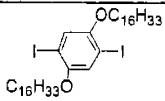
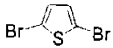
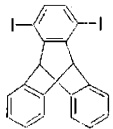
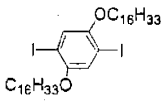
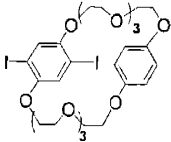
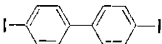
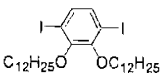
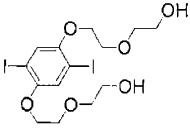
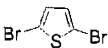
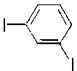
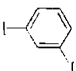
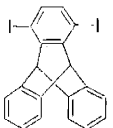
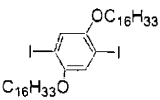


Table 1. Properties of TPPEs as synthesized.

Polymer	Comonomer	$M_n / 10^3$	pdi	Polymer	Comonomer	$M_n / 10^3$	pdi
8		8.2	1.0	16		45	2.5
9		114	1.4	17	N/A	8.0	1.4
10		54	1.6	18		79	2.4
11		103	1.5	19	N/A	200	5.5
12		39	1.9	20		34	3-19
13		92	4- 121	21		31.5	2.2
14		7.8	1.3	22		32	4.2
15		58	3.1	23		76	2.8

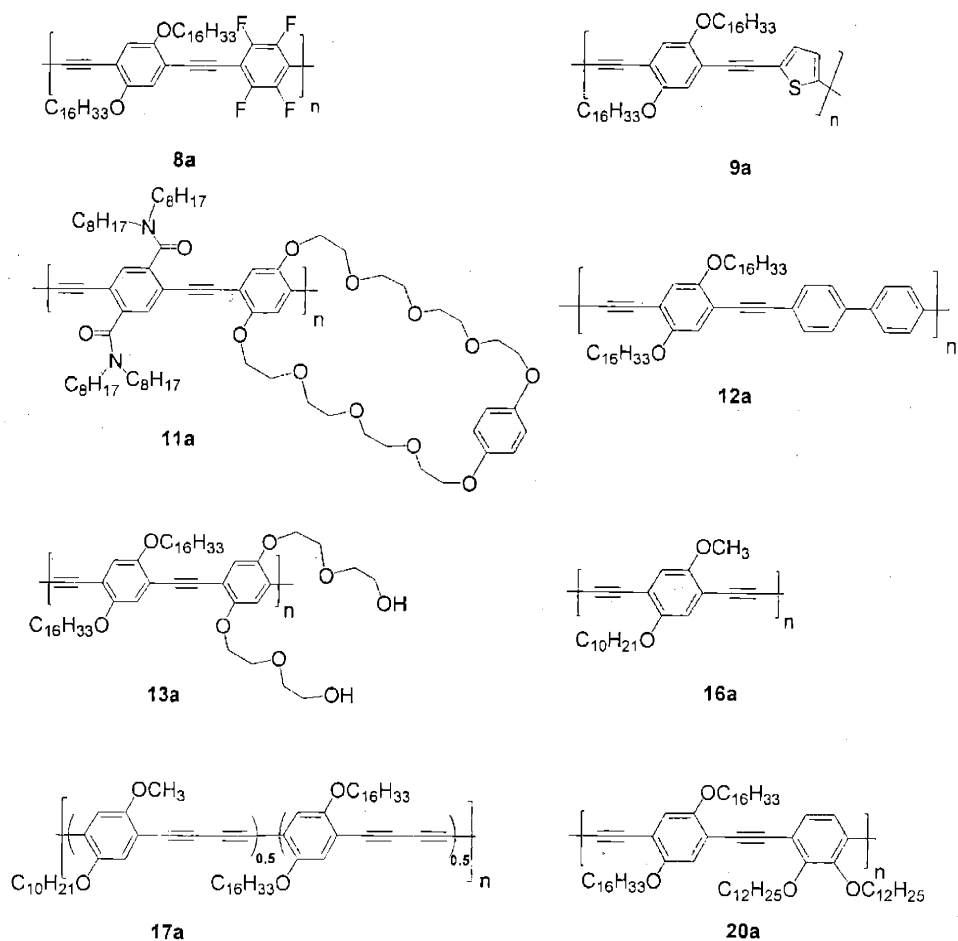
Key improvements in Scheme 1 were effected in steps 2 and 3. The initial target of halogenation in step 2 was the bromo derivative, to be homocoupled with N-bromosuccinimide (NBS) to yield the biphenyl. This coupling was not efficient enough to circumvent rigorous purification of the resulting mixture of biphenyl and dehalogenated

bromo derivative. We alternatively approached the biphenyl via the iodinated intermediate. We enjoyed complete conversion to the biphenyl in the subsequent zinc and palladium coupling. This eliminated the need for purification. With regard to the iron trichloride coupling (step 4), hydrochloric acid generated *in situ* resulted in the cleavage of a single ethylhexyl sidechain from the resulting triphenylene. The byproduct is similar enough in polarity to side product to make chromatographic separation extremely difficult. We found, however, that bubbling argon gas continually through the reaction mixture drives off enough of the hydrochloric acid to prevent sidechain cleavage, yielding triphenylene nearly quantitatively. This reaction offers an alternative to the conventional Ullmann coupling. These simple modifications allowed us to enjoy overall monomer yields in excess of 12%, affording enough material to copolymerize with many other monomers. This allowed us to synthesize a library of TPPEs with which to conduct our studies (Chart 1). Some physical properties of the TPPEs synthesized are summarized in Table 1.

2.2. Model polymer synthesis

In order to compare the photophysical enhancement achieved in excited state lifetime and energy migration by triphenylene incorporation, matched PPEs to TPPEs were synthesized for comparative studies (Chart 2). Comonomers for polymers **8a**, **9a**, **11a**, **12a**, **13a**, and **20a** are identical to those used in TPPEs with the *p*-diactelyde

Chart 2. Model polymers (PPEs) synthesized.



(21) (Chart 3) substituted for the triphenylene monomer. Polymer **11a** was synthesized by Dr. Quin Zhou. Polymer **16a** was synthesized by Mr. Sean K. McHugh from the corresponding diiodo and diacetylide precursors.

Polymer **17a** is regio-random structure and to maintain solubility at high-molecular weights **17a** was synthesized as a random copolymer. Some physical properties of the PPEs synthesized are

Chart 3. PPE monomer **21**.

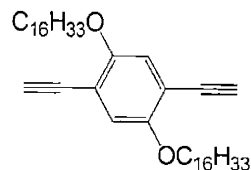


Table 2. Properties of PPEs as synthesized.

Polymer	$M_n/10^3$	pdi	Polymer	$M_n/10^3$	pdi
8a	4.8	1.3	13a	22	2.8
9a	57	2.1	16a	40	1.1
11a	29	1.9	17a	104	3.4
12a	9.9	1.4	20a	22	2.0

3. Conclusions

A novel, high yielding route to a unique triphenylene monomer was developed. Subsequent polymerizations resulted in high molecular weight, fluorescent triphenylene-based conjugated polymers. Model polymers, identical except for the triphenylene chromophores, were also synthesized. This allowed us to assess the changes in photophysical behavior resulting from triphenylene incorporation, as discussed in detail in the next chapter.

4. References

- ¹ Handbook of Conducting Polymers, **1998**, Skotheim, T. A.; Elsenbaumer, R. L.; Reynolds, J. R. eds. Marcell Dekker, Inc. New York, NY.
- ² Shim, H. K.; Jin J. I. *Polymers for Photonic Applications I Advances in Polymer Science* **2002**, *158*, 193.
- ³ Nguyen, T.Q.; Doan, V.; Schwartz, B.J. *J. Chem. Phys.* **1999** *110*, 4068.

-
- ⁴ Friend, R. H.; Gymer, R. W.; Holmes, A. B.; Burroughes, J. H.; Marks, R. N.; Taliani, C.; Bradley, D. D. C.; Dos Santos, D. A.; Bredas, J. L.; Logdlund, M.; Salaneck, W. R. *Nature* **1999**, *397*, 121.
- ⁵ Sariciftci N. S. *Curr. Opin. Solid-State. Mater. Sci.* **1999**, *4*, 373.
- Bao, Z *Adv. Mater.* **2000**, *12*, 227.
- ⁶ Sirringhaus, H.; Tessler, N.; Friend, R. H. *Science* **1998**, *280*, 1741.
- ⁷ (a) Zhou, Q.; Swager, T. M. *J. Am. Chem. Soc.* **1995**, *117*, 7017. (b) Zhou, Q.; Swager, T. M. *J. Am. Chem. Soc.* **1995**, *117*, 12593. (c) Yang, J.-S.; Swager, T. M. *J. Am. Chem. Soc.* **1998**, *120*, 5321.
- ⁸ Devadoss, C.; Bharathi, P.; Moore, J. S. *J. Am. Chem. Soc.* **1996**, *118*, 9635.
- ⁹ Ley, K. D.; Whittle, C. E.; Bartberger, M. D.; Schanze, K. S. *J. Am. Chem. Soc.* **1997**, *119*, 3423.
- ¹⁰ Guillet, J. *Polymer Photophysics and Photochemistry: An Introduction to the Study of Photoprocesses in Macromolecules*, **1987**, Cambridge University Press: Cambridge, U.K.
- ¹¹ (a) Byers, J. D.; Friedrich, M. S.; Friesner, R. A.; Webber, S. E. *In Molecular Dynamics in Restricted Geometries*; Klafter, J., Drake, J. M., Eds.; Wiley: New York, 1988; pp 99-144. (b) Kiserow, D. J.; Itoh, Y.; Webber, S. E. *Macromolecules* **1997**, *30*, 2934. (c) Levitsky, I. A.; Webber, S. E. *J. Lumin.* **1998**, *78*, 147.
- ¹² Förster, T. *Discuss. Faraday Soc.* **1953**, *27*, 7.
- ¹³ Dexter, D. L. *J. Chem. Phys* **1953**, *21*, 836.
- ¹⁴ Bunz, U. H. *Chem. Rev.* **2000**, *100*, 1605.
- ¹⁵ Markovitski, D.; Germain, A.; Millie, P.; Lecuyer, P.; Gallos, L. K.; Argyrakakis, P.; Bengs, H.; Ringsdorf, H. *J. Phys. Chem.* **1995**, *99*, 1005.

-
- ¹⁶ Etchegoin, P. *Phys Rev. E* **1997**, *56*, 538.
- ¹⁷ (a) Warman, J. M.; Schouten, P. G. *J. Phys. Chem.* **1995**, *99*, 17181.
(b) van de Craats, A. M.; de Haas, M. P.; Warman, J. M. *Synth. Met.* **1997**, *86*, 2125.
- ¹⁸ Markovitski, D.; Lecuyer, I.; Lianos, P.; Malthete, J. *J. Chem. Soc., Faraday Trans.* **1991**, *87*, 1785.
- ¹⁹ Matheson, I.M.; Musgrave, O.C.; Webster, C.J. *Chem. Comm.* **1965**, 278.
- ²⁰ Boden, N.; Bushby, R. J.; Ferris, L.; Hardy, C.; Sixl, F. *Liq. Crystals* **1986**, *1*, 109.
- ²¹ Bechgaard, K.; Parker, V. D. *J. Am. Chem. Soc.* **1972**, *94*, 4749.
- ²² Boden, N.; Bushby, R. J.; Cammidge, A. N. *Chem. Comm.* **1994**, 465.
- ²³ Bacher, A.; Erdelen, C. H.; Paulus, W.; Ringsdorf, H.; Schimdt, H.-W.; Schuhmacher P. *Macromolecules*, **1999**, *32*, 4551.
- ²⁴ Jacob, P.; Callery, P. S.; Shulgin, A. T.; Catagnoli, N. *J. Org. Chem.* **1976**, *41*, 3627.
- ²⁵ Sonogashira, K.; Tohda, Y.; Hagihara, N. *Tetrahedron Lett.* **1975**, 4467.
- ²⁶ Williams, V. E.; Swager, T. M. *J. Polym. Sci. A* **2000**, *33*, 4069.

5. Experimental Section

All manipulations were performed under a nitrogen atmosphere using standard Schlenk techniques or an Innovative Technologies dry box. Tetrahydrofuran was distilled from sodium benzophenone under nitrogen. Toluene and diisopropylamine were distilled from sodium under nitrogen and then degassed. NMR spectra were recorded on a Varian VXR-500 spectrometer at 500 (^1H), 125 (^{13}C) MHz using CDCl_3 as solvent. The chemical shifts are reported in ppm relative to TMS. Infrared spectra were collected as Nujol mulls on a Mattson Galaxy 3000 spectrometer, using KBr cells. Elemental analyses were performed by Desert Analytics. The molecular weights of polymers were determined using a Hewlett Packard series 1100 HPLC instrument equipped with a PLgel 5 μm Mixed-C (300 x 7.5 mm) column and a diode array detector at 245 nm at a flow rate of 1.0 mL/min in THF. The molecular weights were calibrated relative to polystyrene standards purchased from Polysciences, Inc. Compounds were purchased from Aldrich. The compound 1,2-di(2-ethylhexyloxy)benzene was prepared according to literature procedures.

1,2-di(2-ethylhexyloxy)benzene. In a 2 L flask were combined 2-ethylhexylbromide (127.9 mL, 0.719 mol), KI (21.71 g, 0.131 mol), K_2CO_3 (180.8 g, 1.31 mol), and catechol (36.0 g, 0.327 mol). The flask was purged with N_2 for 10 min. and 1 L butanone was added. The mixture was heated at reflux for 22 d. The reaction mixture was then cooled, filtered and the solids washed with ether. The filtrate was washed several times with water, dried (MgSO_4) and concentrated under reduced pressure. The crude product was distilled (80 $^\circ\text{C}$ / 0.02 mmHg) to give **1** as a colorless oil in 79% yield. ^1H NMR (500 MHz): δ 0.87 - 0.93 (m, 12H), 1.20 - 1.54 (m, 20H), 1.72 - 1.76 (m, 2H), 3.82 - 3.86 (m,

4H), 6.86 (s, 3H). ^{13}C NMR (125 MHz): δ 11.38, 14.33, 23.31, 24.10, 29.34, 30.79, 39.78, 71.77, 113.99, 121.01, 149.78. IR (KBr, cm^{-1}): 2958 s, 2928 s, 2872 m, 2859 m, 1592 m, 1503 m, 1465 m, 1380 w, 1254 m, 1222 m, 1122 m, 1033 m, 738. HRMS (FAB): found m/z 334.2875 (M^+); calcd for $\text{C}_{22}\text{H}_{38}\text{O}_2$ m/z 334.2872 (M^+). Anal. Calcd for $\text{C}_{22}\text{H}_{38}\text{O}_2$: C, 78.99; H, 11.45. Found: C, 78.96; H, 11.24.

4-iodo-1,2-di(2-ethylhexyloxy)benzene (1). 1,2-di(2-ethylhexyloxy)benzene (37.19 g, 0.1112 mol) was added to a mixture of HIO_3 (4.28 g, 0.02445 mol), I_2 (solid, 10.44 g, 0.04114 mol), glacial acetic acid (125 mL), chloroform (33 mL), distilled water (41 mL), and sulfuric acid (1.2 mL). The mixture was stirred at 40 °C for 12 hours. The reaction mixture was cooled to room temperature and distilled water (100 mL) and chloroform (60 mL) was added. Solution was washed (3x) with 2 M KOH and with water (3x). After drying with MgSO_4 , the solvent was removed under reduced pressure. Crude product was distilled (150 °C/ 0.02 mmHg) to give **1** as a light yellow oil in a 90% yield. ^1H NMR (300 MHz): δ 0.85 – 0.97 (m, 12 H), 1.27- 1.56 (m, 16 H), 1.57 - 1.77 (m, 4H), 3.82 - 3.85 (m, 4H), 6.20 (d, 1H, $J = 8.5$ Hz), 6.72 (d, $J = 3.0$ Hz, 1 H), 7.12 (d d, 1H, $J = 8.4$ Hz, $J = 2.1$ Hz).

3,3',4,4'-tetrakis(2-ethylhexyl)biphenyl (2). Zn powder and Pd (10%) on carbon were suspended in water (150 mL) and acetone (150 mL) and heated to 50 °C with stirring for 30 min. **1** (16.87 g, 0.0366 mol) in 10 mL acetone was slowly added. The mixture was stirred for 12 hours. The reaction mixture was cooled to room temperature, filtered through a plug of silica, and eluted with diethyl ether. The organic fraction was washed with water (2x), and sat. NaCl solution (1x), dried with MgSO_4 . Solvent was removed under reduced pressure and the remaining yellow oil (90% yield) was used in next step

without purification. ^1H NMR (500 MHz): δ 0.85 - 0.94 (m, 24H), 1.30 - 1.56 (m, 32H), 1.74 - 1.78 (m, 4H), 3.85 - 3.92 (m, 8H), 6.90 (d, 2H, $J = 8.5$ Hz), 7.03 (d, 2H, $J = 8.5$ Hz), 7.04 (s, 2H). ^{13}C NMR (125 MHz): δ 11.42, 14.34, 23.32, 24.12, 29.36, 30.80, 39.84, 72.00, 113.11, 114.06, 119.34, 134.53, 148.99, 149.79. IR (NaCl, neat, cm^{-1}): 2961 s, 2923 s, 2872 s, 2860 s, 1602 m, 1570 m, 1499 s, 1466 s, 1417 w, 1380 m, 1310 w, 1251 s, 1217 m, 1184 w sh, 1139 m, 1057 w sh, 1031 m, 929 w, 846 w, 799 m, 728 w. HRMS (FAB): found m/z 666.5579 (M^+); calcd for $\text{C}_{44}\text{H}_{74}\text{O}_4$ m/z 666.5587 (M^+). Anal. Calcd for $\text{C}_{44}\text{H}_{74}\text{O}_4$: C, 79.22; H, 11.18. Found: C, 79.39; H, 11.31.

1,4-dimethoxy-6,7,10,11-tetrakis(2-ethylhexyloxy)triphenylene (3). Oil 2 (11.96 g, 0.01793 mol) was added to an ice cold suspension of anhydrous FeCl_3 (23.27 g, 0.1434 mmol) in dry CH_2Cl_2 (700 mL). Within 2 min, 1,4-dimethoxybenzene (9.91 g, 0.07172 mmol) was added to the green reaction mixture. Dry Ar gas was bubbled continuously through the reaction mixture. The reaction mixture was allowed to warm slowly to room temperature and then stir for an additional 12 h. The reaction mixture was quenched with anhydrous MeOH (100 mL). The volume of the mixture was reduced under reduced pressure. The remaining mixture was poured into water and extracted twice with dichloromethane. The organic fractions were washed with water, dried with MgSO_4 and concentrated under reduced pressure. The excess 1,4-dimethoxybenzene was sublimated out of the resulting oil (0.02 mmHg, 90 $^\circ\text{C}$, 12 hours) and the remaining oil (95 % yield) was used without further purification. ^1H NMR (500 MHz): δ 0.88 - 1.00 (m, 24H), 1.30 - 1.63 (m, 40H), 1.85 - 1.89 (m, 4H), 3.97 (s, 6H), 4.04 - 4.12 (m, 8H), 7.07 (s, 2H), 7.79 (s, 2H), 9.12 (s, 2H). ^{13}C NMR (125 MHz): δ 11.42, 11.55, 14.36, 14.38, 23.35, 23.37, 24.21, 29.37, 29.40, 30.89, 30.91, 30.94, 39.67, 39.79, 57.44, 71.63, 71.96, 106.40,

110.58, 112.98, 112.59, 123.16, 125.57, 148.22, 149.23, 152.69. IR (KBr, pellet, cm^{-1}): 2960 s, 2929 s, 2873 m, 2859 m, 1614 w, 1598 w sh, 1543 w, 1514 m, 1457 s, 1433 m sh, 1415 w sh, 1379 w, 1372 w sh, 1280 w sh, 1261 m sh, 1243 s, 1187 m, 1168 w, 1123 s, 1078 w, 1035 w, 999 w, 864 w, 831 w, 799 w, 768 w, 723 w, 605 w. HRMS (FAB): found m/z 800.5938 (M^+); calcd for $\text{C}_{52}\text{H}_{80}\text{O}_6$ m/z 800.5955 (M^+). Anal. Calcd for $\text{C}_{52}\text{H}_{80}\text{O}_6$: C, 77.95; H, 10.06. Found: C, 78.14; H, 10.35.

6,7,10,11-tetrakis(2-ethylhexyloxy)triphenylene-1,4-dione (4). An aqueous solution (1 mL) of $(\text{NH}_4)_2\text{Ce}(\text{NO}_3)_6$ (0.035 g, 0.064 mmol) was added dropwise to a THF solution (5 mL) of 1,4-dimethoxy-6,7,10,11-tetrakis(2 ethylhexyloxy) triphenylene (0.029 g, 0.032 mmol). The reaction mixture immediately turned deep red. After 6 h, the reaction mixture was poured into ether and washed with a saturated solution of NaHCO_3 and water. The organic layer was dried with MgSO_4 and the solvent removed under reduced pressure. The crude product was purified by column chromatography on silica gel (1:1 CH_2Cl_2 /hexane) to afford **3** as a deep red waxy solid in 70% yield (mp = 105 – 107 °C). ^1H NMR (500 MHz): δ 0.87 - 1.01 (m, 24H), 1.32 - 1.60 (m, 32H), 1.84 - 1.90 (m, 4H), 4.08 (d, 4H, $J = 9.5$ Hz), 4.14 (d, 4H, $J = 9.5$ Hz), 6.85 (s, 2H), 7.73 (s, 2H), 8.92 (s, 2H). ^{13}C NMR (125 MHz): δ 11.52, 11.60, 14.23, 14.34, 16.21, 23.31, 24.25, 29.39, 30.97, 39.6671.22, 71.45, 103.83, 109.35, 122.44, 126.96, 129.16, 138.04, 151.33, 151.74, 189.88. IR (KBr, pellet, cm^{-1}): 2959 s, 2930 s, 2873 m, 2860 m, 1640 m, 1612 m, 1522 w sh, 1507 m, 1461 m, 1436 m, 1382 m, 1333 w, 1264 s, 1186 w, 1159 w, 1082 s, 1047 w, 1020 w, 863 w, 823 w. HRMS (FAB): found m/z 770.5496 (M^+); calcd for $\text{C}_{50}\text{H}_{74}\text{O}_6$ m/z 770.5485 (M^+). Anal. Calcd for $\text{C}_{50}\text{H}_{74}\text{O}_6$: C, 77.88; H, 9.67. Found: C, 77.66; H, 9.75.

(5). Compound 4 (1 g, 1.30 mmol) was dissolved in 1,3-cyclohexadiene (20 mL). The mixture was heated to 80 °C for 12 h. The excess 1,3-cyclohexadiene was then removed under reduced pressure. The remaining viscous oil was transferred to a hydrogenation vessel (50 mL capacity) along with CH₂Cl₂ (10 mL) and 10% Pd on carbon (10 mg). This mixture was degassed and then shaken under H₂ (40 psi) for 24 h. The reaction mixture was then filtered through a short plug of silica and evaporated to dryness. The remaining solid was added to glacial acetic acid (40 mL) and heated to 100 °C. Two drops of concentrated HBr were added causing the solution to turn dark red. After 5 min an aqueous solution (10 mL) of KBrO₃ (0.016 g, 0.096 mmol) was added and the mixture was heated for an additional 10 min. The solution was allowed to cool and then extracted with two portions of CH₂Cl₂. The combined organic fractions were washed with water, dried with MgSO₄ and evaporated to dryness. The crude product was purified by column chromatography on silica gel using a 1:9 dichloromethane/hexane solvent mixture affording 5 in 50% yield over the 3 steps. ¹H NMR (500 MHz): δ 0.90 (t, 12H, *J* = 6.5 Hz), 0.95 - 1.00 (m, 12H), 1.31 - 1.63 (m, 44H), 1.79 (d, 4H, *J* = 7.5 Hz) 1.83 - 1.90 (m, 4H), 3.52 (s, 2H), 4.08 - 4.14 (m, 8H), 7.73 (s, 2H), 8.97 (s, 2H). ¹³C NMR (125 MHz): δ 11.55, 11.61, 14.36, 23.32, 23.33, 24.24, 24.26, 24.30, 24.33, 25.79, 27.27, 29.41, 29.43, 30.97, 39.68, 39.77, 71.10, 71.45, 103.90, 109.70, 122.90, 127.43, 128.89, 149.25, 151.07, 151.35, 187.06. IR (KBr, pellet, cm⁻¹): 2957 s, 2927 s, 2870 m, 2860 m, 1636 m, 1613 m, 1521 w sh, 1506 m, 1459 m, 1434 m, 1378 m, 1335 w, 1259 s, 1214 w, 1197 w, 1162 w, 1082 w, 1032 m, 922 w, 865 w, 820 w, 773 w. HRMS (FAB): found *m/z* 850.6119 (M⁺); calcd for C₅₆H₈₂O₆ *m/z* 850.6111 (M⁺). Anal. Calcd for C₅₆H₈₂O₆: C, 79.01; H, 9.71. Found: C, 79.36; H, 9.66.

6,7,10,11-tetrakis(2-ethylhexyloxy)-1,4-ethynyltriphenylene (7) A hexane solution of *n*-BuLi (8.81 mL, 1.57 M, 14.10 mmol) was added to a THF solution (60 mL) of trimethylsilylacetylene (2.00 mL, 14.10 mmol) that had been precooled to -78 °C. The mixture was allowed to warm to -10 °C and stirred at that temperature for 30 min. The solution was then cooled to -78 °C and a THF solution (30 mL) of **5** was added dropwise. During the addition the red color of the quinone dissipated. After the addition was complete the reaction mixture was allowed to warm to room temperature and then stirred for an additional 12 h. The reaction mixture was then poured into ether and enough dilute HCl was added to make the solution slightly acidic. The organic layer was then quickly washed with several portions of water and dried with MgSO₄. The solvent was removed under reduced pressure and the remaining light brown oil was dissolved in acetone (300 mL). To this solution was added dropwise a solution of SnCl₂·2 H₂O (2.76 g, 12.22 mmol) in 50% HOAc (30 mL). After 12 h the reaction mixture was poured into ether and washed with water, a saturated solution of NaHCO₃ and again water. The organic layer was dried with MgSO₄, and the solvent was removed under reduced pressure. Product was obtained as a yellow oil in 55% yield over 3 steps to form **6,7,10,11-tetrakis(2-ethylhexyloxy)triphenylene-1,4-di(2-trimethylsilyl) acetylene (6)**. This compound was then deprotected to form **(7)** as follows. Solid K₂CO₃ (1.79 g, 13.0 mmol) was added to a 1:1 THF/MeOH solution (100 mL) of **7,10,11-tetrakis(2-ethylhexyloxy)triphenylene-1,4-di(2-trimethylsilyl) acetylene** (3.3 g, 3.25 mmol). The reaction mixture was allowed to stir for 12 h. It was then poured into ether and washed with water. The organic layer was dried with MgSO₄ and the solvent removed under reduced pressure. The product was purified by flash chromatography on silica gel using a 1:3 CH₂Cl₂/hexane solvent

mixture. Compound 5 was obtained as a yellow oil in 85% yield ^1H NMR (500 MHz): δ 0.93 - 1.05 (m, 24H), 1.2 - 1.7 (m, 36H), 1.86 - 1.95 (m, 8H), 3.72 (s, 2H), 3.98 (s, 2H), 4.08 - 4.11 (m, 4H), 4.16 (d, 4H, $J = 5.5$), 7.78 (s, 2H), 9.39 (s, 2H). ^{13}C NMR (125 MHz): δ 11.46, 11.58, 14.35, 14.38, 23.35, 24.25, 24.27, 25.69, 29.41, 29.43, 30.94, 30.97, 31.82, 32.30, 39.76, 39.84, 71.78, 72.01, 84.47, 86.17, 106.36, 111.78, 112.67, 123.59, 125.12, 130.05, 146.55, 147.95, 149.55. IR (KBr, pellet, cm^{-1}): 3306 m, 2957 s, 2928 s, 2863 m, 1613 m, 1537 w sh, 1513 s, 1464 m, 1421 m, 1380 m, 1343 w, 1287 m, 1243 s, 1189 m, 1145 w, 1099 m, 1034 m, 1013 w, 908 w, 855 w, 831 w, 808 w, 768 w, 734 w. HRMS (FAB): found m/z 868.6352 (M^+); calcd for $\text{C}_{60}\text{H}_{84}\text{O}_4$: m/z 868.6370 (M^+).
Anal. Calcd for $\text{C}_{60}\text{H}_{84}\text{O}_4$: C, 82.90; H, 9.74. Found: C, 82.56; H, 9.74.

Chapter 3

Combining excited state lifetime measurements and polarization spectroscopy to track energy migration.

Portions of this chapter have appeared in print:

Rose, A.; Lugmair, C. G.; Swager, T. M. *J. Am. Chem. Soc.* **2001**, *123*, 11298-11299.

1. Introduction

Time-resolved luminescence of conjugated polymers (CPs) can reveal information on their excited state behavior such as lifetime, migration and decay pathways. The dynamic nature uncovered by these measurements has invited both research and speculation.¹ Excited state absorption, intersystem crossing and energy migration are some of the contributors that confuse absorption/emission profiles in CPs. We are interested in excited state processes in CPs because excited state dynamics provide amplification in our sensory schemes.

In efforts to maximize amplification, we designed and synthesized materials with extended excited state lifetimes. We rely on time-resolved spectroscopy to quantify achieved enhancements in lifetime. Because multiexponential excited state depopulation is especially pronounced in solid state measurements, we chose to pursue lifetime measurements in solution. In addition to simplifying comparisons, this eliminates variables associated with processing and interchain interactions. Model polymers, i.e. without triphenylene chromophores, were synthesized as described previously (Ch.2), and their photophysics were compared to the triphenylene polymers. In these studies, we seek to assess the effects on the excited state when longer-lived chromophores are incorporated into a conjugated polymer (CP) backbone. We hope to chronicle an increase in the extent of exciton migration, therefore improving sensory response.

2. Results and discussion

2.1. Experimental

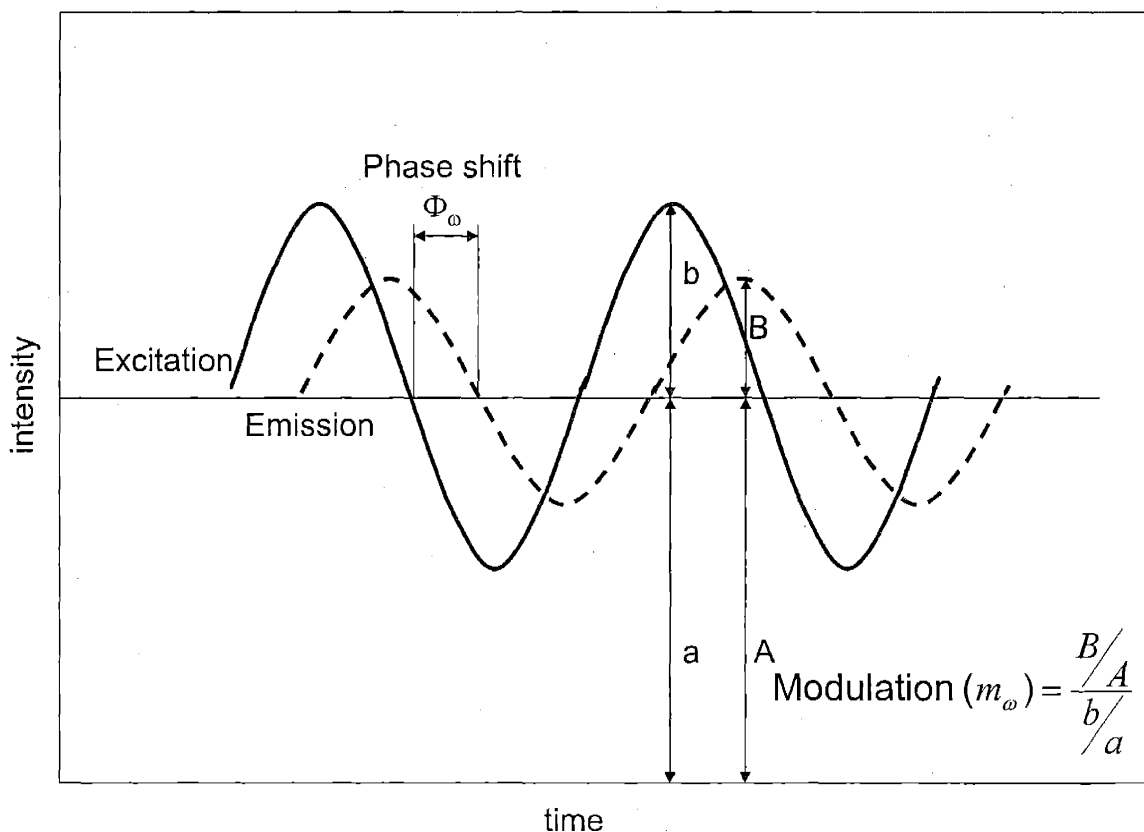


Figure 1. Frequency-domain lifetime measurements. Drawing adapted from Lakowicz.²

Lifetimes were measured in the frequency domain (Fig. 1).² In this technique, the excitation light is modulated at a high frequency compared to the lifetime of the sample. The emission is consequentially modulated but delayed due to the time lag between absorption and emission. This results in a phase shift (Φ_ω) and modulation change (m_ω) relative to the excitation beam. Demodulation and phase shift are measured at a range of frequencies and provide two independent variables for lifetime calculations. As frequency (ω) increases, the finite lifetime of the emission produces greater shift of phase and demodulation. For single exponential decay, the decay time (τ) can be described by:

$$\tan \Phi_{\omega} = \omega\tau$$

$$m_{\omega} = (1 + \omega^2\tau^2)^{-1/2}$$

where ω is the circular frequency ($2\pi \times$ Hz) of the excitation. Emission experiments were performed using a SPEX Fluorolog- τ 2 fluorometer (model FL112, 450W xenon lamp) equipped with a model 1935B polarization kit. Time decay of fluorescence was determined by using modulation frequencies between 10 and 200 MHz.

The molecular weights of polymers were determined and selected using a Hewlett Packard series 1100 HPLC instrument equipped with a Pl Gel 5 μ m Mixed-C (300 x 7.5 mm) column and a diode array detector at 245 nm at a flow rate of 1.0 mL/min in THF. The molecular weights were calibrated relative to polystyrene standards purchased from Polysciences, Inc.

2.2 Monomer spectroscopy

The syntheses described in Chapter 2 were designed to successfully impart the lifetime elongation expected in triphenylene monomer **7** onto a series of CPs. If this approach is valid, spectroscopic characteristics of **7** can therefore be used to predict photophysical behavior of triphenylene-based poly(*p*-phenyleneethynylene)s (TPPEs). To assess this, excited state lifetimes of the triphenylene monomer **7** and a PPE monomer **24** were measured in methylene chloride solution along with their absorption and emission spectra (Fig 2). Both emission and absorption are significantly redshifted in **7** due to added electron density from the extended aromatic core. This red-shift proved transferable to resulting polymers and was essential to the development of cascade energy

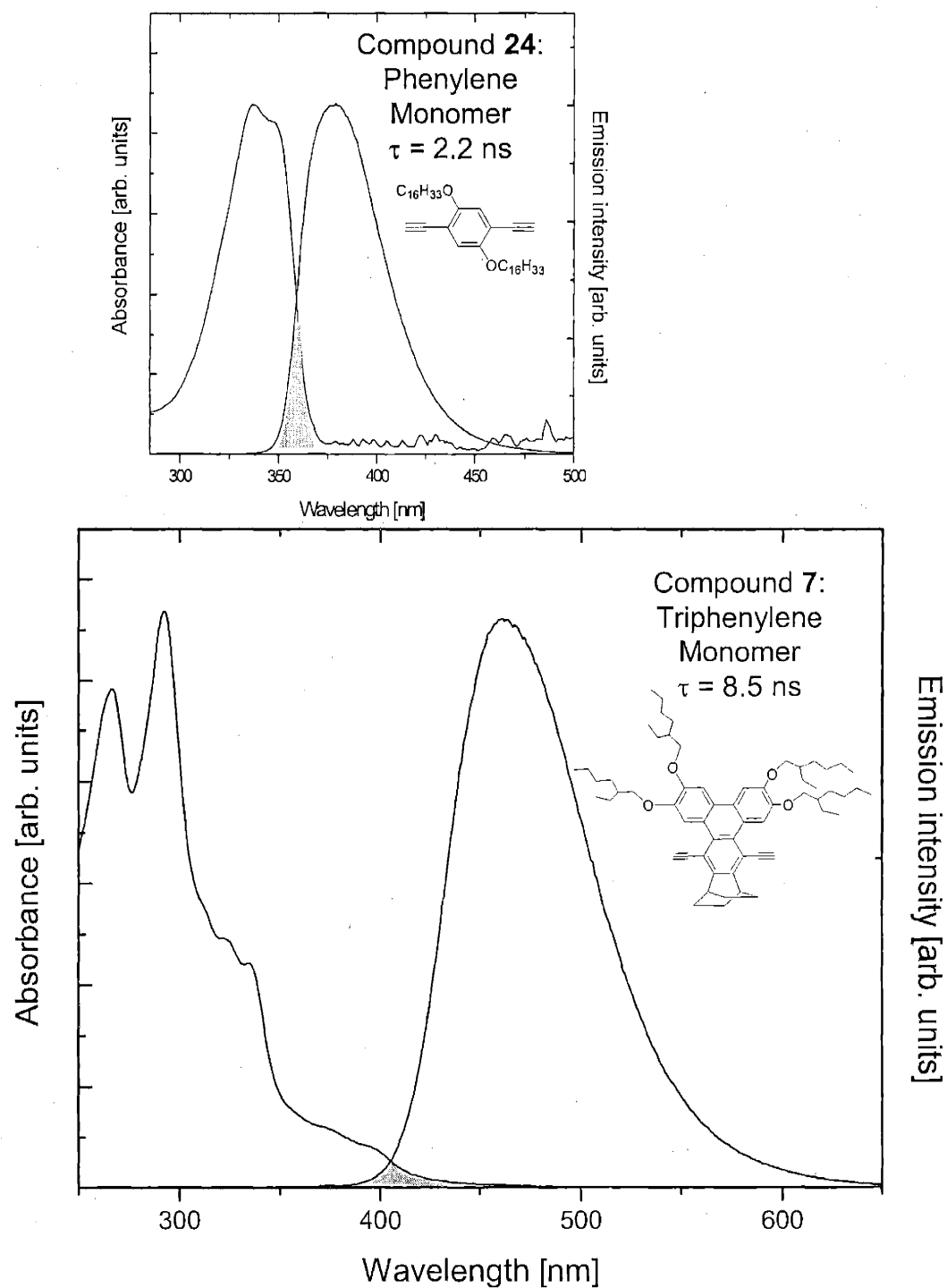


Figure 2. Phenylene and triphenylene monomer spectra with lifetime values and chemical structures. The small overlap between absorption and emission (colored in gray) in the triphenylene monomer spectra indicates a weakly allowed ground state transition.

transfer films.³ The oscillator strength at the band edge of **7** is significantly diminished relative to **24**. This indicates the ground state transition in **7** is still weakly-allowed despite minor synthetic desymmetrization. Consequentially, **7**'s lifetime is about 4 times longer than that of **24** (8.5 ns vs. 2.2 ns, respectively). With this information in hand, we sought to compare the photophysics from polymers of **7** and **24**.

2.3. Polymer spectroscopy

Polymers and model polymers described in the previous chapter (Chart 1 and Chart 2 respectively in Chapter 2) were initially studied as synthesized.¹ Absorption and emission spectra of polymers in methylene chloride solutions are documented at the end of this chapter, and photophysical properties are tabulated below (Table 1). Model polymers were studied similarly (Appendix 2 and Table 2). Comparison between model polymers (PPEs) and TPPEs indicates we universally enforced the targeted lifetime trends (Fig. 3). Every TPPE we synthesized demonstrates a longer excited state lifetime, though the magnitude of this difference varies. Interestingly, among PPEs, there is only about a 10% deviation of any observed lifetime from the average value. In comparison, the variation among TPPEs is large. This indicates that lifetime modulation exhibited in TPPEs is exceptional. The combination of τ and Φ data demonstrate enhanced lifetimes are principally due radiative rate suppression in TPPEs, not an increase of non-radiative rates.

Some persistent trends surface from comparisons among this class of polymers. In polymers where the excitation is more localized, the lifetime enhancing effect of the

¹ Simple purification protocols involved repeated precipitations with non-solvent to isolate highest molecular weight fractions.

Table 1 Photophysical properties of TPPEs.

	$\lambda_{\text{max abs.}}$ [nm]	$\lambda_{\text{max em.}}$ [nm]	Stokes shift [nm]	τ_{obs} [ns]	Φ	$\tau_{\text{rad}}/[10^8 \text{ s}]$	$\tau_{\text{non-rad}}/[10^8 \text{ s}]$
8	435	558	123	4.0	0.08	0.2	2.3
9	464	519	55	0.72	0.40	5.5	8.3
10	435	487	52	1.49	0.42	2.8	3.9
11	495	510	15	0.70	0.30	4.3	10
12	410	482	72	2.2	0.31	1.4	3.1
13	477	504	27	1.6	0.39	2.4	3.8
14	483	493	10	7.0/1.3*	0.08		
15	434	486	52	2.65	0.27	1.0	2.8
16	470	504	34	0.80	0.30	3.8	8.8
17	490	530	40	1.52	0.22	1.5	5.1
18	464	504	40	0.91	0.28	3.1	7.9
19	497	543	46	2.04	0.23	1.1	3.8
20	462	520	58	2.00	0.20	1.0	4.0
21	462	520	58	0.85	0.15	1.8	10
22	385	509	124	3.3	0.19	0.58	2.5
23	465	504	39	0.77	0.33	4.3	8.7

*could only be modeled with biexponential decay. Weighed fractions are 60:40 respectively.

Table 2. Photophysical properties of PPEs.

	$\lambda_{\text{max abs.}}$ [nm]	$\lambda_{\text{max em.}}$ [nm]	Stokes shift [nm]	τ_{obs} [ns]	Φ	$\tau_{\text{rad}}/[10^8 \text{ s}]$	$\tau_{\text{non-rad}}/[10^8 \text{ s}]$
8a	387	440	53	0.60	0.13	2.2	17.8
9a	449	540	91	0.50	0.40	8.0	12.0
11a	425	455	30	0.62	0.40	6.5	9.7
12a	395	435	40	0.60	0.90	1.4	3.1
13a	440	472	32	0.60	0.55	8.3	8.3
16a	440	475	35	0.52	0.45	8.6	10.6
17a	460	478	18	0.42	0.49	11.6	12.2
20a	442	455	13	0.48			

triphenylene component is more pronounced. For example, **12** consists of a triphenylene monomer and a biphenyl monomer. Because biphenyl planarizes in the excited state, a large Stoke shift is observed in the resulting polymer. The time necessary for this can also serve to localize the excitation, as radiative decay rates become more competitive with

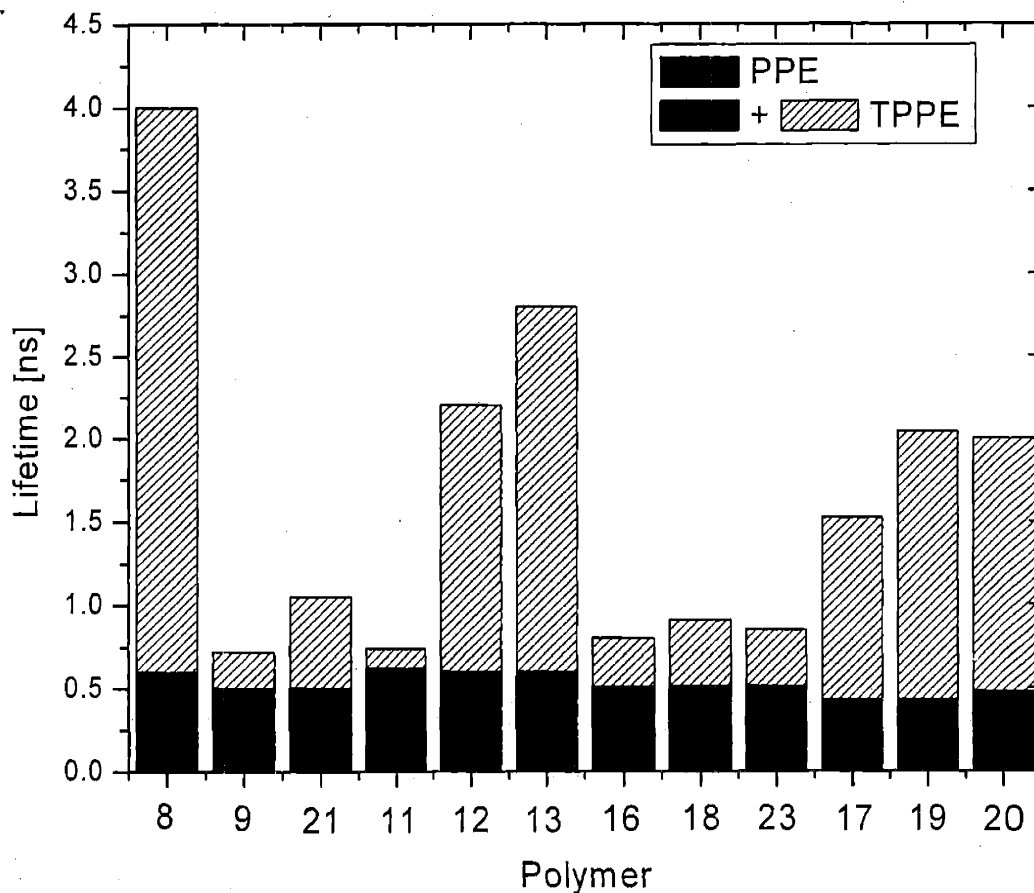


Figure 3. Lifetime comparison of PPEs and TPPEs. PPE lifetimes are shown as a subset of TPPE lifetimes. Black boxes are PPE lifetimes and striped + black boxes are TPPE lifetimes. TPPE excitations in all cases are longer-lived.

energy transfer. Consequentially, Polymer **12**'s lifetime is about three times longer than its PPE analogue. This effect is mirrored in Polymers **14** (60% 7.0 ns: 40% 1.3 ns)ⁱⁱ and **22** (3.3 ns). The meta linkage in **14** and **22** disrupts conjugation, insulating the excitation. This results in some of the longest lifetimes in TPPEs.

Electrostatic variation in TPPEs can lead to excited state interactions. In Polymer **8**, an exciplex is likely formed between the triphenylene and its electron deficient tetrafluorinated comonomer. The very long excited state lifetime (4 ns) and broad, redshifted emission spectra are clear indications of this phenomenon. The absence of these characteristics in its PPE analogue suggests the flat, electron-rich nature of triphenylene is necessary induce exciplex formation. One can imagine exploiting this interaction to produce a 'turn-on' type sensor. If an electron deficient analyte interacts with our triphenylene materials to produce an exciplex, a new, redshifted emission would result. The electrostatic variation within the triphenylene materials could select for an analyte with given energetics.

To further support our assertion that the triphenylene chromophore is responsible for lifetime extension, we synthesized Polymers **17** and **19**. They are homopolymers, coupling only the diactylede units (see Chapter 1), hence directly linking triphenylene monomers. Polymers with a larger triphenylene component demonstrate more pronounced lifetime enhancement. Resulting lifetimes in these materials are several multiples above that of their PPE analogue. Differences were even manifested by the bicyclooctane moiety on the triphenylene monomer, a relatively small perturbation to the triphenylene core. Polymers **16**, **18**, and **23** share identical comonomers and differ only

ⁱⁱ Polymer **14**'s lifetime could only be modeled by a biexponential decay. This probably results from its short chain length. This is the only polymer synthesized that could not be satisfactorily modeled by a single component lifetime.

by substitutions on the triphenylene ring. Conformational changes that might be imparted by side chain group variation do not seem have a significant effect on lifetime as indicated by polymers with different alkoxy substituents. However, the bicyclooctane substitution diminishes lifetime enhancement. This effect is reproduced throughout the series of polymers. Polymers **10** (1.49 ns) and **15** (2.65 ns) demonstrate a wide variation in an otherwise similar materials. Polymers **17** (1.52 ns) and **19** (2.04 ns) as well as **9** (0.72 ns) and **21** (0.85 ns) confirm this trend.

2.4. Chain length selection and spectroscopy

Solubility differences among monomers yielded polymers with a wide range of molecular weights (Ch. 2). Because we aimed to study the range of energy migration, an accurate comparison demanded materials of similar chain length. We used size-exclusion gel permeation chromatography (GPC) and selected fractions of TPPEs and PPEs with similar degree of polymerization. For small chain lengths, photophysical properties in CPs change exponentially as repeat units are added, leveling off usually after 10-15 units. In most cases, we choose to select the longest chains attainable to ensure we surpassed the small chain length regime. Therefore, the size-exclusion GPC did not need to precise to one repeat unit to yield comparable samples. In addition, variation in GPC size selection due to differences in polymer conformation would have less effect. A range of chain lengths was studied to verify the static molecular weight regime was reached.

Lifetime values in size selected molecular weight materials were similar to polydispersed samples, varying by less than 10%. However, definite trends were demonstrated among different molecular weights of the same CP. As expected, higher

molecular weights exhibited slightly shorter lifetimes at a given wavelength of emission. Extended communication afforded by longer chain lengths increase the chance of an excitation encountering a trap site, thereby increasing non-radiative rate of decay and the observed lifetime. This decrease truncates at high molecular weights as the distance the exciton can travel is now limited by its radiative decay rate, and additional repeat units will not be sampled. The magnitude of these variations were small enough not to effect conclusions made on polydispersed samples.

2.5. Polarization spectroscopy

Our synthetic strategies universally invoked the lifetime trends we targeted. These pursuits however were entirely in the interest of extending energy migration in CPs. Therefore, it was necessary to correlate the suppression of radiative rates with energy migration enhancement. One might envision that although an excitation is longer lived, if the transfer step between chromophores is slower, then the overall distance it covers will not be extended. In fact, this behavior is predicted by the Förster equation,⁴ as it poises the through-space energy transfer rate inversely proportional to the lifetime of the donor, i.e. the allowedness of the transition. However, the Dexter⁵ formulation makes no such limitation, as it describes energy transfer resulting from direct wavefunction overlap. Therefore, transition allowedness does not affect overall rates. Typically, one draws on Förster's approach because the energy transfer it describes extends over much larger distances ($\sim 50 \text{ \AA}$) so it accurately portrays chromophores that are not covalently bound, for example energy transfer in photosynthetic systems and between small molecules. In the instance of isolated CPs in solution, chromophores are conjugated, maximizing

wavefunction overlap. Dexter transfer may therefore be the dominant mechanism in these systems. The implications of this determination include improved materials design and further amplification of sensory response as detailed in the introduction.

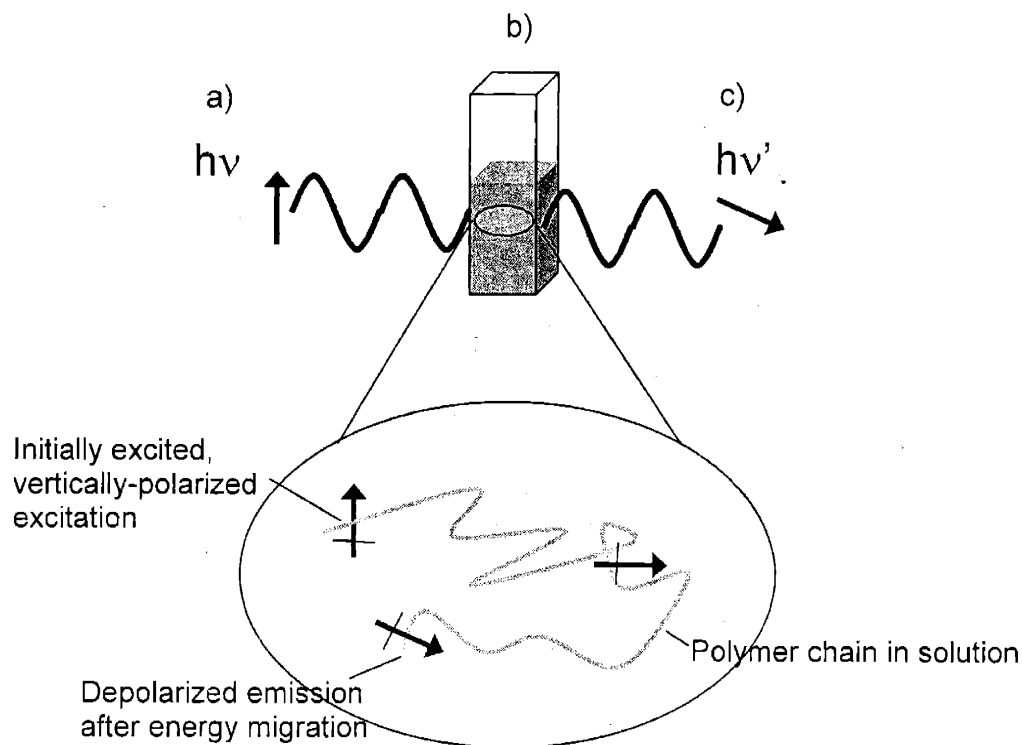


Figure 4. A simplified pictorial of depolarization due to energy migration in conjugated polymers (CPs). (a) Excitation beam is vertically polarized therefore only vertical transition dipoles are initially excited on the CP chain. (b) Vertically polarized excitations on the polymer chain migrate. As they move over a disordered polymer chain, they lose their initial polarization. (c) Emission of polymer is depolarized relative to the excitation beam. This amount of measured depolarization indicates the extent of energy migration in the conjugated polymer.

One may distinguish between energy transfer mechanisms via fluorescence depolarization measurements. All polymers studied are high molecular weight materials and can be considered rotationally static over the emission lifetime of the polymer. Therefore, energy migration is the major contributor to the fluorescence depolarization in

conjugated polymers; the exciton loses more of its initial polarization as it diffuses along a disordered polymer chain (Fig. 4). The polarization value, P , has been determined from standard equation $P = (I_{vv} - GI_{hv}) / (I_{vv} + GI_{hv})$, where I_{vv} and I_{hv} are the intensities of emissions detected parallel and perpendicular to the polarization vector of the incident light and G is an instrumental correction factor. Because our polymers exhibit reduced transition dipoles, Förster-type migration should be suppressed. A Dexter mechanism however, would dictate an increase in depolarization over that observed in PPEs because a longer lifetime allows excitations to migrate further.

Concurring with lifetime data, depolarization is universally more pronounced in TPPEs. This is showcased in Figure 5 which compares TPPE depolarization to that of corresponding PPE when excited at their respective absorption maxima. It is difficult to qualitatively link lifetime to polarization throughout the entire class of polymers as differences between dipole orientation and solution conformation can affect measured results. To normalize for these variations, we synthesized model polymers, identical except for the triphenylene chromophores. However, a cursory comparison of TPPEs polarization behavior underscores some important points. In the case of Polymers **8** and **8a**, the kinked thiophene linkage results in much greater depolarization than in other polymers studied. A greater scrambling per migration step results. Polymer **12**, with its localizing biphenyl monomer, retains almost the highest polarization value. This is consistent with slightly reduced energy migration as the biphenyl takes time to planarize in the excited state. The highest polarization value among TPPEs is observed in Polymer **8**. The energy minimum formed by its exciplex should quickly trap the wandering excitation, reducing energy migration. Collectively, these observations correlate expected

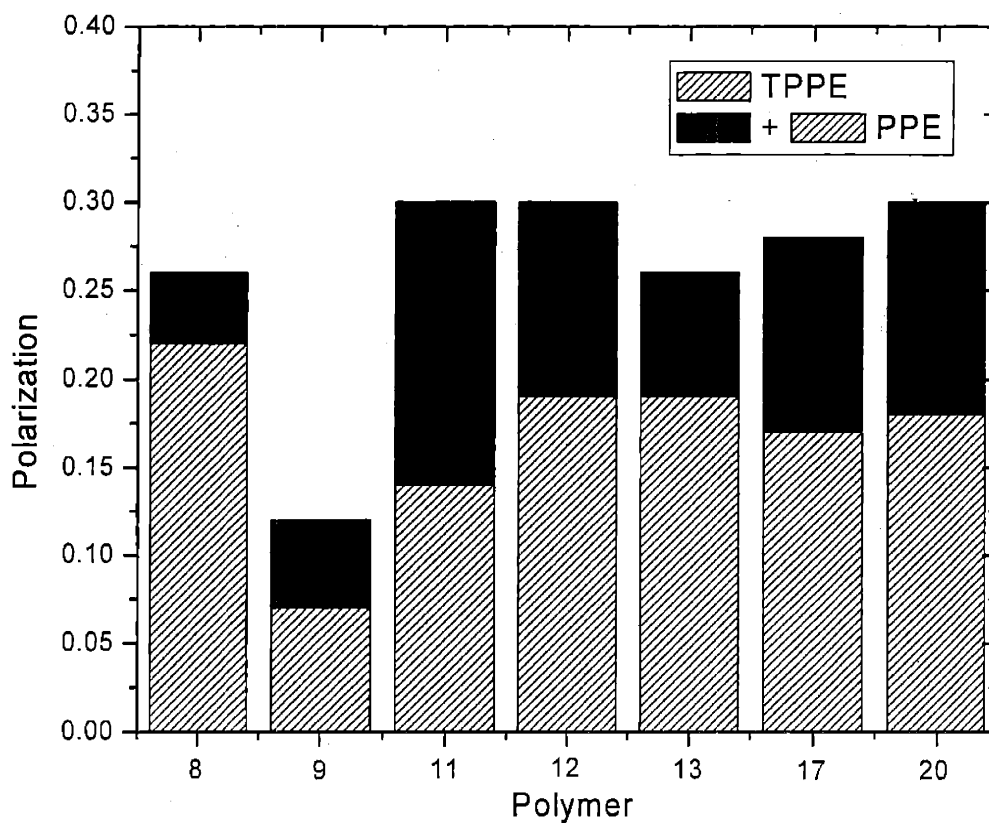


Figure 5. Polarization comparison of PPEs and TPPEs. Black + striped bars are polarization values for PPEs excited at λ_{\max} . Stripped boxes are polarizations for TPPEs excited at λ_{\max} . In every instance, TPPEs exhibit greater depolarization, indicating more extensive energy migration.

trends in energy migration with observed polarization data, validating our assessment approach.

The full range of allowable excitation energies for a subset of polymers was investigated to separate depolarization due to energy migration from that due to absorption/emission dipole alignment. Measurements were performed on materials selected for similar chain length, all above the small molecular weight regime. As excitation energy is increased, both the TPPEs and PPEs display lower P values, consistent with population of higher energy excitons that readily lower their energy by migration to lower energy states. The decrease in emission polarization at higher energies may also be the result of exciting triphenylene localized transitions that have an angular displacement from the emission dipole. In this case, polarization would be expected to decrease more dramatically at certain intervals of wavelengths, not continuously over the range investigated. In TPPEs, a near linear decrease of polarization as a function of excitation wavelength (Fig. 6-9) is observed supporting energy migration as the major contributor to depolarization. Over all wavelengths, the TPPEs consistently revealed lower P values. For TPPEs, the lowest attainable P values are a fraction of the P observed when exciting at λ_{max} . In PPEs however, this value is only about half, indicating the radiative rate of emission limits the extent of energy migration. This limitation is

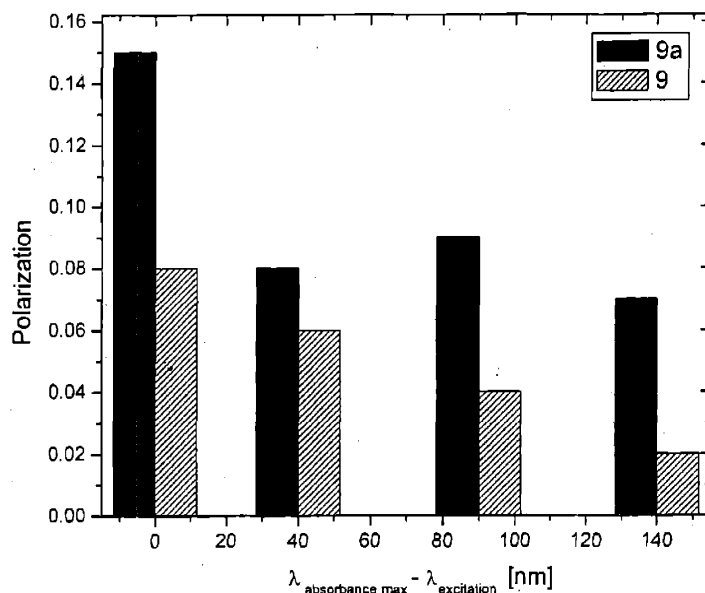


Figure 6. Polarization comparison as a function of excitation wavelength in **9a** (a PPE) and **9** (a TPPE). Polarization values truncate as excitation moves from λ_{max} in **9a**. In **9**, polarization continued to decrease with shorter wavelengths of excitation, indicating radiative rates are not competitive with energy migration as they are in **9a**.

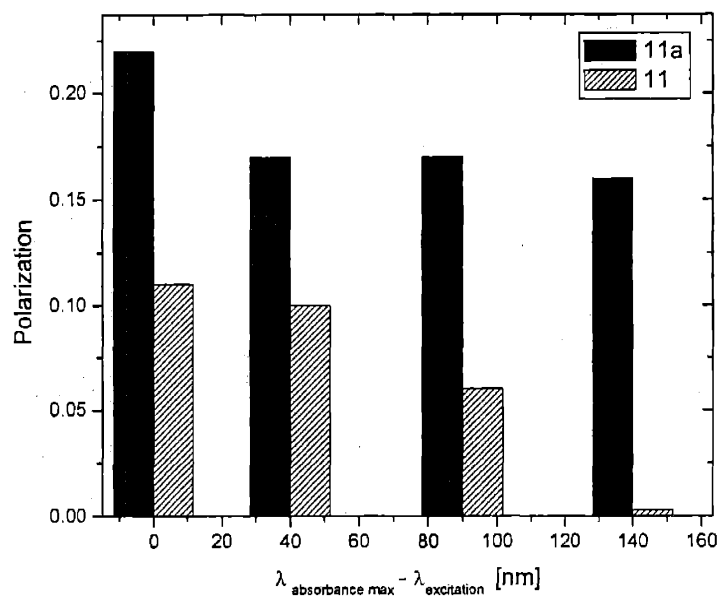


Figure 7. Polarization comparison as a function of excitation wavelength in **11a** (a PPE) and **11** (a TPPE). Polarization values truncate as excitation moves from λ_{max} in **11a**. In **11**, polarization continued to decrease with shorter wavelengths of excitation, indicating radiative rates are not competitive with energy migration as they are in **11a**.

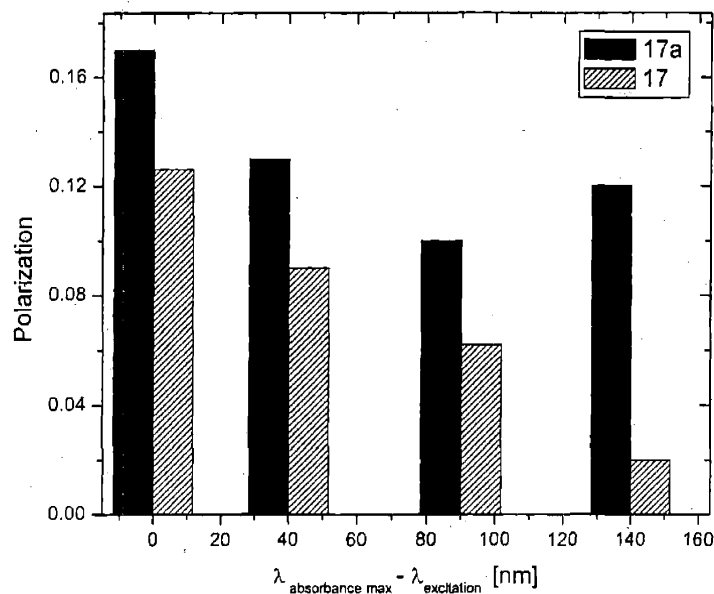


Figure 8. Polarization comparison as a function of excitation wavelength in **17a** (a PPE) and **17** (a TPPE). Polarization values truncate as excitation moves from λ_{max} in **17a**. In **17**, polarization continued to decrease with shorter wavelengths of excitation, indicating radiative rates are not competitive with energy migration as they are in **17a**.

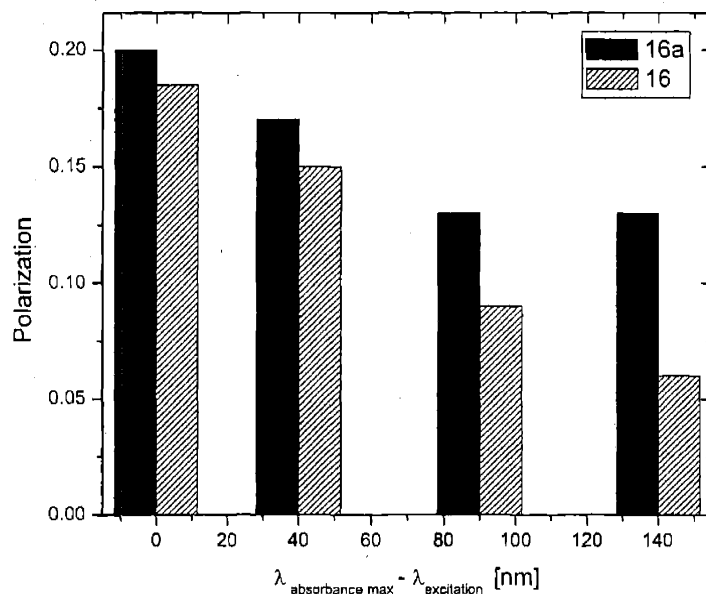


Figure 9. Polarization comparison as a function of excitation wavelength in **16a** (a PPE) and **16** (a TPPE). Polarization values truncate as excitation moves from λ_{max} in **16a**. In **16**, polarization continued to decrease with shorter wavelengths of excitation, indicating radiative rates are not competitive with energy migration as they are in **16a**.

overcome in the longer-lived TPPE systems as near 0 P values are obtainable in most of the materials. Studies of polarization as a function of chain length support these conclusions. If the Förster mechanism dominated, then enhanced radiative rates in PPEs would encourage more extensive migration. This is not observed, pointing to the Dexter mechanism as the dominant intramolecular energy transport process in these materials.

2.6. Chain length selection and spectroscopy

Polarization and lifetime studies as a function of chain length on selected polymers support energy migration as the major contributor to depolarization. We detail these results in Figure 10 for Polymers **11** and **11a**. For shorter chain lengths, depolarization increases and lifetime decreases as expected. Once the static molecular weight regime has been reached, both parameters should remain relatively constant as additional repeat units are added. This is attained in PPEs of about 100 repeat units or greater. At the highest molecular weights synthetically obtainable (< 230 repeat units) in TPPEs, polarization continued to decrease. This is consistent with more extensive energy migration in TPPEs. If dipole displacement was the main contributor to depolarization, then depolarization would be relatively insensitive to chain length. In particular, it should stabilize among shorter chain lengths of TPPEs than PPEs. Observation of the reciprocal trend indicates enhanced energy migration in TPPEs.

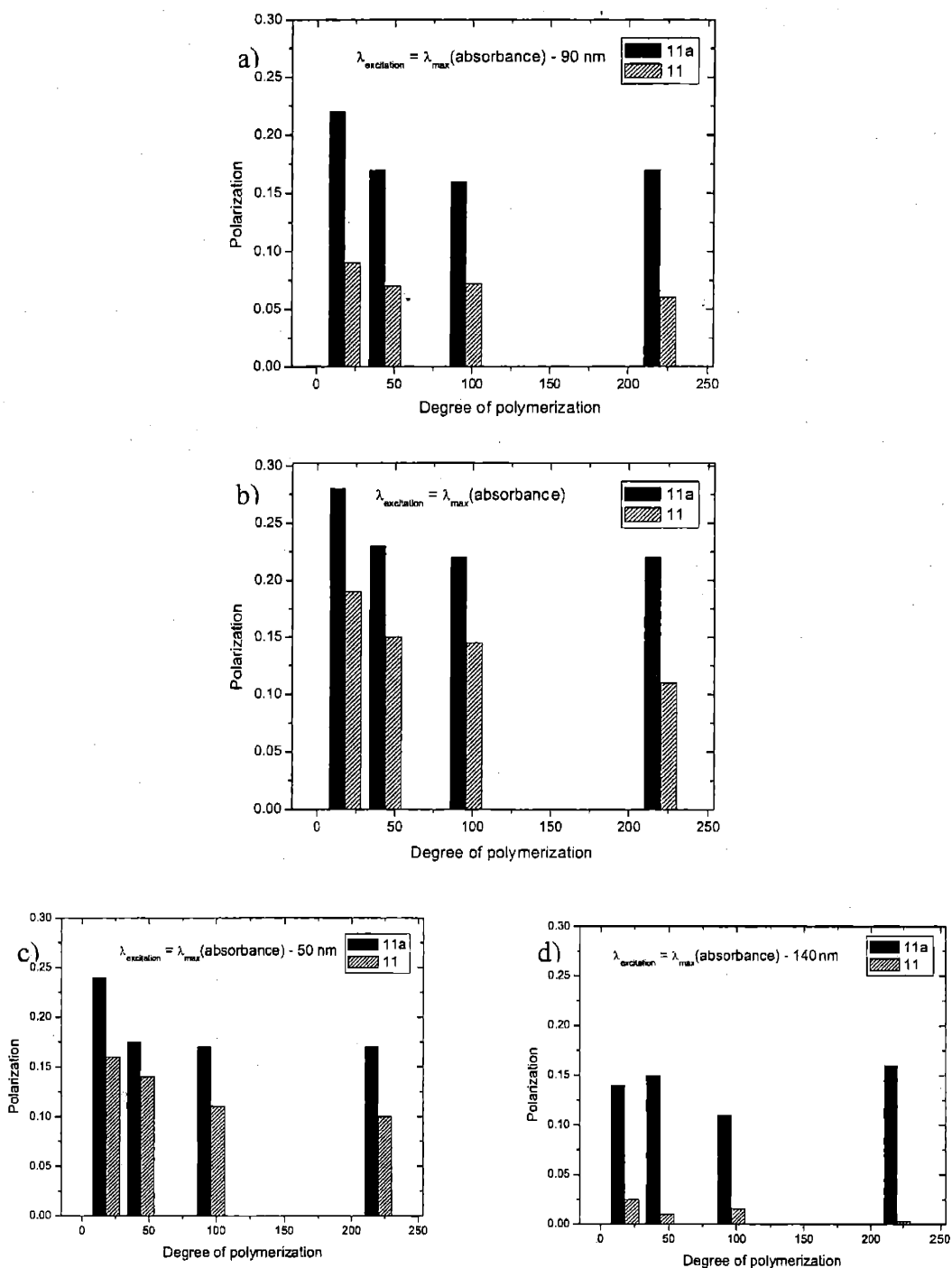


Figure 10. Polarization as a function of chain length at different excitation wavelengths for 11 (striped boxes) and 11a (black boxes). Polarization values stop decreasing at shorter chain lengths in the PPE. In the TPPE, polarization continued to decrease with longer chain lengths, indicating energy can migrate longer distances in these systems as additional repeat units are sampled by the excitation.

3. Conclusions

It is possible to engineer the lifetimes of CPs. By incorporating chromophores with a long-lived excited state into a PPE backbone, we universally lengthened the resulting polymers lifetimes compared to polymers without these chromophores. For isolated polymer chains in solution, this increase allowed more extensive energy migration before radiative decay as determined through polarization measurements. This general paradigm has applied in the design of other long-lived chromophores in our laboratory, as detailed in the next chapter. Its influence on sensory response was qualitatively assessed, and these design principles appear to augment sensory response to TNT.

4. References

¹ (a) Lemmer, U.; Mahrt, R.F.; Wada, Y.; Greiner, A.; Bassler, H.; Gobel, E. O. *Chem. Phys. Let.* **1993**, *209*, 243.

(b) Rauscher, U.; Bassler, H.; Bradley, D. D. C.; Hennecke, M. *Phys. Rev. B* **1990**, *42*, 9830.

(c) Kennedy, S. P.; Garro, N.; Phillips, R. T. *Phys Rev B* **2001**, *64*, 115206.

(d) Hayes, G. R.; Samuel, I. D. W.; Phillips, R. T.; *Phys. Rev. B* **1997**, *56*, 3838.

² *Principles of fluorescence spectroscopy* Joseph R. Lakowicz. Edition : 2nd ed. New York : Kluwer Academic/Plenum, **1999**.

³ Kim, J.; Rose, A.; Zhu, Z.; Swager, T. M. *J. Amer. Chem. Soc* **2001**, *123*, 11489.

⁴ (a) Förster, Th *Discuss. Faraday Soc.* **1953**, *27*, 7.

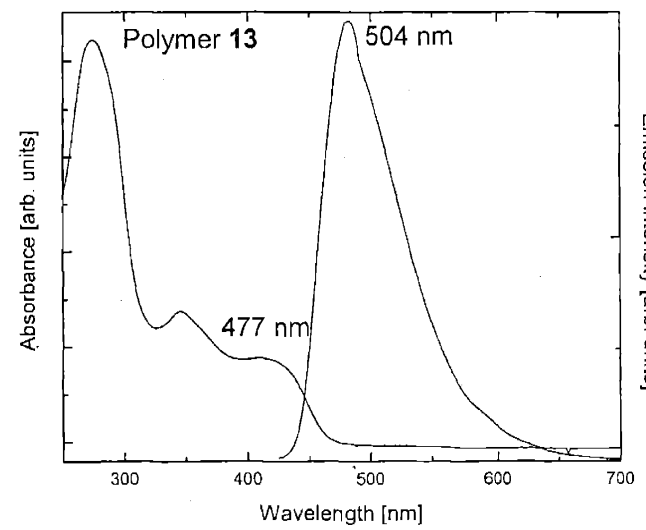
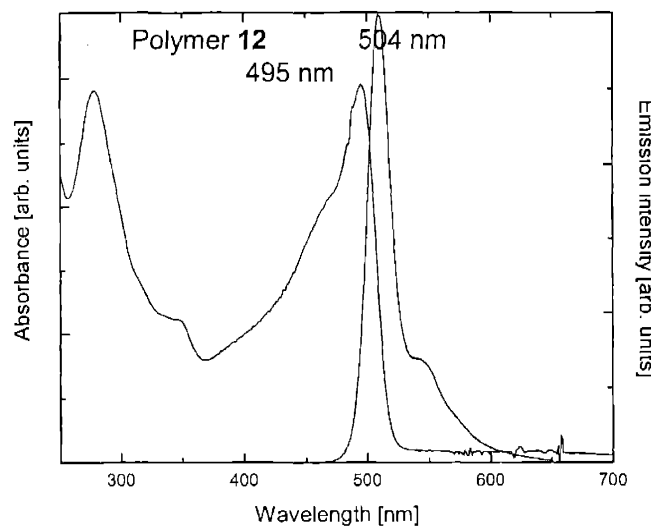
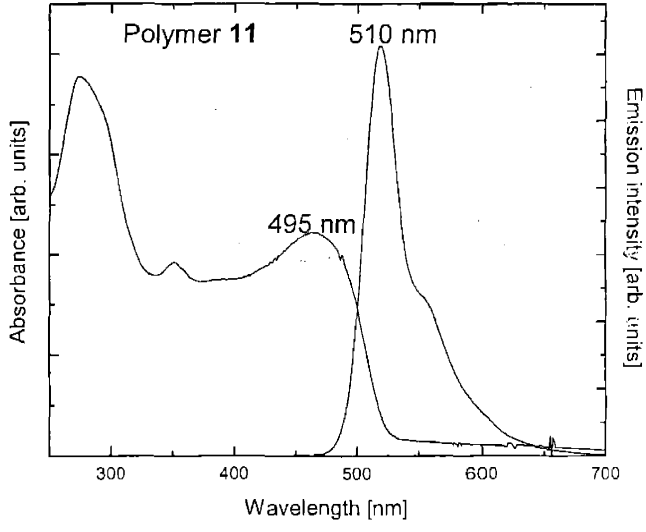
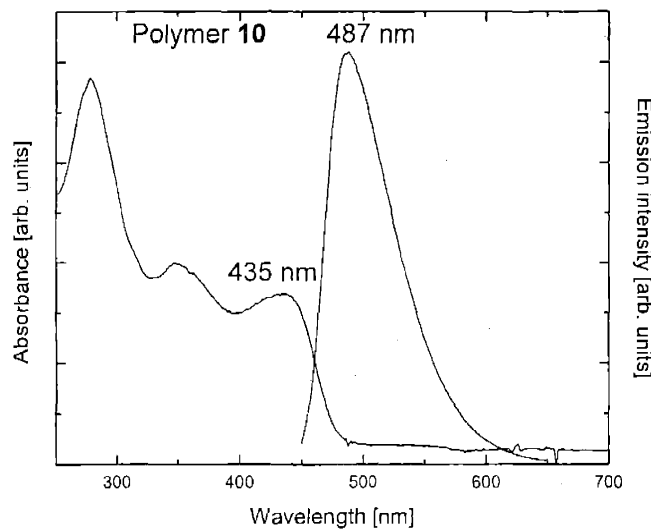
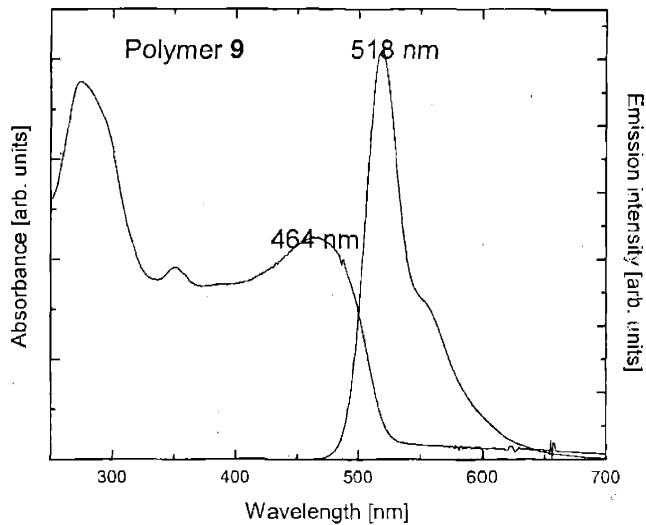
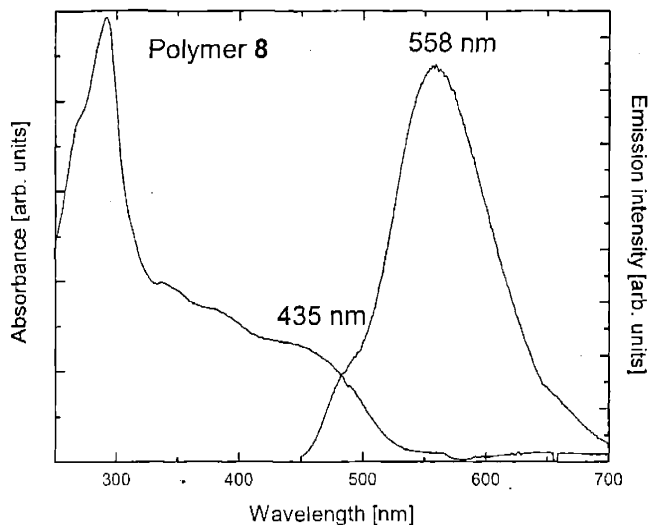
(b) Förster, Th. in: O. Sinanoglu (Ed.), *Modern Quantum Chemistry, Part III*, Academic Press, New York, 1965.

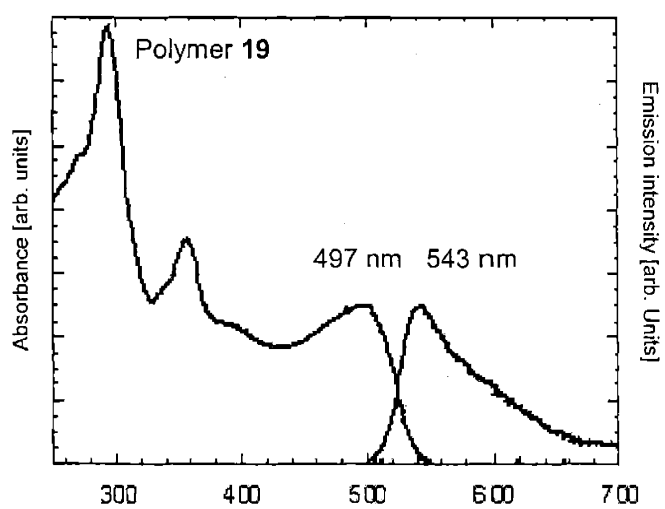
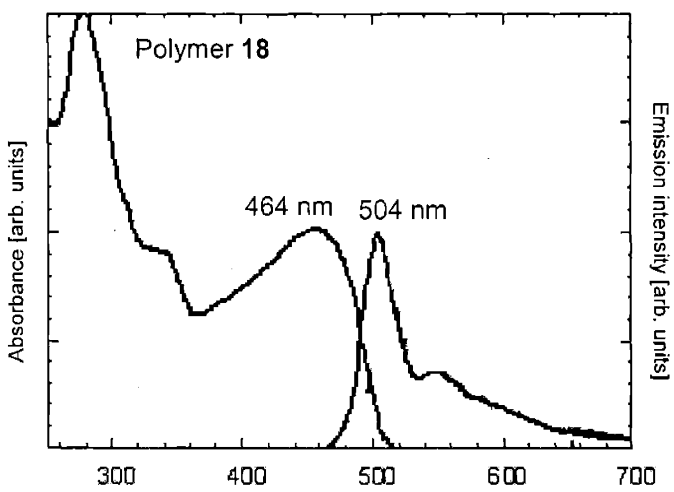
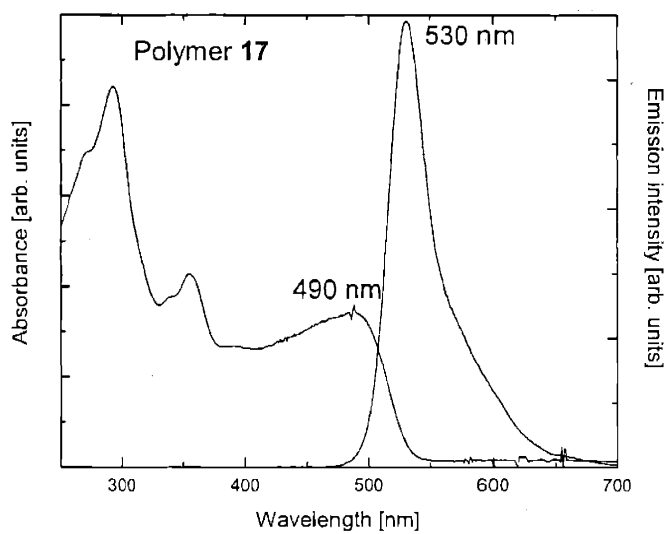
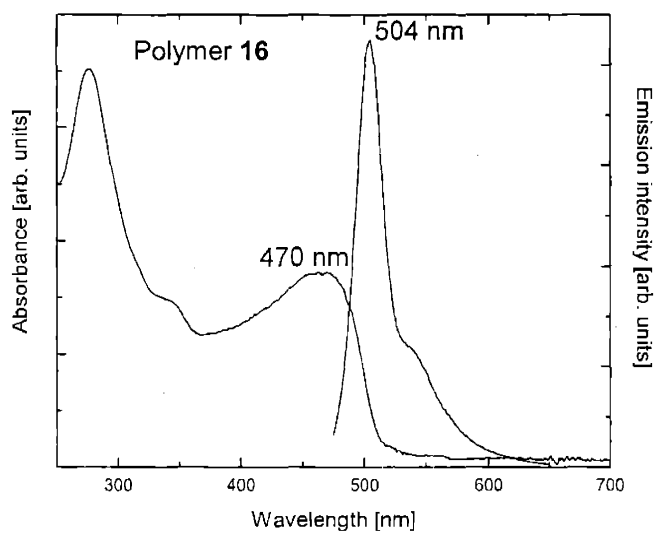
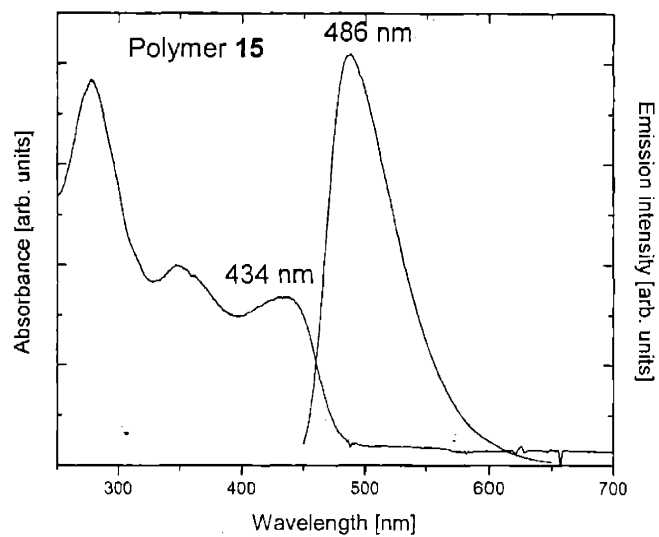
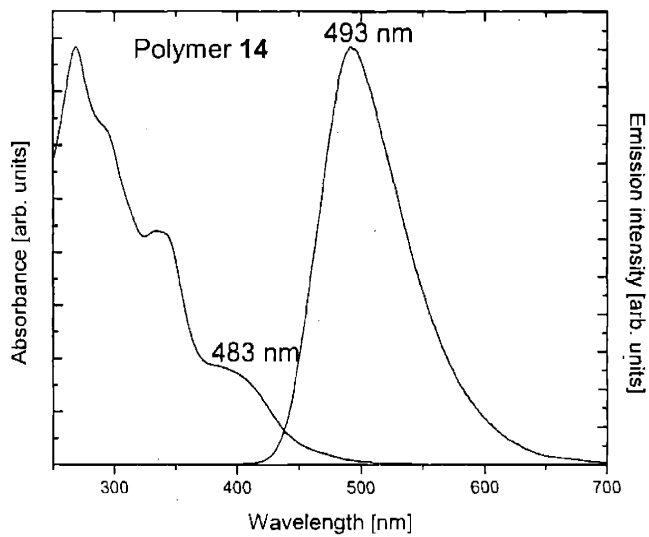
⁵ Dexter, D. L. *J. Chem. Phys.* 1953, 21, 836.

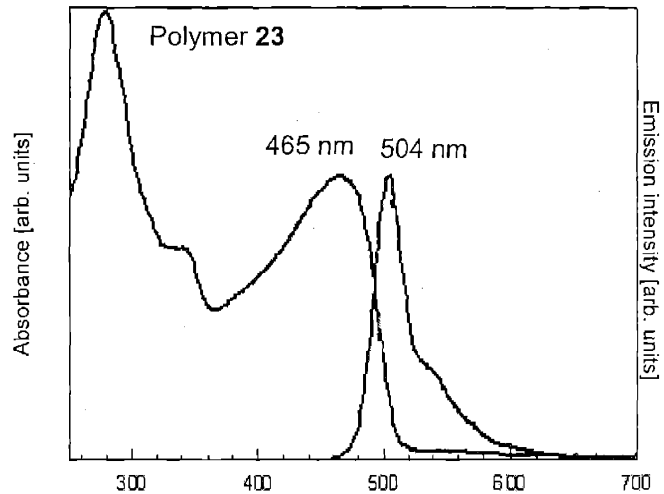
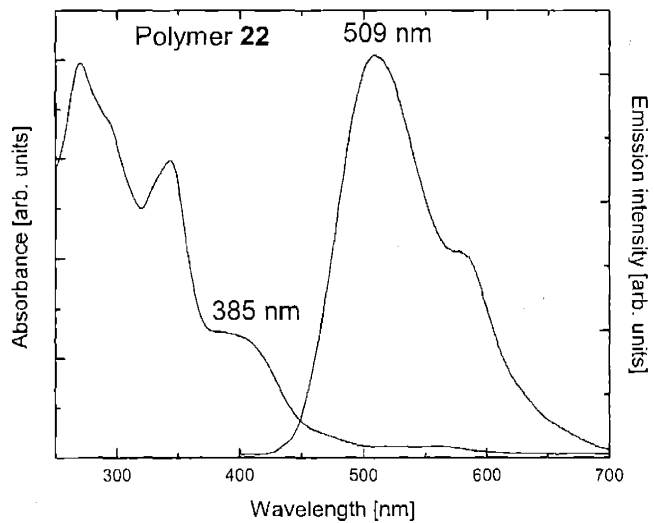
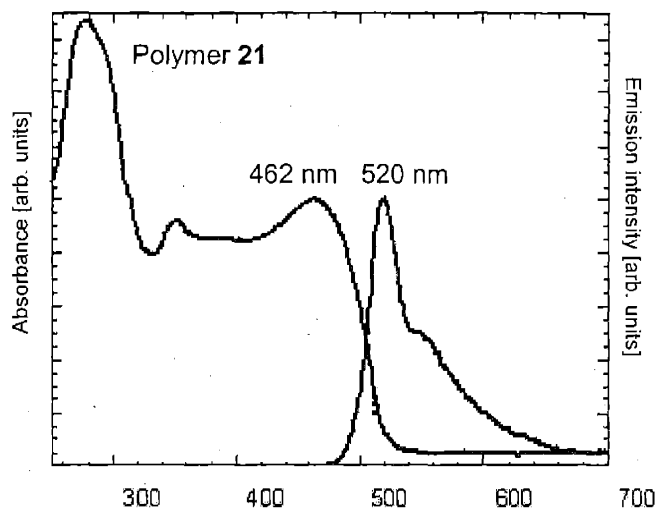
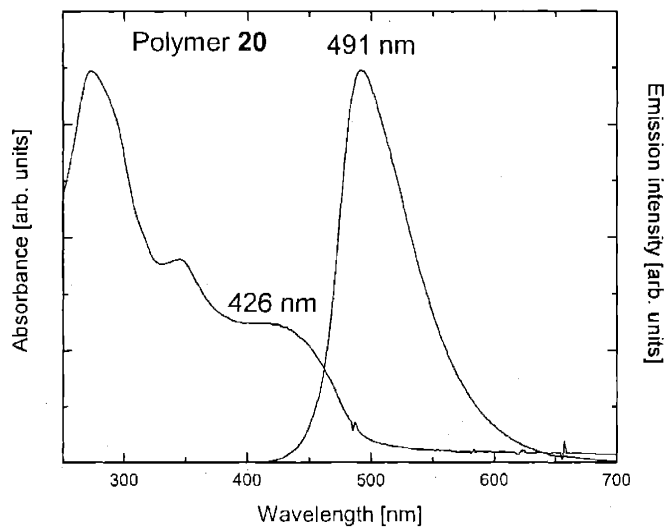
Chapter 3

Appendix 1

TPPE spectra.



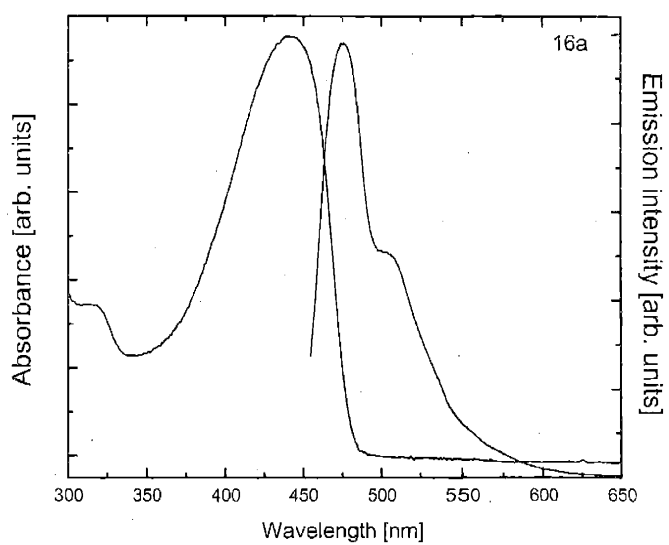
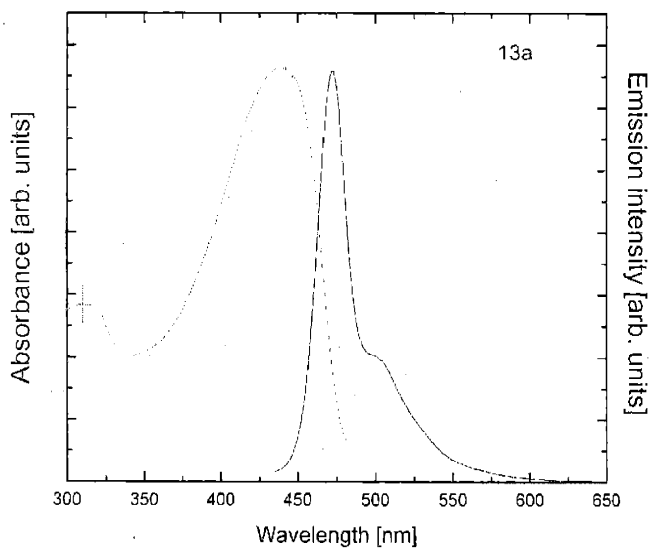
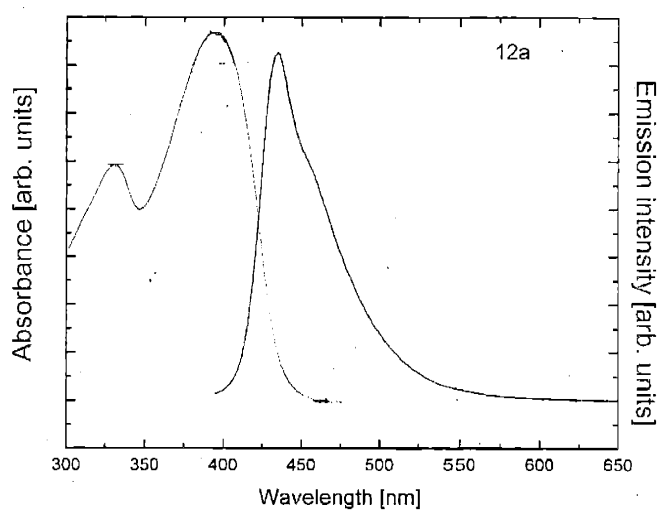
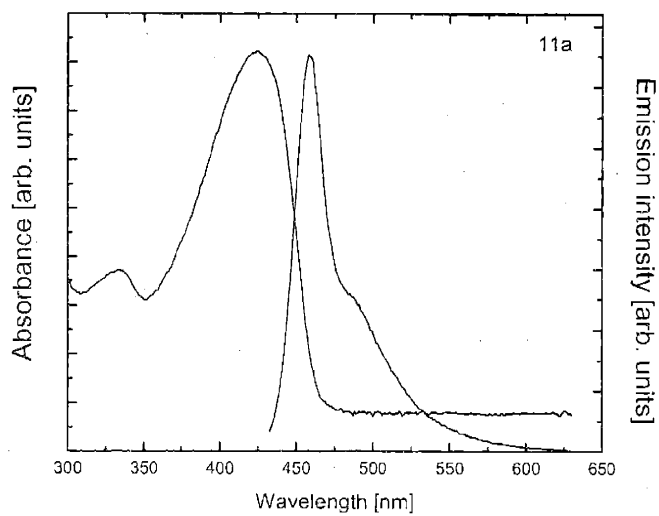
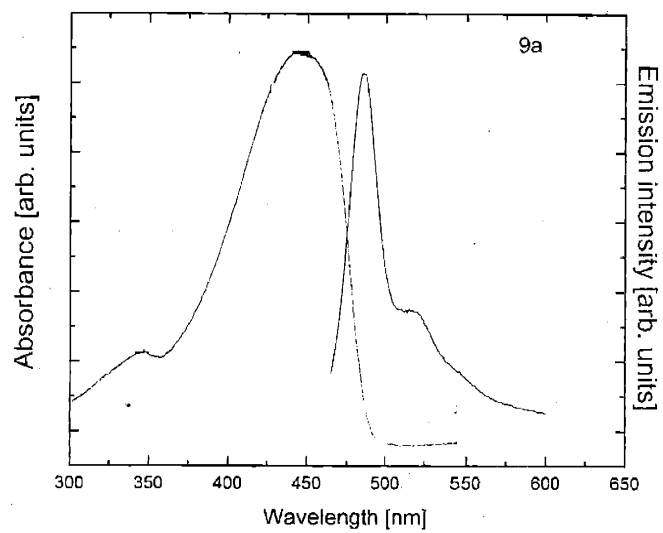
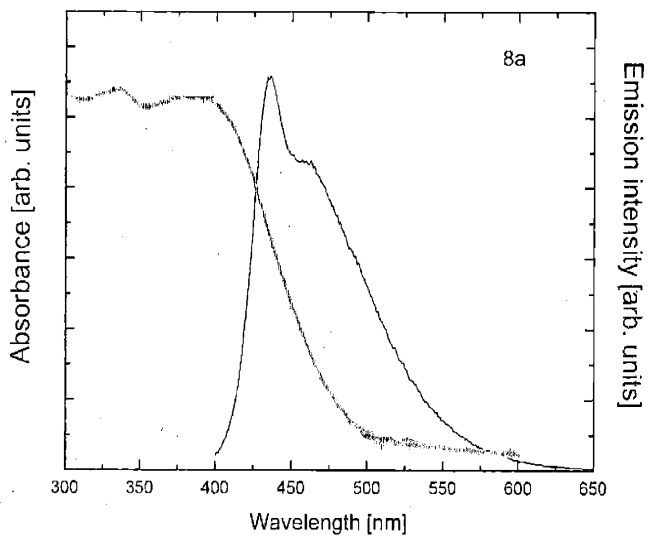


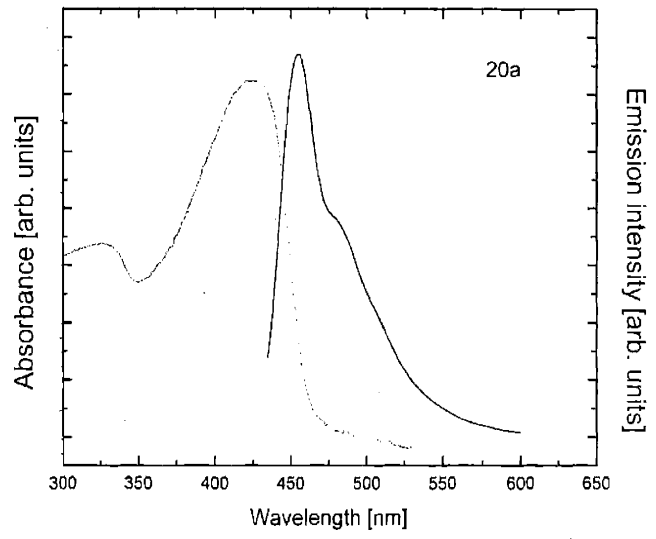
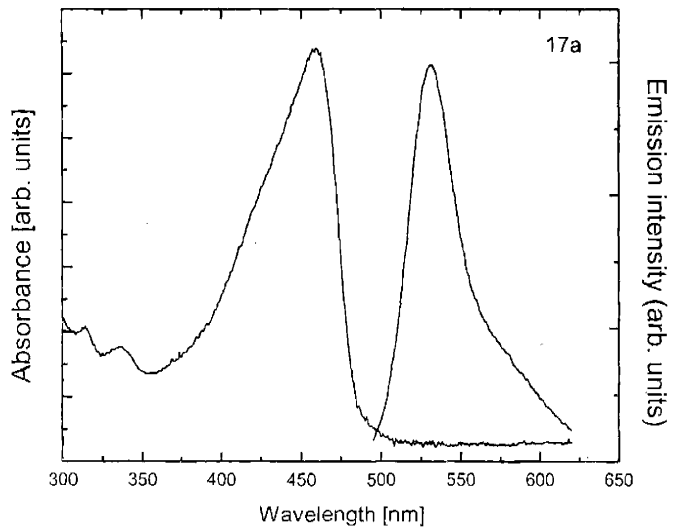


Chapter 3

Appendix 2

PPE spectra.





Chapter 4

Lifetime engineering in conjugated polymers ~ chromophore design for the extension of energy migration.

Portions of this chapter have appeared in print:

Tovar, J. D.; Rose A.; Swager, T. M. *J. Am. Chem. Soc.* **2002**, *124*, 7762-7769.

1. Introduction

The previous chapter detailed how desired photophysical properties can be incorporated into a conjugated polymer (CP). This study underscored the utility of the chromophore in the design of CPs. Specifically, excited state lifetime and energy migration in poly (*p*-phenyleneethylenes) (PPEs) were increased by conjugating triphenylene chromophores, known to have symmetrically forbidden ground state transitions, into the polymer backbone. In the interest of designing better sensory materials, we sought to demonstrate the widespread applicability of this approach. Many other extended aromatic chromophores also have symmetrically forbidden or weakly allowed transitions. Therefore, we pursued incorporation of other long-lived chromophores into the PPE backbone and studied their photophysics similarly.

Further insight into the control of energy migration in CPs was provided through unique conjugated polymers synthesized in our laboratory. Dibenzo[*g,p*]chrysene (Chart 1) polymers have extended aromatic cores. They therefore allowed us to assess the effects of rigidifying and symmetrizing the backbone of the polymer. We then sought to look more rigorously at the varying effective conjugation pathways and their implications before and after chromophore cyclization. Matched pairs of uncyclized and cyclized polymers allowed us to assess the impact of rigidification and aromatization. Collectively, these triphenylene, chrysene and thiophene-based systems afforded us a more complete understanding of the interplay of rigidification, symmetrization, lifetime, and energy migration in conjugated polymers.

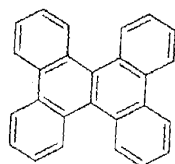
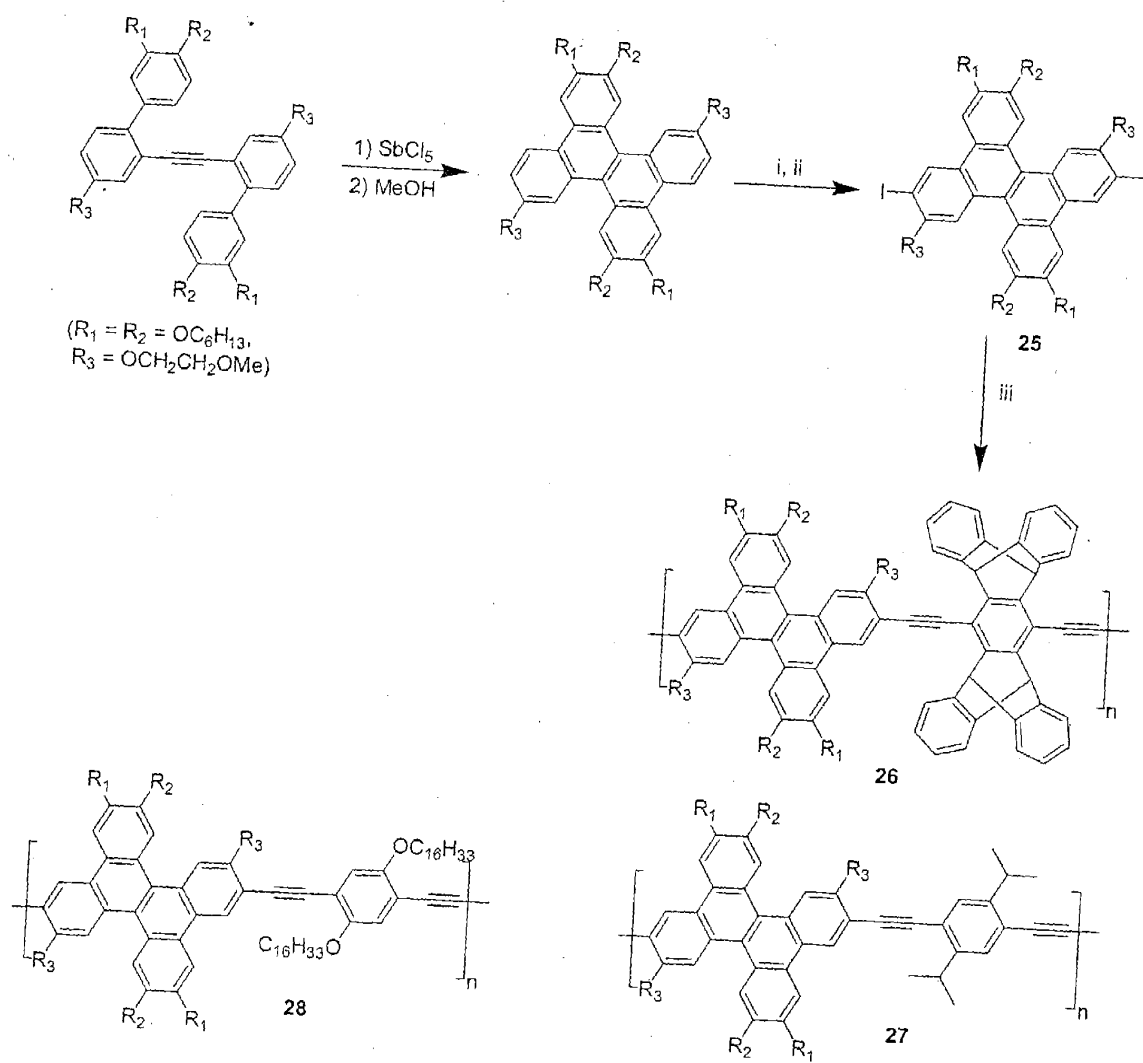


Chart 1. Dibenzo[*g,p*]chrysene.



Reagents and conditions: i) *t*-BuLi, Et_2O , rt; ii) $\text{ICH}_2\text{CH}_2\text{I}$, -78°C ; iii) appropriate diethynylarene, $\text{Pd}(\text{PPh}_3)_4/\text{CuI}$, toluene/*i*-Pr₂NH.

Scheme 1.

2. Results and Discussion

2.1 Dibenzo[*g,p*]chrysene polymers

Similar to triphenylene, dibenzo[*g,p*]chrysene has demonstrated interesting liquid crystalline properties.¹ In concert with our desire to augment energy migration in the solid state, the strong coupling between chromophores in liquid crystalline systems facilitates exciton and charge migration. In addition, dibenzo[*g,p*]chrysene's rigid structure and weakly-allowed transitions² was postulated to convey similar photophysical properties to those observed in triphenylene-based PPEs (TPPEs), i.e. longer excited state lifetimes and more extensive energy migration. These considerations prompted the integration of the dibenzo[*g,p*]chrysene into a PPE backbone. We now had a unique handle on our investigations into lifetime extension.

Synthetic approaches to the dibenzo[*g,p*]chrysene class of materials had previously been limited to a few types of classical syntheses.³ Professor Shigehiro Yamaguchi, a visiting scholar in our laboratory, developed a new oxidative acetylene cyclization route to these materials as depicted in Scheme 1.⁴ Photophysical properties of CPPEs are summarized in Table 1. Absorbance and emission spectra (Figure 1) reveal a weakly allowed ground state transition in the dibenzo[*g,p*]chrysene monomer, **25**. In contrast to the TPPE's however, the disallowed transition is not entirely preserved upon polymerization: the lowest energy absorptions strengthen in the polymer spectra. Perhaps this is due to greater π conjugation along the main chain resulting from the more inflexible aromatic structure effecting. This would augment the comonomer contribution to the oscillator strength in this region of the spectrum. Despite the strengthening of these

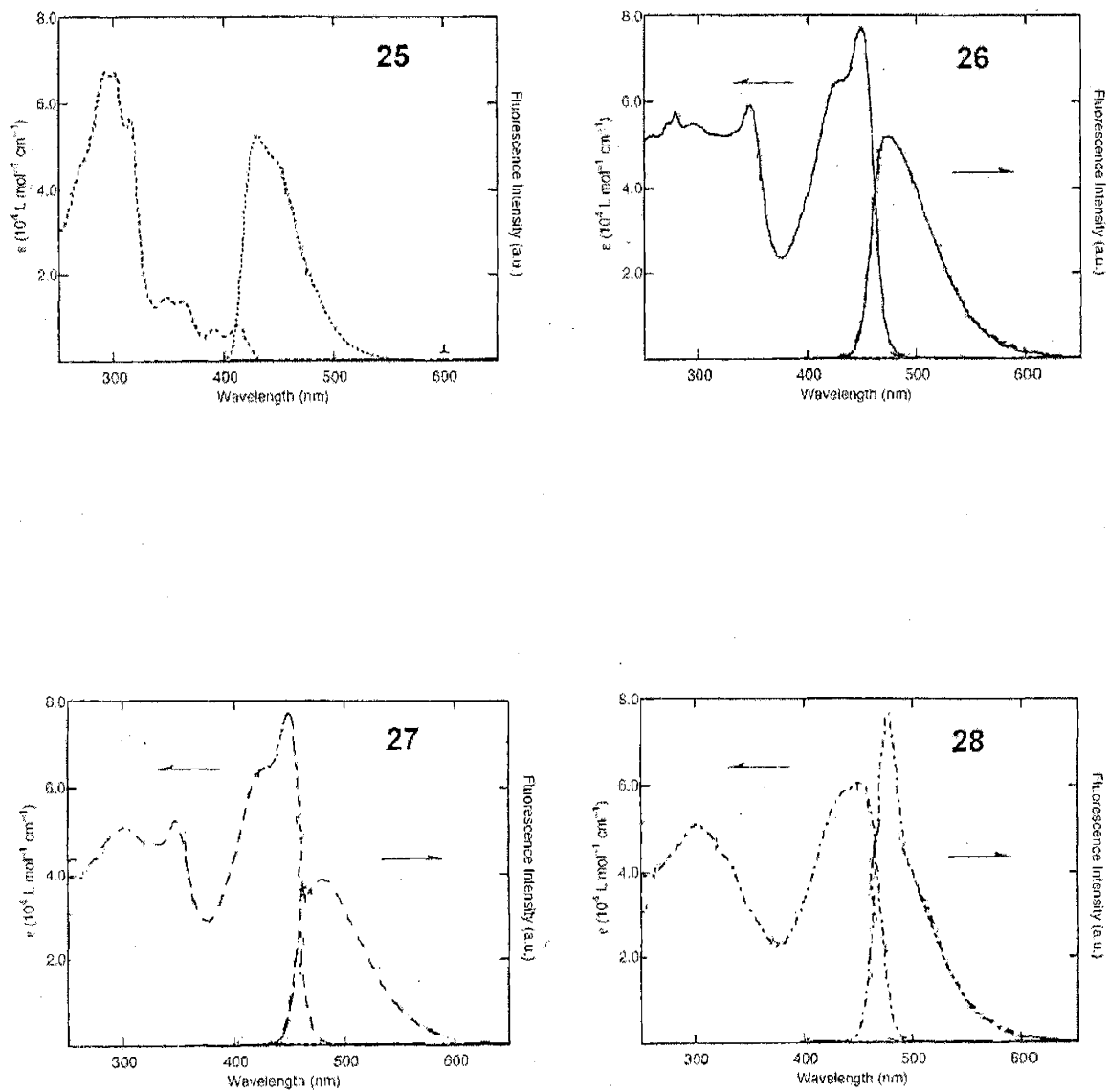


Figure 1. Absorption and emission spectra of **25-28**, dibenzo[*g,p*]chrysene monomer (**25**) and polymers (**26-28**).

Table 1. Photophysical Data for Dibenzo[*g,p*]chrysene Derivatives and Polymers^a

	UV-vis absorption		fluorescence				
	λ_{\max} [nm] ^b	log ϵ	λ_{\max} [nm] ^c	Φ_f ^d	τ [ns]	$k_{\text{rad}}[10^8 \text{ s}^{-1}]$	$k_{\text{non-rad}}[10^8 \text{ s}^{-1}]$
25	412	3.91	431	0.29	-	-	-
26	450	4.89 ^e	474	0.31	2.5	1.2	4.0
27	444	4.83 ^e	480	0.25	2.6	0.96	2.9
28	453	4.78 ^e	478	0.35	1.6	2.2	4.0

^a In dichloromethane. ^b Only the longest λ_{\max} are given. ^c Excited at the absorption maximum wavelengths. ^d Determined with quinine sulfate as a standard. ^e Per monomer unit.

transitions, very long lifetimes are observed in these polymers. This is may be due to the fact that there is a larger polycyclic aromatic component, per mass, in the repeat unit of each CPPE. We previously observed in TPPEs that this resulted in further lifetime extension. Polymers **26** and **28** have all-phenyl analoguesⁱ (Chart 2) with lifetimes several times shorter than those exhibited in the dibenzo[*g,p*]chrysene-based PPEs (CPPEs). This disparity is quantified in Figure 2. We did not have the phenyl analogue for Polymer **27** in hand however it also has a long lifetime (2.6 ns) compared to any PPE we have measured.

We were most concerned to demonstrate extended energy migration in these materials. Polarization spectroscopy, as implemented in Chapter 3, assessed energy migration in CPPEs. Size-exclusion gel-permeation chromatography selected CPPEs and PPEs of similar chain length for an accurate comparison. We again targeted the highest molecular weights attainable to enjoy stable photophysical properties as a function of chain length.

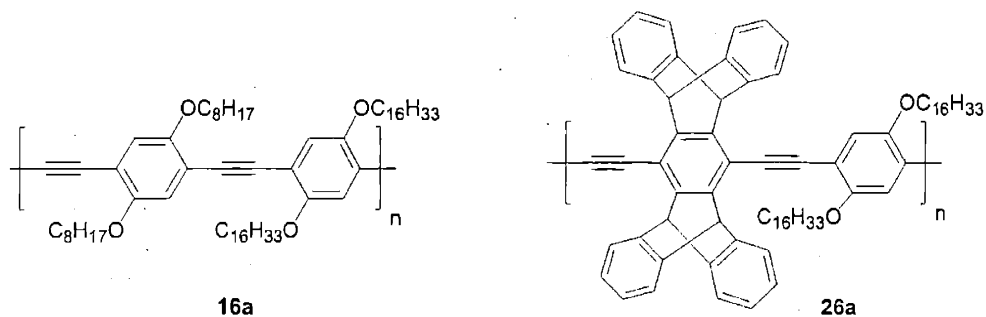


Chart 2. PPE analogues.

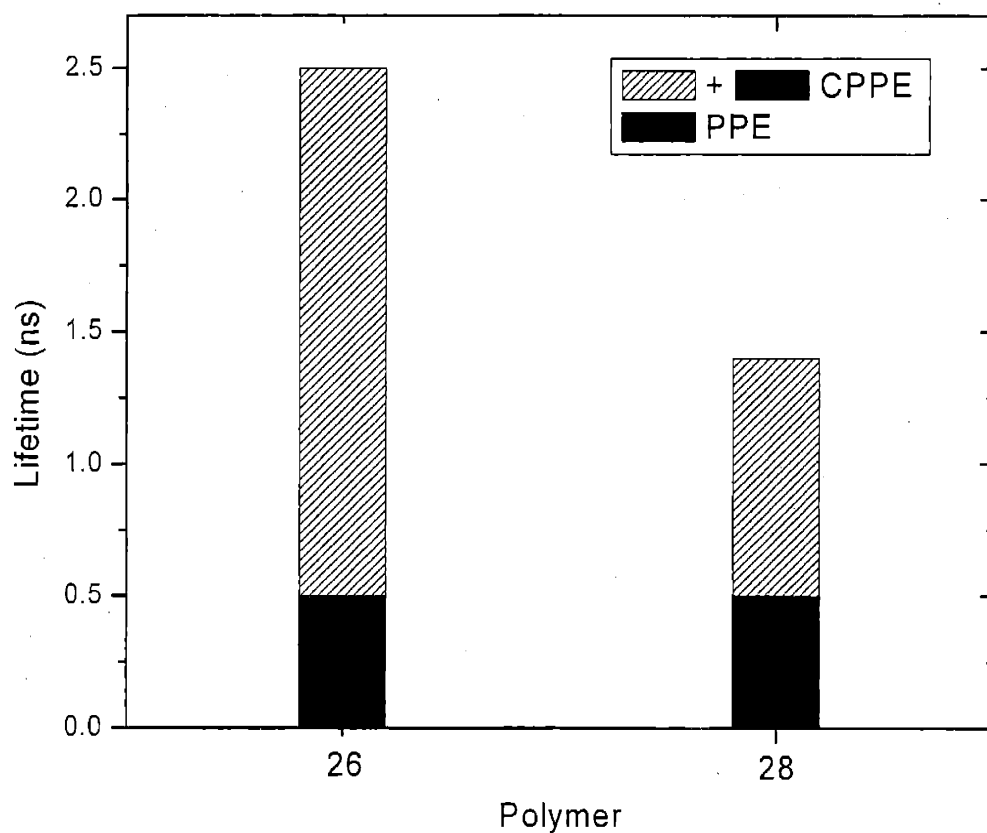


Figure 2. Lifetime comparison of PPEs and CPPEs. PPE lifetimes are shown as a subset of CPPE lifetimes. Black boxes are PPE lifetimes and stripped + black boxes are TPPE lifetimes. CPPE excitations in both cases are longer-lived.

ⁱ Polymer 26a was synthesized by Dr. Joon Ho Moon and Polymer 16a was synthesized by Mr. Sean K. McHugh.

For all chain lengths and at all excitation wavelengths, CPPEs exhibited lower polarization values than their PPE analogues (Fig. 3-6). In most cases, the values were about half those in the corresponding PPEs. However, one is always concerned that a larger absorption and emission dipole displacement is the main contributor to the disparity in depolarization. In this case, polarization would be expected to decrease more dramatically at certain intervals of wavelengths, not continuously over the range investigated. This is discounted by polarization data as a function of excitation wavelength. As excitation energy is increased, both the CPPEs and PPEs display lower P values, consistent with population of higher energy excitons that readily lower their energy by migration to lower energy states.

A near linear decrease of polarization as a function of excitation wavelength in Polymer **26** (Fig. 3) is observed supporting energy migration as the major contributor to depolarization. In addition, the lowest attainable P values are a fraction of the P obtained when exciting at λ_{max} . In **26a** however, this value is only about half, indicating the radiative rate of emission limits the extent of energy migration. This limitation is overcome in the longer-lived CPPE system as near 0 P values are obtainable. Because only very high molecular weights were the focus of this study, we observe very little change in polarization as a function of chain length in **26** and **26a** (Fig. 4). However, a small decrease in polarization persists in **26** while **26a** stabilizes. This indicates radiative decay does not supercede energy migration in **26** even for the longest chain lengths.

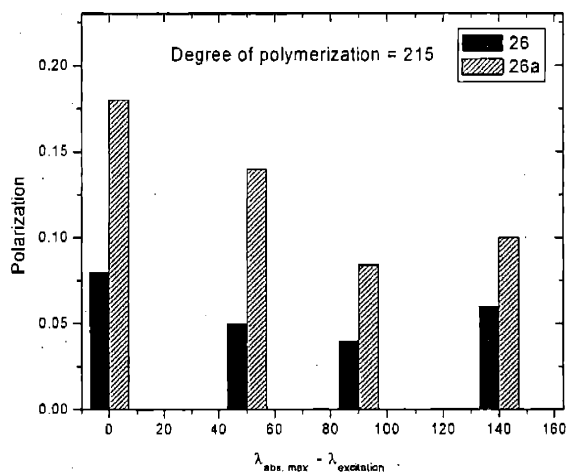
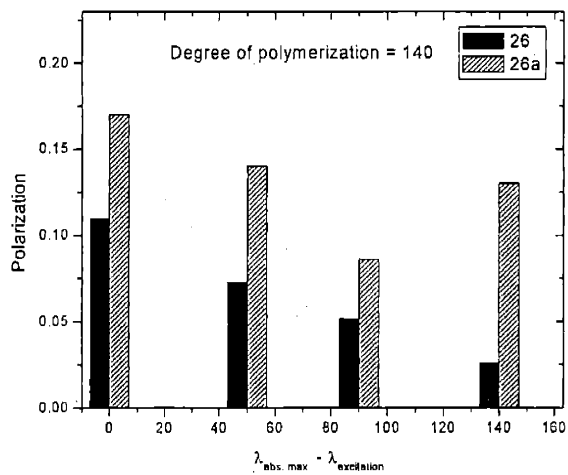
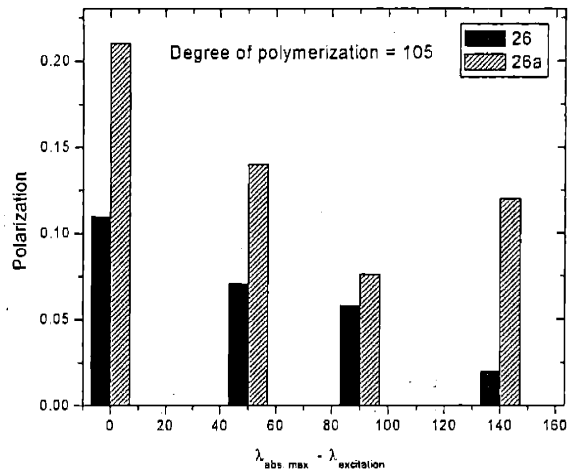


Figure 3. Polarization comparison as a function of excitation wavelength in **26** and **26a**. Wavelength units are nm.

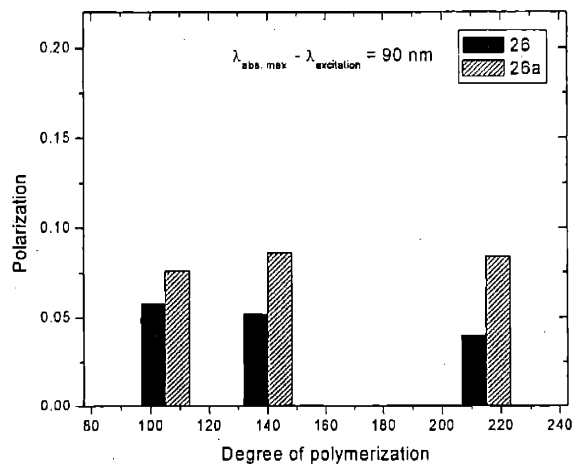
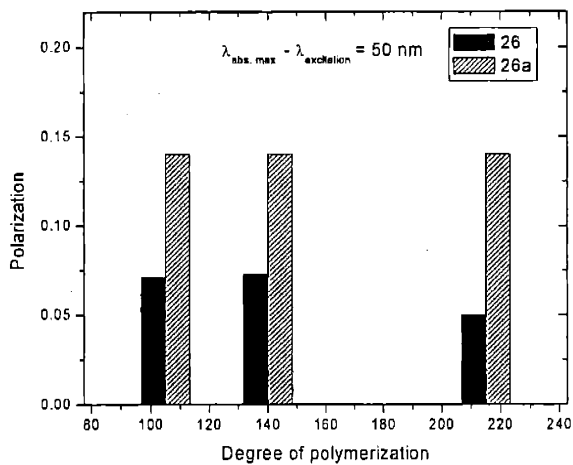
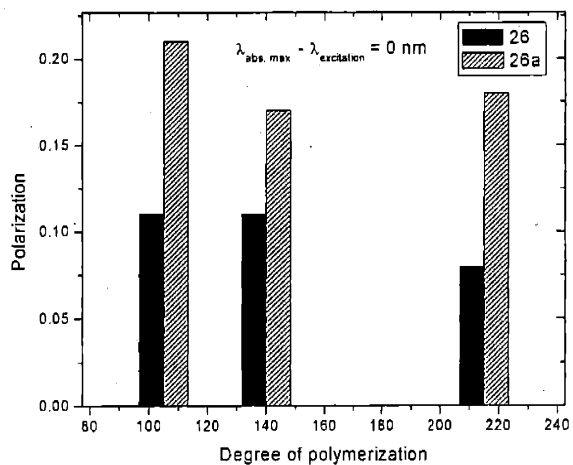


Figure 4. Polarization comparison in 26 and 26a as a function of degree of polymerization for various excitation wavelengths.

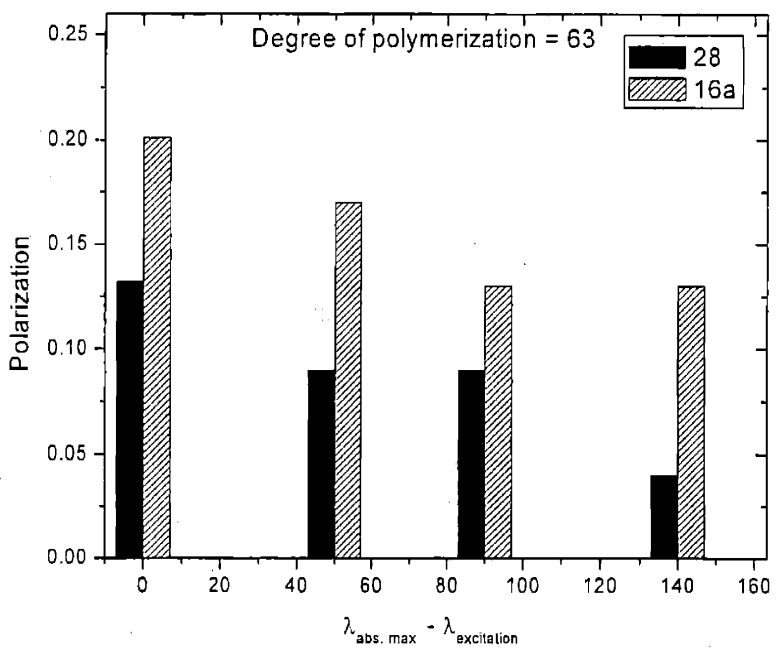
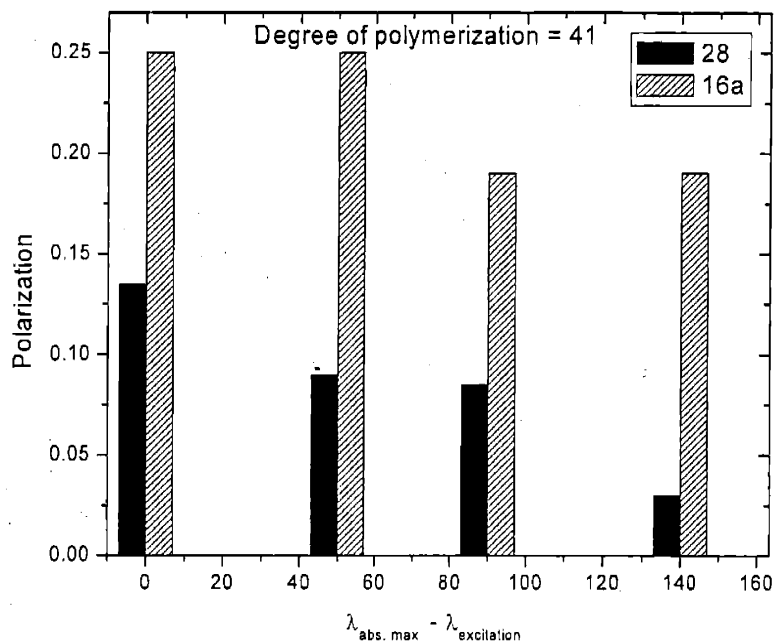


Figure 5. Polarization comparison as a function of excitation wavelength in 28 and 16a. Wavelength units are nm.

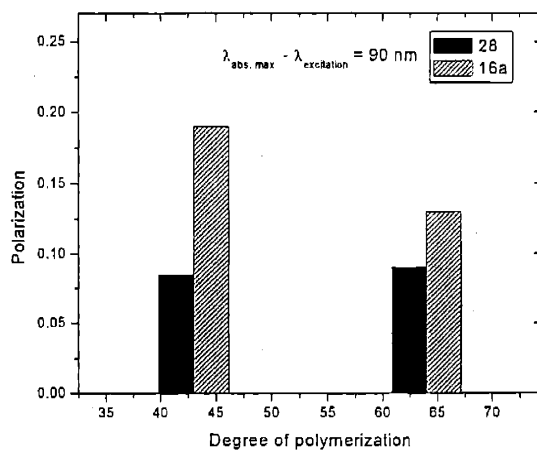
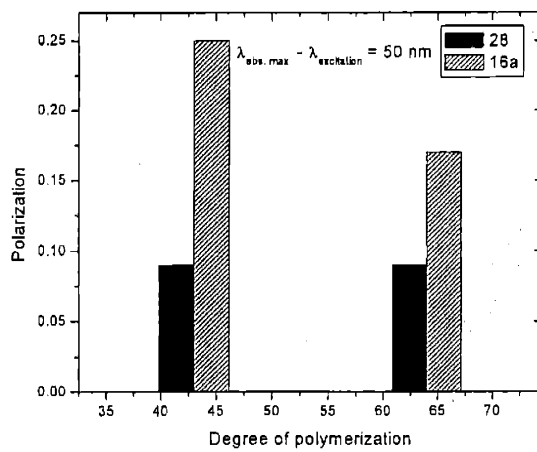
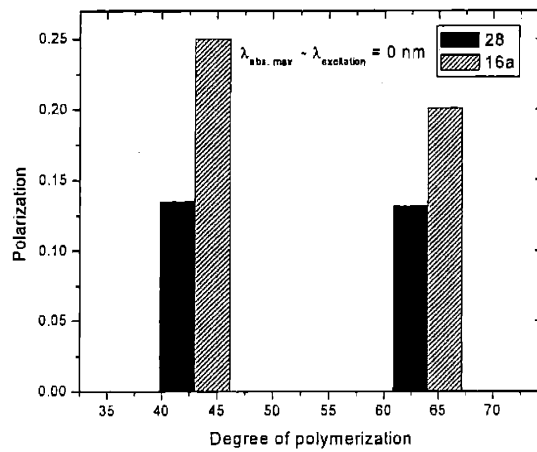


Figure 6. Polarization comparison in **28** and **16a** as a function of degree of polymerization for various excitation wavelengths.

Comparisons between **28** and **16a** were somewhat limited due to the fact that only relatively short chain lengths of **16a** were synthetically attainable. However, the trends observed in **26** along with the entire class of TPPEs (Ch. 3) are mirrored in this system as well. In all experiments, **28** exhibits greater depolarization (Fig. 4 and 5). As in the other materials, a decrease in polarization is observed as excitation wavelength increases, however this levels off in **16a** while it continues to decrease in **28**. This supports the assertion that energy migration is not truncated by radiative decay in CPPEs as it is in PPEs.

2.2. An uncyclized triphenylene

In an elegant complement to the investigation of chromophore-imposed lifetime elongation, Dr. John D. Tovar designed some materials to shed further light on this phenomenon. Polymer **29** is perhaps the ideal model polymer with which to compare photophysical properties of TPPEs. It has a repeat unit analogous to the triphenylene without the bonds that provide symmetry. It is therefore expected to be identical in electronic properties and solution conformation but missing the rigid aromatic core responsible for disallowed transitions. We compared the lifetime and polarization behavior of this polymer to that observed in **16** and **16a** to further describe the impact of triphenylene incorporation.

Some significant singularities emerge upon photophysical characterization of **29** (Table 2). The lifetime of **29** and **16a** are nearly identical at 0.47 ns and 0.52 ns emerge upon photophysical characterization of **29** (Table 2). The lifetime of **29** and **16a** are nearly identical at 0.47 ns and 0.52 ns respectively for a sample of approximately 70

Table 2. Photophysical properties of **16**, **16a** and **29**.

	$\lambda_{\text{max}}^{\text{abs}}$ [nm]	$\lambda_{\text{max}}^{\text{em}}$ [nm]	Stokes shift [nm]	τ_{obs} [ns]	Φ	τ_{rad} [10^8 s^{-1}]	$\tau_{\text{non-rad}}$ [10^8 s^{-1}]
16	470	504	34	0.80	0.30	3.8	10
29	463	470	7	0.47	0.22	4.6	16.7
16a	440	475	35	0.52	0.45	8.6	10.6

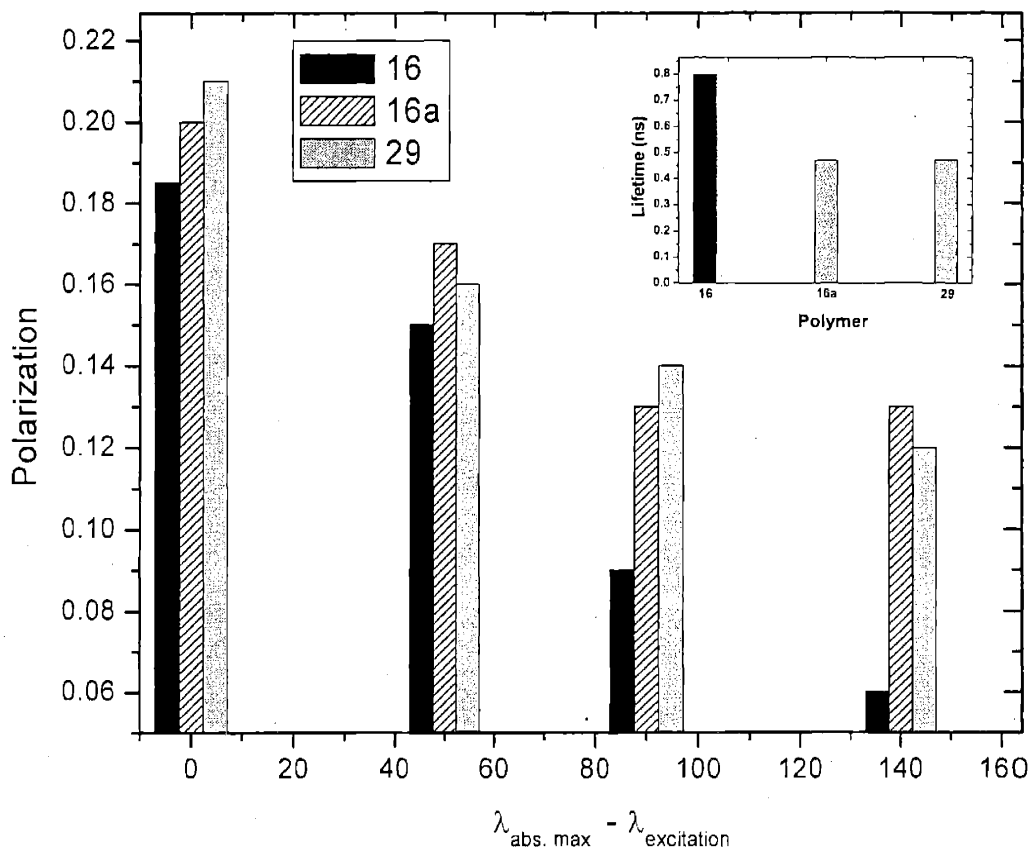


Figure 7. Polarization comparison as a function of excitation wavelength in **16**, **16a**, and **29**. Wavelength units are nm. Inset: lifetime comparison among polymers. Degree of polymerization = 71.

repeat units. For the same size chain, **16**, the triphenylene containing polymer, has a lifetime of 0.72 ns. While this appears a modest extension of lifetime when compared to those observed in CPPEs, TPPEs do not possess the same structural rigidity that can reduce conformational defects and hence non-radiative decay. More importantly, quantum yield measurements revealed that a significant component of lifetime extension in **16** is due to suppression of radiative rates, not merely a non-radiative rate increase.

Polarization studies as a function of excitation wavelength again confirm enhanced energy migration in the TPPE. Polarization values are lowest for **16** in all measurements (Fig. 7). In addition, depolarization increases throughout the wavelength range for **16** but levels off in **16a** and **29**. This study validates our hypothesis that symmetry imposed selection rules can extend lifetime and enhance energy migration through a Dexter-type transport mechanism.

2.3. Thiophene-based model compounds and polymers

Other polymers with novel architectures designed and synthesized by Dr. Tovar further illuminate lifetime extension. Through unique methodologies, he produced

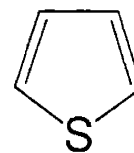


Chart 3. Thiophene.

model compounds and polymers with pendant thiophenes (Chart 3). Sulfur incorporation benefits materials properties in part because of the larger radial extension of its bonding. This promotes cofacial electronic interactions between stack molecules which could enhance energy transfer. In addition, the facile functionalization of a thiophene monomer offers relatively efficient synthetic solutions to band-gap tuning, solubility and

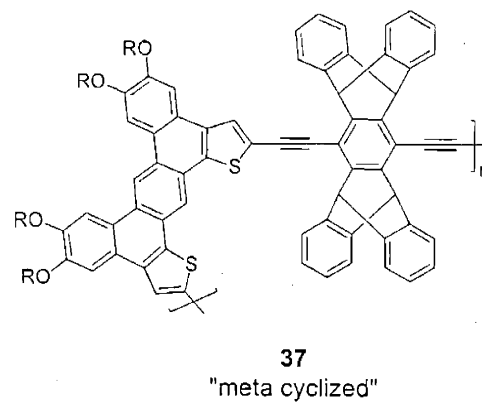
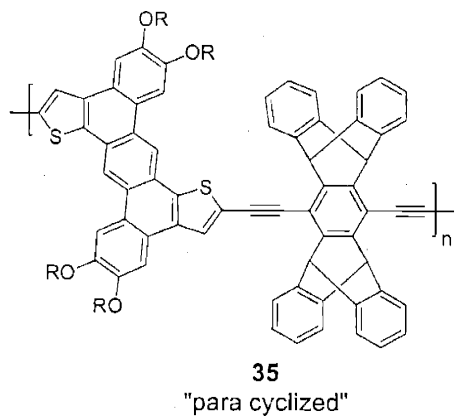
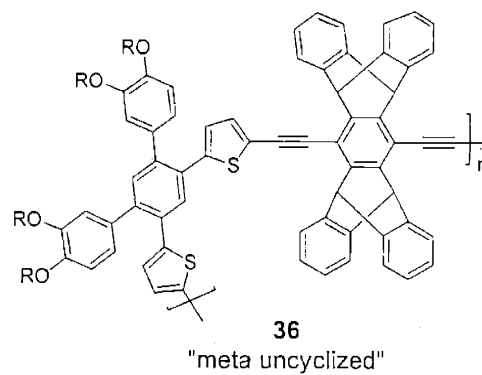
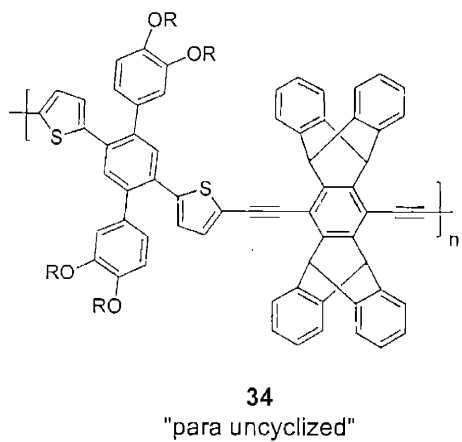
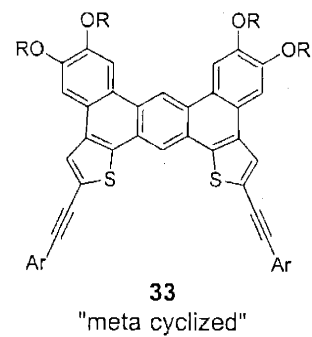
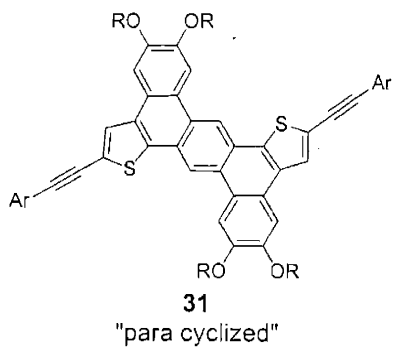
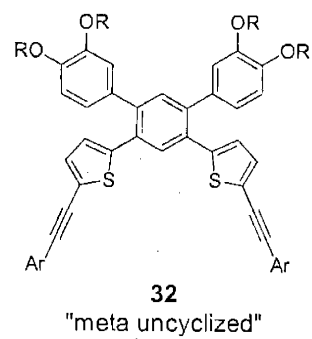
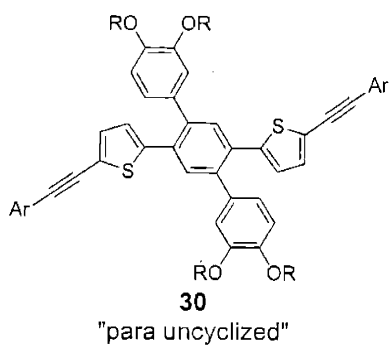


Chart 4. Thiophene-based model compounds and conjugated polymers.

processability.¹ Indeed, the series of thiophene-based materials (Chart 4) produced by Dr. Tovar allowed us to better understand the photophysical behavior of conjugated polymers with varied symmetries and structural constraints. We took the same approach as in our studies of **29**, interrogating both a cyclized and non-cyclized version of each model compound and polymer to assess the effects of imposed symmetry and rigidity. With both meta and para linkages represented, this family of polymers allowed us to explore effects of different degrees of aromatization in addition to probing cyclization effects.

Model compounds **30**, **31**, **32** and **33** provided systems with precisely defined conjugation lengths, allowing us to separate planarization effects from the effective conjugation length variations which play a key role in most polymer photophysical properties. We can use these model compounds to predict the behavior of polymers bearing them in the backbone and also to normalize for discrepancies in such behavior when in comparisons between polymer systems. Indeed, a simple examination of the absorption and emission spectra of these materials provide insight into cyclization phenomena (Fig. 8). The cyclized compounds **31** and **33** show a sharpening of vibronic structure concomitant with a decrease in Stokes' Shift as degrees of freedom are reduced. The oscillator strength of the (0,0) transition is significantly reduced in the meta system **33** ($\epsilon = 3.63$) when compared with the para isomer **31** ($\epsilon = 4.69$) and is reflected in a disparity in lifetime (5.00 ns vs. 1.12 ns respectively) between the isomers. Perhaps more relevant to these studies is the lifetime extension that arises from the cyclization of a

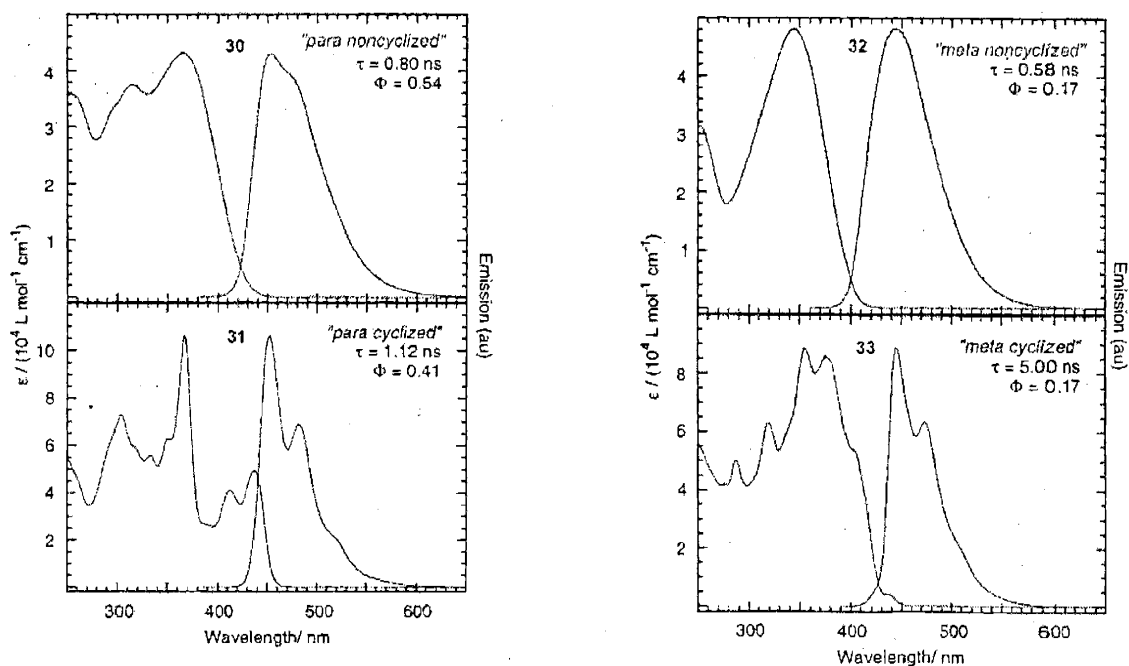


Figure 8. Absorbance and emission spectra of **30-33**.

particular isomer. The meta system sees a 9-fold increase (**32**: 0.58 ns, **33**: 5.0 ns) in lifetime. The lifetime increase in the para system is more modest (**30**: 0.80 ns, **31**: 1.12 ns). While a sharpening of emission spectra occurs, there is not a significant wavelength shift in either system upon aromatization. This suggests there is planarization in the excited state of **30** and **32** to allow for greater delocalization.

In support of the hypotheses originating this work, the photophysical properties of the model compounds are reflected with fidelity in the corresponding polymers. The absorption spectra of rigid, aromatized **35** and **37** displays sharper vibronic structure and a decrease in Stokes' Shift. The meta polymer **37** displays a much lower oscillator strength at the band edge than its para analogue, also predicted by the model compound spectra. Aromatization effects only slight shifts in emission maxima in both the para and

meta systems. As in **30** and **32**, this may attest to excited state planarization in the flexible systems.

The strengthening of band edge absorptions upon aromatization makes spectroscopic polarization as an expression of energy migration more complex. Because emission maxima are relatively stable, the Stokes' Shift in **35** and **37** is markedly diminished. Therefore, band edge excitations will not migrate far in energy before emission. Our previous method for comparison was designed to account for a shift in both absorption *and* emission maxima between model polymers and the more electron-rich, red shifted TPPEs and CPPEs. We monitored polarization values for these materials by comparing polarization upon excitation at discreet differences between absorption maximum and emission maximum ($\Delta E = 0, 50, 90, 140$ nm). Because absorption profiles

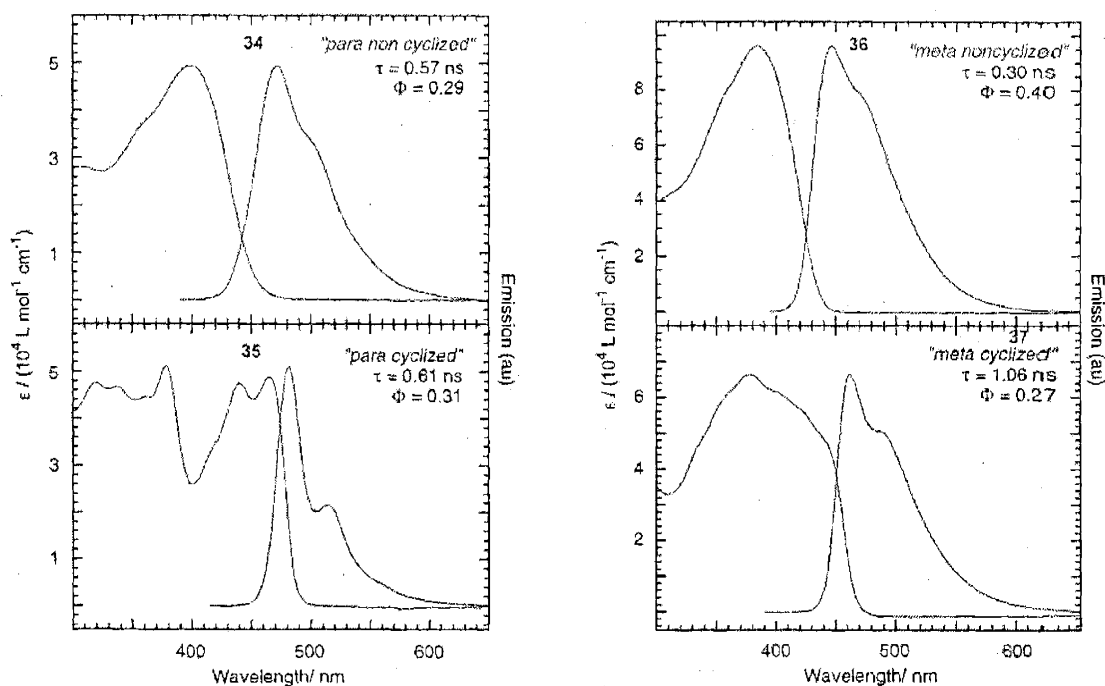


Figure 9. Thiophene polymer absorption and emission spectra.

of our model polymers and our studied polymers were similar, excitations were populated with similar probabilities for migration. Polarization data of different materials sets were therefore analogous. In other words, population of higher energy sites on the polymer chain invariably leads to migration to lower energy site before radiative decay. We accounted for this in previous measurements by comparing polarizations at varying differences from the absorption maximum. Stokes Shifts were similar, so higher energy excitations had a similar energy profile to migrate down before emission. In the materials at hand however, Stokes Shift varies significantly between related materials so a more revealing comparison would correlate polarization values observed when exciting at a given difference in energy from the *emission* maximum. This is plotted for **34** and **35** in Figures 11 and **36** and **37** in Figure 12.

A look at the para isomers reveals that polarization in the cyclized system tends to decrease only at specific intervals of wavelengths. The more pronounced vibronic structure in this polymer reflects a more quantized energy distribution. Therefore, a dipole with different angular displacement can be excited as energy is varied, contributing significantly to depolarization. In fact, polarization decreases rapidly with excitation wavelengths greater than 100 nm away from the emission maximum. This coincides with a new manifold of states in the absorption spectrum, supporting dipole displacement as a contributor to depolarization. The “para noncyclized” polymer **34** displays more expected behavior, with a polarization decrease at each successive excitation wavelength. Interestingly, the polarization values are similar for both **34** and **35**. While aromatization is formally increased in **34**, lifetime is not affected; **34** and **35**

registering identical lifetimes. Model compounds **30** and **31** demonstrate only a small variation in lifetime when compared to their meta counterparts, **32** and **33**. Lifetime correspondence to this trend was therefore expected in the polymers. It can also be correlated with the similarity in polarization values between **34** and **35** (Fig. 10). Discounting the highest energy excitations as due to dipole displacement, polarization values in **33** and **34** are roughly similar. This suggests that without lifetime enhancement, greater energy migration is not enhanced. It also underscores an important distinction: simply rigidifying the backbone of the polymer is not enough to extend lifetime and energy migration. One must carefully consider chromophore photophysics when attempting to impart these properties onto CPs.

Both meta systems, **36** and **37**, exhibit very low polarization values (Fig. 11) as expected from their kinked structure. A single hop along the twisted polymer backbone would significantly decrease initial polarization. However, the cyclized version **37** exhibits the extreme of this effect, reaching near 0 polarization values at higher excitation energies. Because here, as in the previous case, we cannot discount dipole displacement at higher energies, it is most important to notice for the lowest excitation energies, the cyclized isomer still exhibits lower polarization. This concurs with the observed lifetime disparity (**36**: 0.30 ns, **37**: 1.06 ns) that facilitates energy migration. It is likely again in this case the excited state behavior is encoded by the choice of chromophores. Cyclization in meta-substituted model compounds affords significant lifetime extension (**32**: 0.58 ns, **33**: 5.00 ns) mainly due to radiative rate suppression (**32**: 2.9×10^8 , **33**: 0.34×10^8). This augmentation is transferred to the PPE backbone, resulting in longer lived excitations and enhanced energy migration.

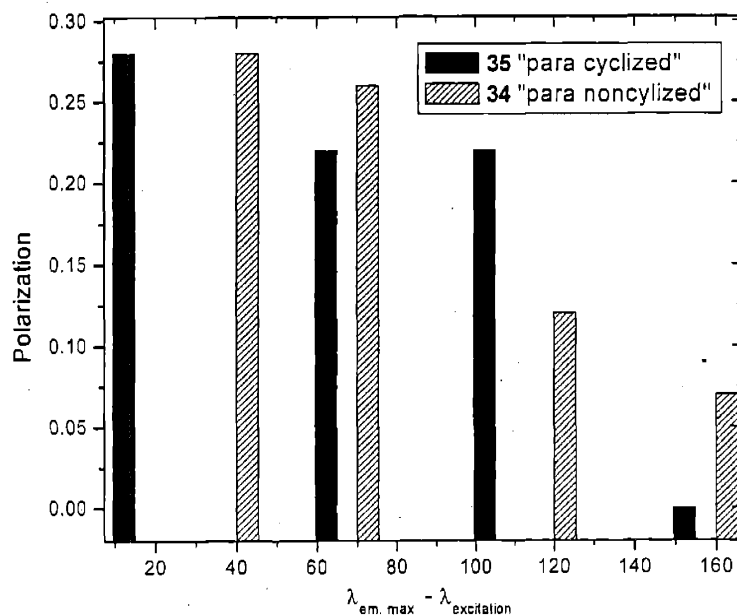


Figure 10. Polarization comparison as a function of excitation wavelength in 34 and 35. Wavelength units are nm.

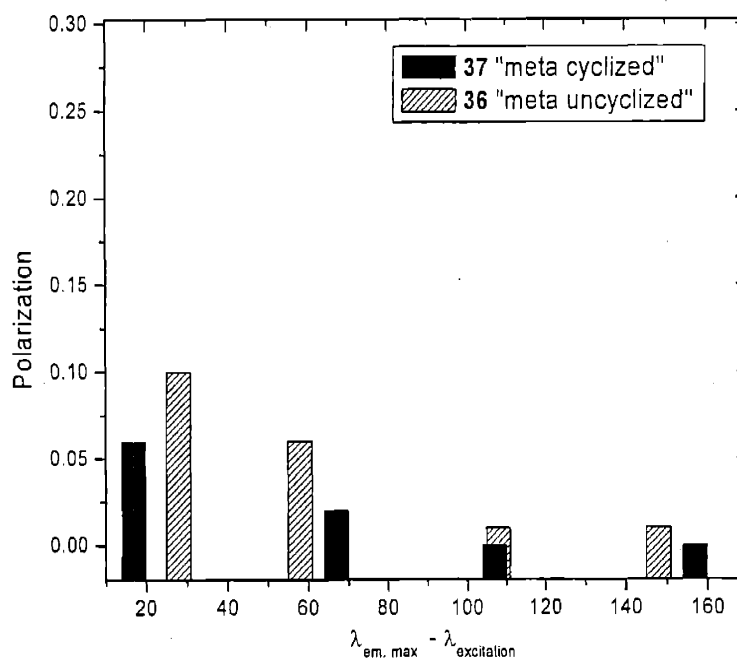


Figure 11. Polarization comparison as a function of excitation wavelength in 36 and 37. Wavelength units are nm.

3. Conclusions

The symmetrization and aromatization design principles pioneered with triphenylene- based PPEs were applied to novel molecular and polymeric systems. The consistent photophysical properties presented in this chapter demonstrated lifetime extension in conjugated polymers can be effected through deliberate chromophore design. Prior to the development and interrogation of these molecular systems, there had been no criterion for excited state lifetime extension in conjugated polymers. The high self-consistency of these results suggests a universal platform has been developed with which to design better sensory materials.

4. References

- ¹ Kumar, S.; Varshney, S. K. *Mol. Cryst. Liq. Cryst.* **2002**, *378*, 59.
- ² Berlman, I. B. *Handbook of Fluorescence Spectra of Aromatic Molecules*; Academic Press: New York, **1971**.
- ³ (a) Bergmann, F.; Eschinazi, E. *J. Am. Chem. Soc.* **1944**, *66*, 183. (b) Clar, E.; Guye-Vuilleme, J. F.; Stephen, J. F. *Tetrahedron* **1964**, 2107. (c) Suzuki, K.; Fujimoto, M.; Murakami, M.; Minabe, M. *Bull. Chem. Soc. Jpn.* **1967**, *40*, 1259. (d) Talapatra, S. K.; Chakrabarti, S.; Mallik, A. K.; Talapantra, B. *Tetrahedron* **1990**, *46*, 6047. (e) Klumpp, D. A.; Baek, D. N.; Prakash, G. K. S.; Olah, G. A. *J. Org. Chem.* **1997**, *62*, 6666.
- ⁴ Yamaguchi, S., Swager, T. M. *J. Am. Chem. Soc.* **2001**, *123*, 12087.
- ⁵ Roncali, J. *Chem. Rev.* **1997**, *97*, 173-205

Chapter 5

Chemosensing lasing action in conjugated polymers.

1. Introduction

The study of amplified spontaneous emission (ASE) and lasing action in conjugated polymers (CPs) is a relatively new field. Ten years ago, Moses reported the first evidence of stimulated emission by optically pumping a solution of poly(2-methoxy, 5-(2'-ethyl-hexyloxy)-*p*-phenylene-vinylene) (MEH-PPV).¹ However, reproducing this phenomenon in the solid state proved challenging. It was not for another four years that Heeger *et al* observed ASE in the solid state in MEH-PPV by dispersing it in polystyrene with TiO₂ nanocrystals.² True lasing in a neat film was achieved by Friend, Tessler, and Denton by incorporating MEH-PPV polymer into a microcavity.³ One impediment to these advances came from the energy migration inherent in conjugated polymers. If a few impurities are present, many of the excitations will encounter them. Because stimulated processes, such as lasing, are extremely sensitive to any type of competitive process, such as non-radiative decay, extremely pure materials are necessary for their study.

Once high photoluminescence (PL) efficiencies are realized, lasing appears to be a rule rather than exception for CPs⁴ (Fig. 1) as well as small molecule organics.⁵ Among organic semiconductors, CPs are excellent candidates for gain media. The typically low lasing threshold found in CPs is primarily due to large Stokes shifts that minimize the light reabsorption losses. Therefore, energy migration can enhance lasing action, in the absence of impurities. The transport of excitations from high energy sites to regions of lower energy before emission creates the idealized four-level system, allowing a pump beam at higher energy to create a red-shifted population inversion (Fig. 2).

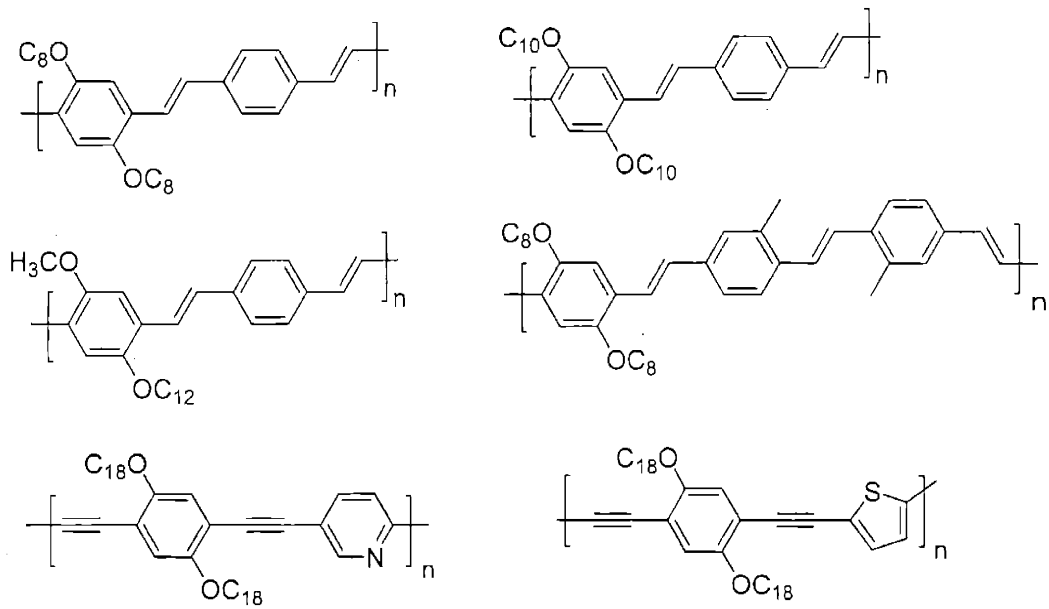
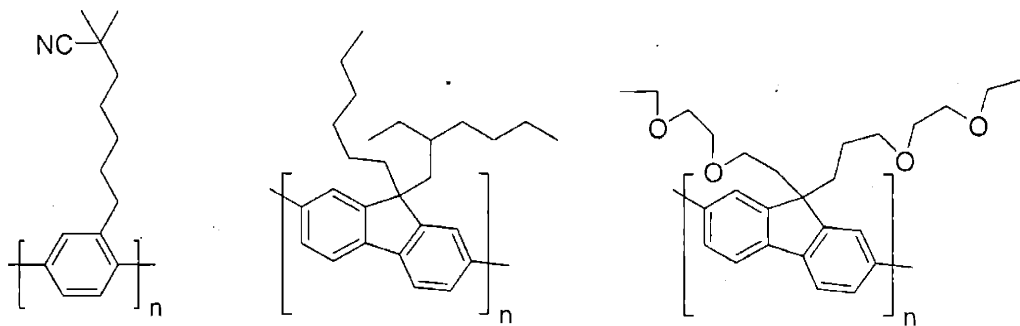
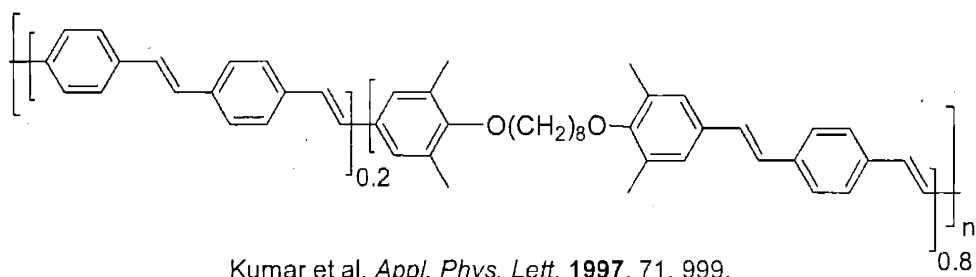


Figure 1. Some conjugated polymers exhibiting stimulated emission.

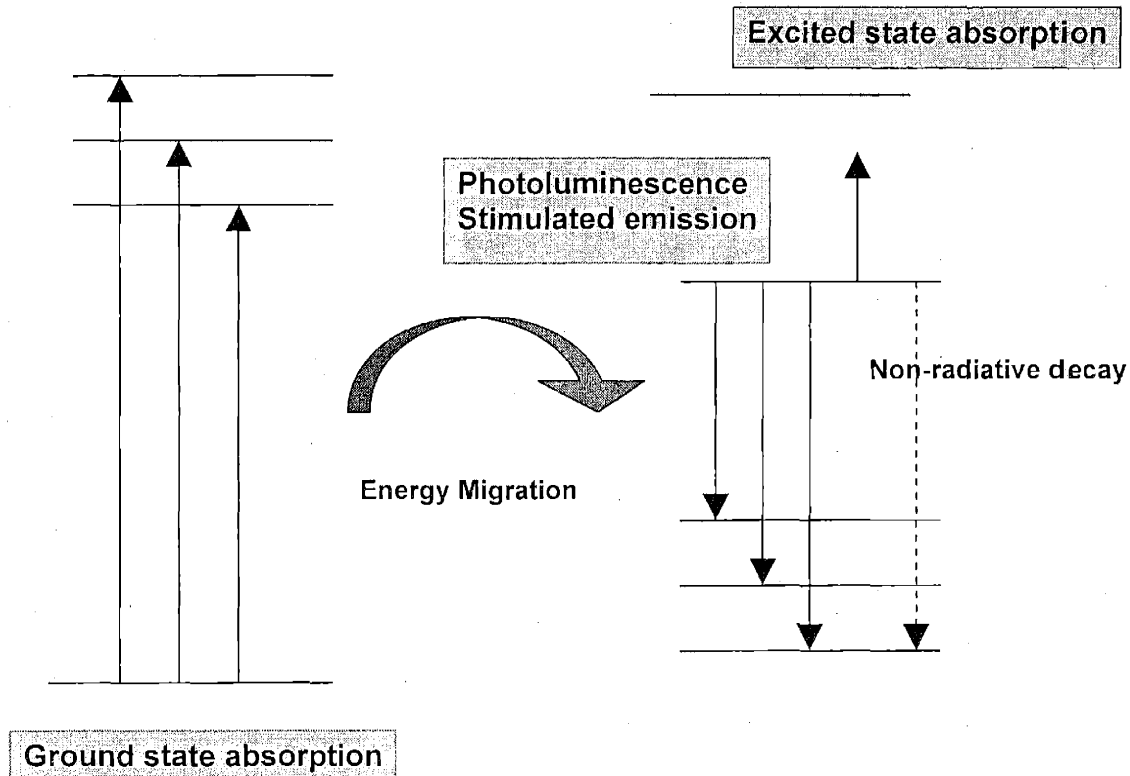


Figure 2. Conjugated polymers as four level systems.

The lasing mechanisms in CPs are compatible to those we exploit for chemosensing. Previous work in our group demonstrated that the fluorescence of electron-rich conjugated polymers can be attenuated upon exposure to electron deficient aromatic analytes. We initially quantified this effect in polymer solutions with paraquat as the target analyte⁶ and more recently have been successful in detecting attograms of 2,4,6 trinitrotoluene (TNT) by observing luminescence quenching of polymer thin films.⁷ The mechanism responsible for the fluorescence quenching is most likely an electron transfer event from the optically excited state of the polymer, an exciton, to the lowest

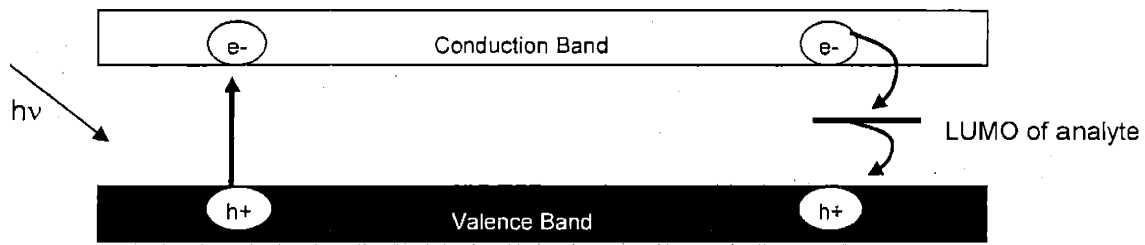


Figure 3. Fluorescence quenching mechanism in CPs. An electron transfer event from the excited state of the PPE to the LUMO of TNT provides non-radiative decay pathway for the exciton.

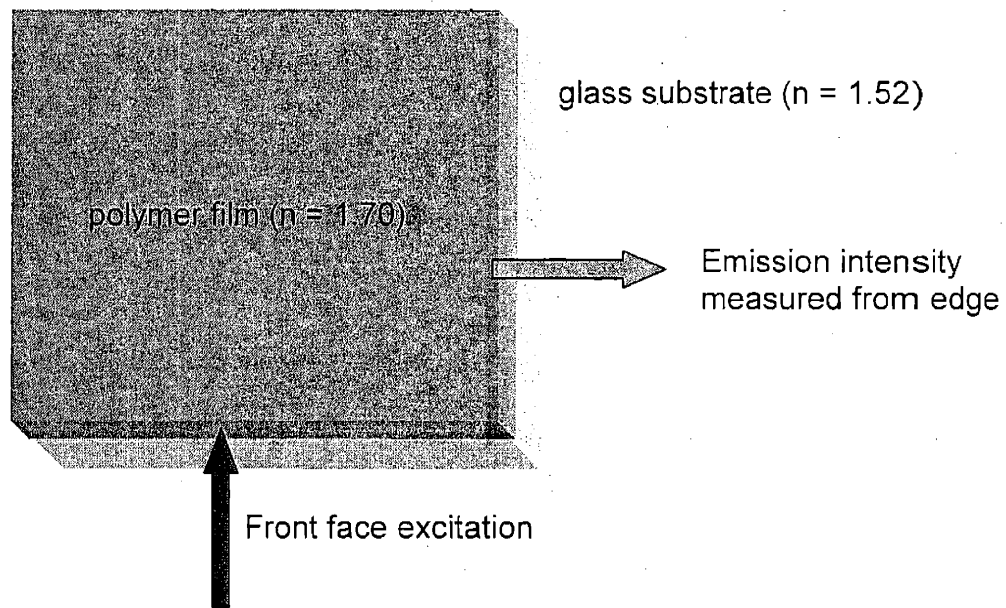


Figure 4. Asymmetric waveguide structures for ASE. Polymer film must be thick enough to support waveguide modes.

unoccupied molecular orbital (LUMO) of the analyte (Fig. 3). We call this in short the 'turn off' mechanism because fluorescence is attenuated upon analyte exposure. The energy alignment of the polymer/analyte molecular orbitals dictates to which compounds a particular polymer will be sensitive, providing for selective response. The rate of the non-radiative processes will increase with the increase in analyte concentration and also for longer diffusion lengths of excitons in the polymer. In an analogous mechanism, lasing can be prevented or shut down by a few sites of non-radiative decay. Our target analyte, TNT, provides a site for non-radiative decay. Because lasing is a non-linear phenomenon, then to 'turn off' a lasing signal rather than spontaneous emission should provide orders of magnitude more signal.

As a primary constituents of most buried landmines worldwide, the explosive TNT and its synthetic by-product, 2,4 dinitrotoluene (DNT) are primary targets for chemical sensor development. Portable devices using our polymers as active materials are currently being pursued for commercialization by Nomadics, Inc. In recent field tests, their machines have been as accurate as the current technology, canine olfaction. Surpassing this milestone means developing materials with enhanced sensitivity. This motivates our interest in optimizing energy migration and the excited state properties of CPs. The lasing approach may supply the enhancement necessary to surpass current demining technology rather than just meeting it.

In this chapter, we put these ideas into practice. We detail how exposure of a polymer thin film to an analyte can increase its lasing threshold or all together prevent lasing. In addition, we demonstrate that attenuation of the lasing emission line can be

used as a chemosensor with over a hundred-fold improvement in chemical sensitivity as compared to sensing by simple fluorescence quenching.

2. Results and Discussion

2.1. Amplified spontaneous emission measurements

We thought the synthetically novel systems developed in our laboratory were apt candidates for ASE due to their extended excited state lifetimes. Longer excited state lifetimes facilitate the creation and persistence of population inversion. We centered our initial investigations on Polymer **11** in part because of its extended excited state lifetime and in part because of its superior solid state luminescence properties. To determine the suitability of a material as a laser gain media, it is convenient to fabricate an asymmetric waveguide structure with glass/air serving as cladding layers (Fig. 4). The threshold for stimulated emission or amplified spontaneous emission can then be readily measured. Excitation power is increased linearly, and emission intensity is recorded. When a non-linear increase in emission intensity is observed with a linear increase in input power, it is likely that ASE or stimulated emission is occurring. Indeed **11** displays a threshold input power above which narrowed emission and non-linear intensity output is observed (Fig. 5).ⁱ These characteristics are clear evidence of stimulated emission.

These preliminary experiments underscored a few important points. ASE is easily induced in our CPs. Input powers are well below those used to pump small molecule systems and quantum dots. Data in Figure 5 was taken at room temperature in an inert

ⁱ These emission measurements were performed by Dr. Hans Eisler and Dr. Vikram Sundar from Professor Bawendi's laboratory with a beam from Professor Dan Nocera's Ti- Sapphire laser.

atmosphere. There was little photobleaching observed over the timescale of these measurements (few hours), indicating a robust material. It became apparent that the real challenge of the ASE measurements lay in the film fabrication. A very thick film (>200 nm), by spin coating standards, is necessary to achieve waveguiding in these structures.

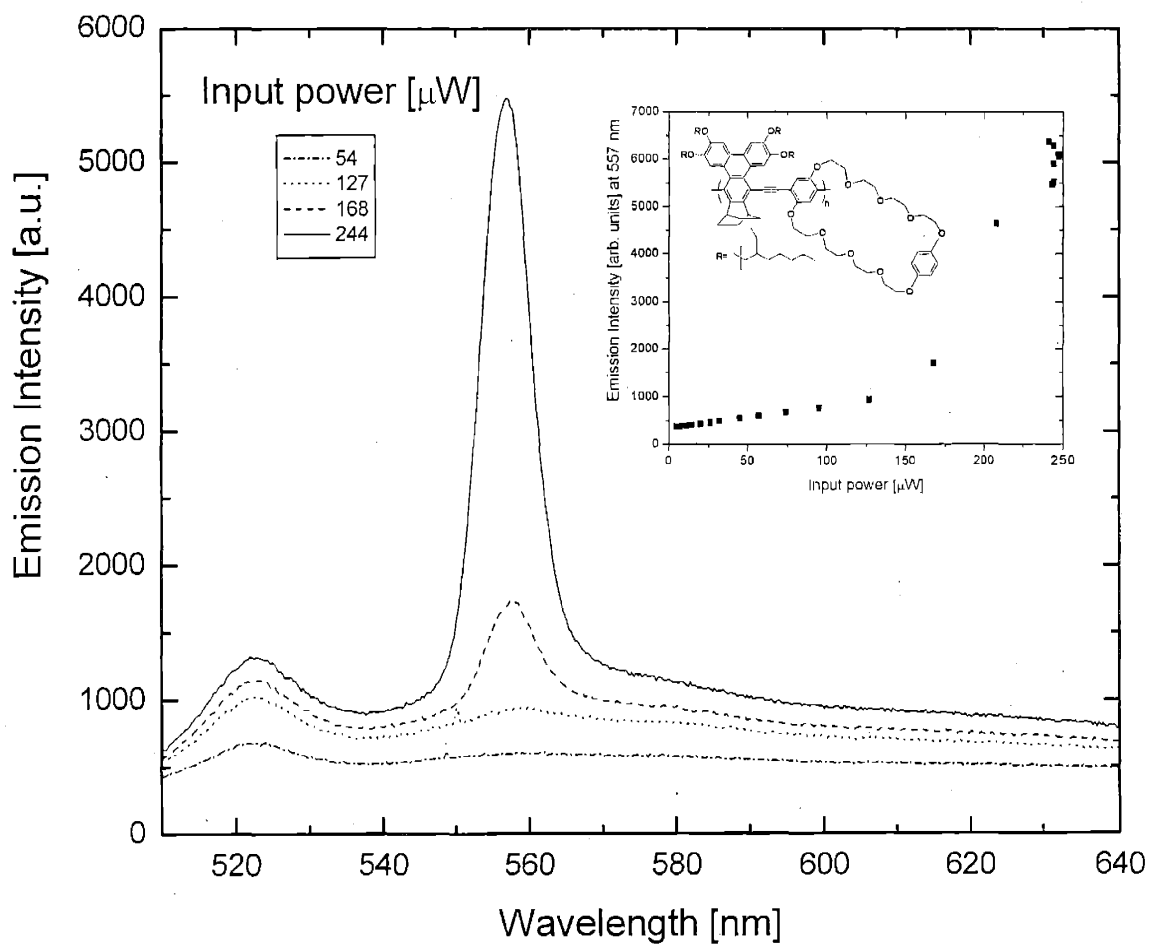
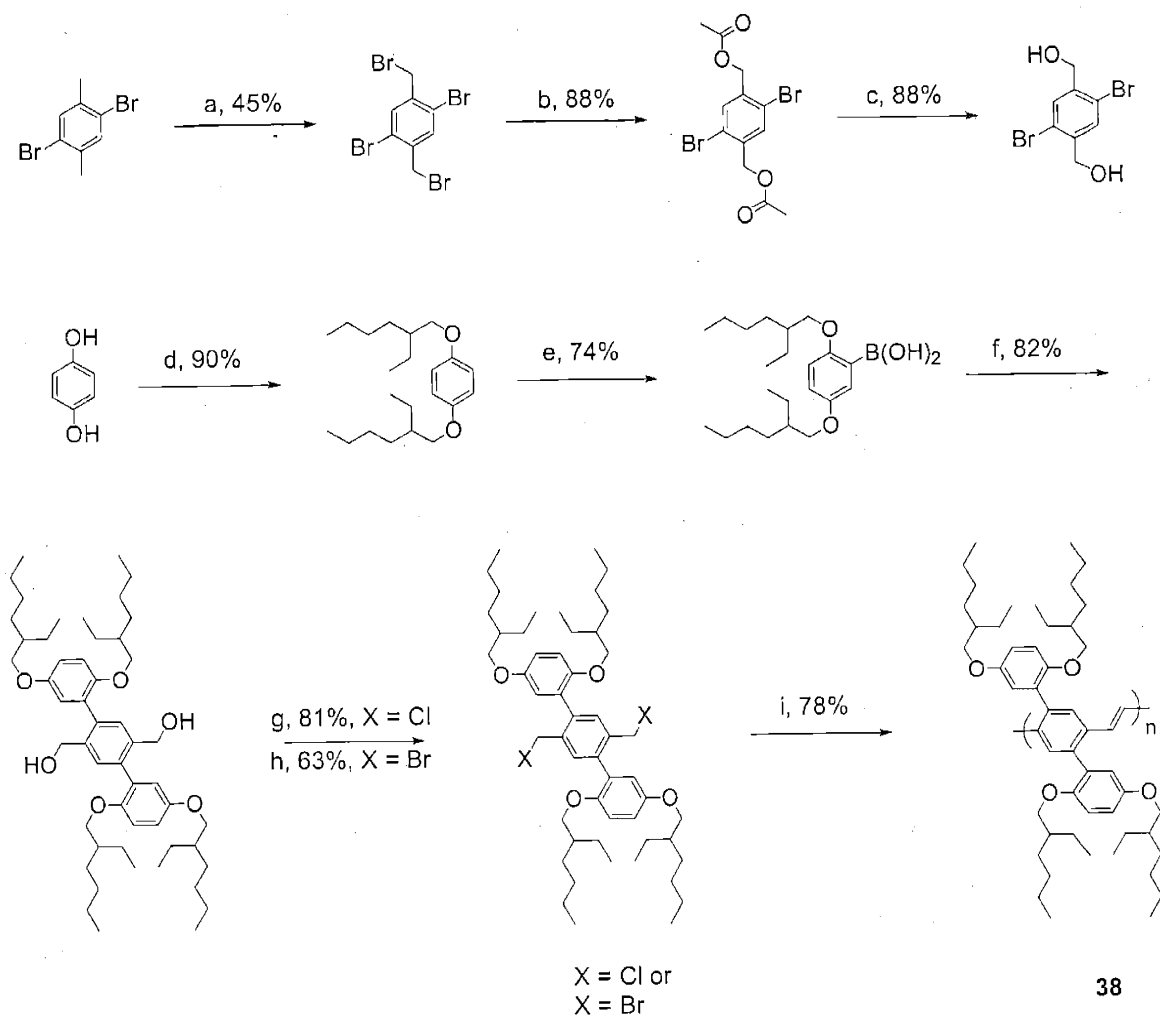


Figure 5. ASE in Polymer **11**. As input power is increased, emission intensity is increases linearly at 525 nm. Above threshold, there is a non-linear increase of emission intensity at 557 nm. Inset: Emission intensity at 557 nm plotted as a function of input power. Non-linear response occurs above input powers of about 130 μW . Chemical structure of Polymer **11** is also shown.

The solution from which these films must be cast will therefore have to be very concentrated (40-50 mg/mL). On the scale of our syntheses, this is a large amount of material. This is perhaps why most literature precedent examining ASE in CPs utilized commercially available materials such as MEH-PPV. However, the synthetically-tailored optical properties of CPs created in our laboratory are superior to most commercially available materials. Therefore, their study is worth pursuing. One must carefully conserve material where possible and target materials which readily yield optically clear, well-behaved films. Attempts at other deposition methods which use less material such as dip coating or drop casting did not produce the smooth, optically clear films necessary for these experiments.

Our ideal material would therefore be in abundant supply, have very high luminescence efficiencies and exhibit extremely low lasing thresholds. For chemically sensitive CP lasing structures that operate in ambient air, the low lasing threshold is essential for extending their operation lifetimes. Indeed, we observed at high pump powers, competitive photo-oxidative processes can significantly degrade the polymer performance. Our best candidate for an air-stable, chemically sensitive lasing CP is Polymer 38. It was synthesized by Dr. Zhengguo Zhu as sketched in Scheme 1, and its absorption and emission spectra are plotted in Figure 6. Its thin film luminescence spectrum (Fig. 6) peaks at $\lambda = 505$ nm and has a radiative lifetime of $\tau = 650$ ps. Rapid radiative relaxation results in the high fluorescence efficiency of the spin-cast thin films of $\Phi_F = 0.80$, when compared to a standard of 9, 10 diphenylanthracene in PMMA ($\Phi_F = 0.83$). Of particular interest, molecular modeling indicated the aromatic side chains orient parallel to the polymer backbone. This can facilitate exciton diffusion by increasing



(a) NBS, heating; (b), NaOAc, acetic anhydride, heating; (c) KOH; (d) 2-ethylhexyl bromide, KOH; (e) i) *n*-Butyllithium, 0 °C, hexanes, ii) trimethyl borate; (f) **3**, (*o*-tolyl)₃P, Pd₂dba₃, CsF, 90 °C; (g) SOCl₂; (h) PBr₃; (i) potassium *tert*-butoxide, THF.

Scheme 1.

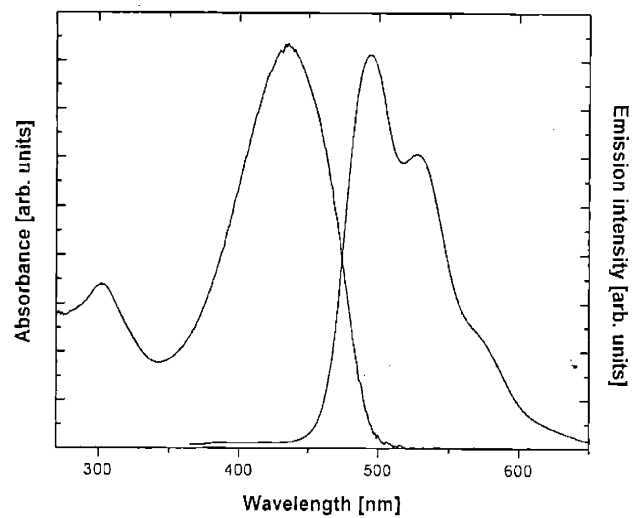


Figure 6. Absorbance and photoluminescence spectrum of Polymer **38** in a 100 nm thick film.

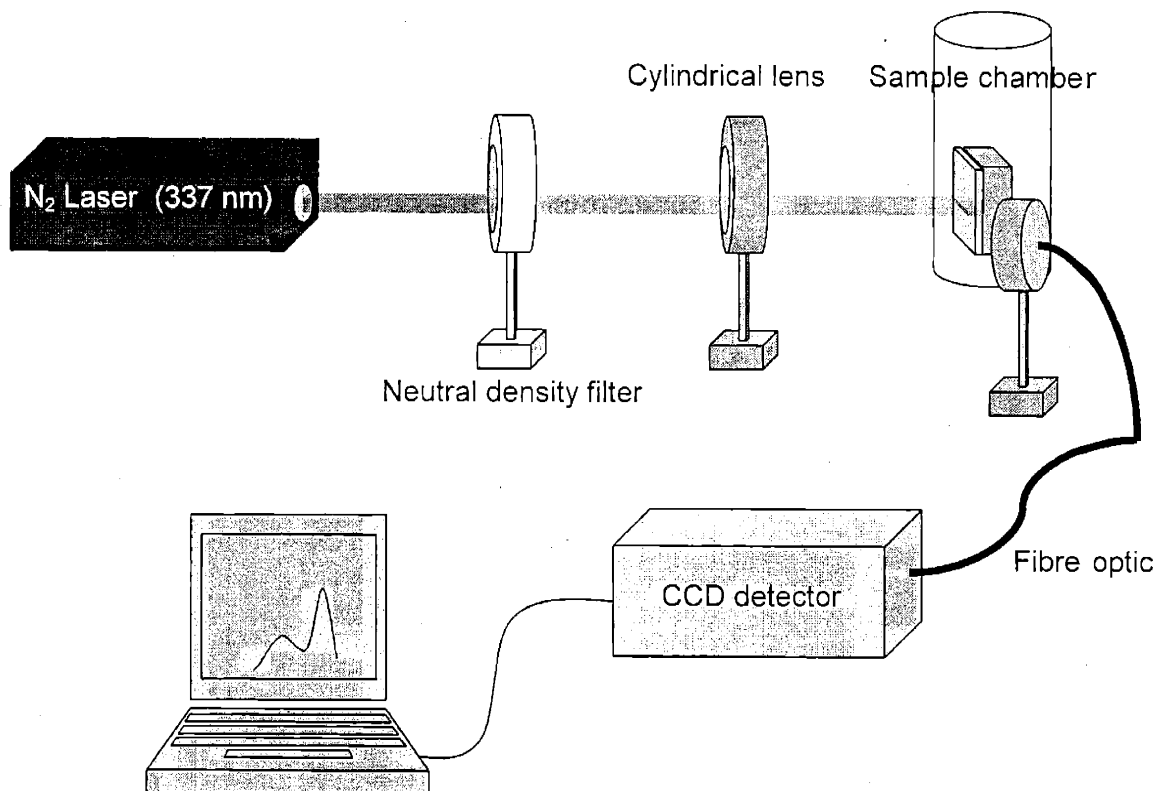


Figure 7. Experimental set-up for optically pumping conjugated polymer films.

π -orbital interactions in the solid state. Diffusion lengths as long as 100 Å were measured in similar material systems. Aromatic side chains are also known to impart rigidity in the solid state, minimizing aggregation of chromophore sites when compared to analogues with only straight chains. Also, chromophore density is increased in this polymer, increasing the stimulated emission cross section.

Because preliminary experiments determined that lasing action is accessible at low powers, we simplified our experimental set-up significantly. The lasing action could be easily be generated by optically exciting thin films of **38** with a N₂ laser that emitted 4 ns long pulses of $\lambda = 337$ nm at the operating frequency of 30 Hz. The beam was focused into a 9 by 0.9 mm stripe with a cylindrical lens and emission collected at a 60° angle from the excitation beam which impinged normal to the substrate (Fig. 7). For the first lasing structures, asymmetric waveguides were formed by spin casting thin films of **38** from 50 mg/mL hexane solution onto glass substrates, with film thickness ranging from 300 Å to 4000 Å. For films thicker than 500 Å, multimode ASE peaked at $\lambda = 535$ nm, coinciding with the first vibronic transition of **38**, as governed by the reabsorption within the thin film (Fig. 8).

2.2. Reducing the active layer: paralene-coated substrates.

In our group, earlier studies found that only the first 16 exposed monolayers of the polymer thin films interact with an adsorbed analyte.⁸ This is due to the fact that

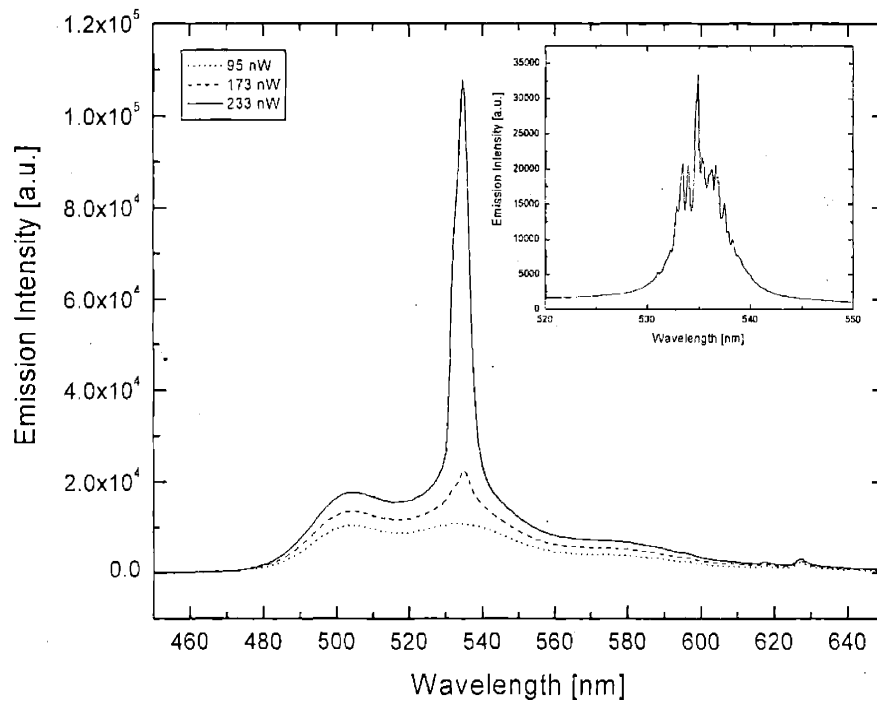


Figure 8. Emission spectrum of the 750 Å thick film of Polymer 38 on a glass substrate for different input powers. ASE peak grows in at higher input powers. Inset: Higher resolution of the 233 nW spectrum showing the detailed, multi-mode emission structure.

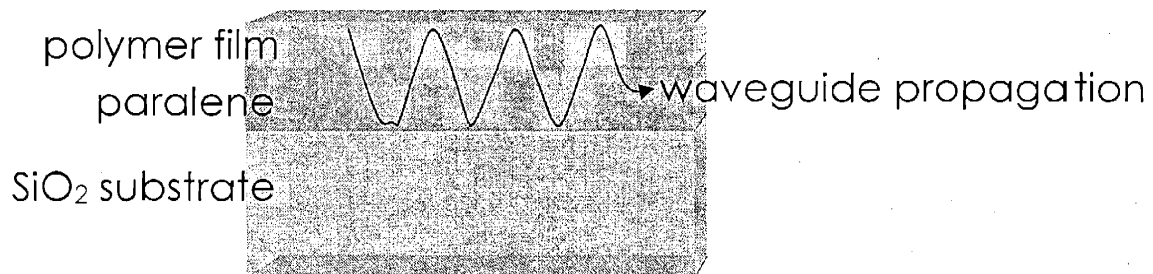


Figure 9. Paralene coated silica substrates with a layer of polymer film. Paralene is index matched with our polymer to allow waveguide propagation.

excitons generated deeper within the film will radiatively decay before migrating to the surface. For thick films the majority of excitations are generated and decay within the bulk. Therefore, in our sensing measurements, thick films only achieve a higher background signal, and thinner polymer films show more pronounced reduction in total fluorescence after analyte exposure. Thin polymer films, however, cannot support waveguided modes necessary for generating the ASE and the lasing action. We remedied this problem by first depositing a 2000 Å thick layer of parylene by chemical vapor deposition on top of silica substrates and then spin casting thin polymer films on top (Fig. 9). Parylenes refractive index of $n = 1.67$ matches the refractive index of the polymer $n = 1.70$ so that two in combination form a waveguide. In these structures we observed ASE emission for polymer layers as thin as 400 Å. For even thinner films, an insufficient amount of light was absorbed in a single excitation pulse.

A myriad of samples were prepared and studied in this manner. We sought to register the lowest the lasing threshold possible and to understand the factors mitigating this phenomenon. One of the lowest thresholds we recorded is shown in Figure 10 which displays the emission intensity of a 600 Å thick film of **38** on glass. At 47 nW of incident power a threshold of ASE emission is observed. With our measured spot sizeⁱⁱ, we calculated a threshold flux of 190 nJ/cm². This is to our knowledge the lowest lasing threshold ever reported for a conjugated polymer. Typically, measured thresholds ranged from 190 nJ/cm² to 4100 nJ/cm² depending on film quality and age though the low limit was easily reproducible and typical of many samples. At these low input powers, signal attenuation due to ambient air exposure is minimized and for short exposure times can be

ⁱⁱ The procedure for measuring spot size and the calculation of flux is detailed in Appendix 1.

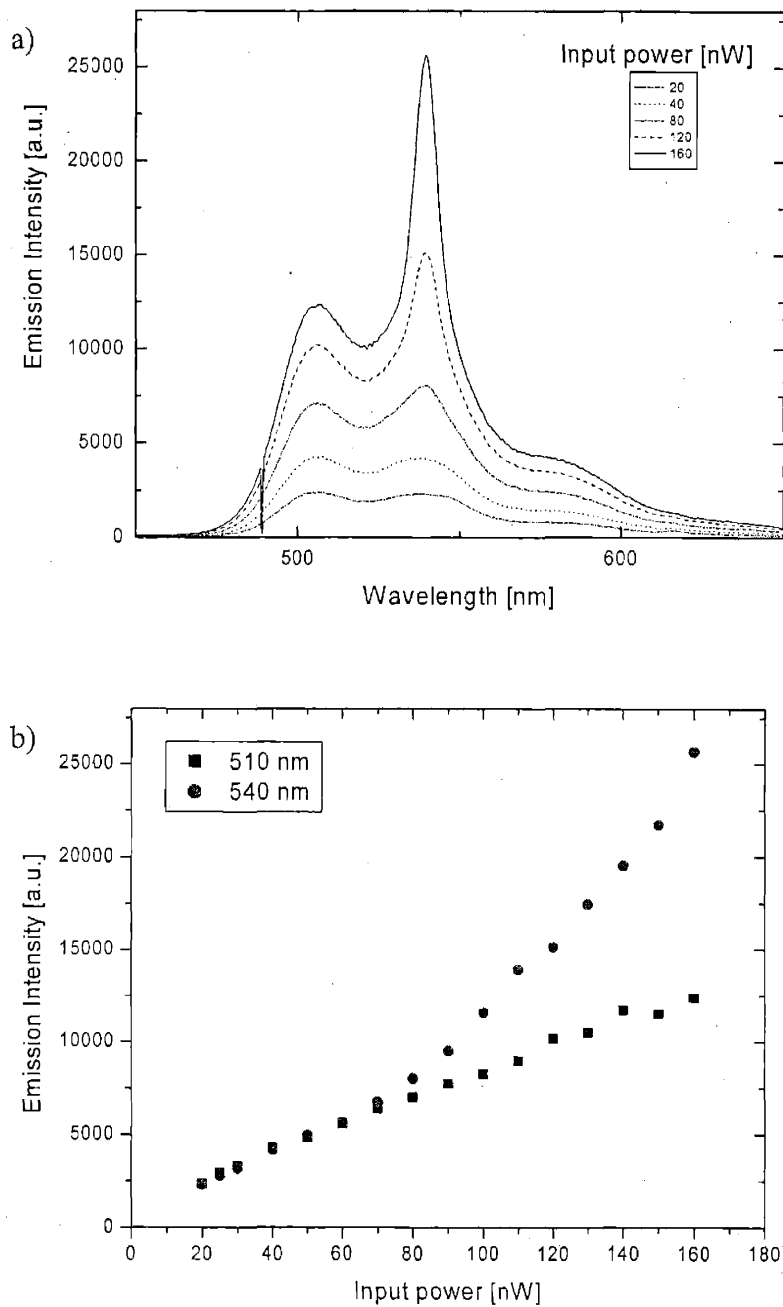


Figure 10. Low lasing threshold of Polymer 38. (a) Emission spectrum of a 100 nm thick film on paralene coated substrates at various input powers. (b) Emission intensity of spontaneous peak (510 nm) and stimulated peak (540 nm) as a function of input power. Lasing threshold is approximately at the inflection point of the 540 nm curve.

neglected altogether. Several spectra were taken before exposure to confirm this and compared to spectra after exposure.

2.3 Chemosensing measurements.

To measure the sensing response, our typical exposure technique involves introducing our sample to the solid state vapor pressure of a target analyte. Initial attempts used TNT as the analyte. However, due in part to the large size of our sample chamber and the low vapor pressure of TNT (5 ppb), we had difficulty introducing TNT directly to the film surface. We then decided to pursue sensing responses from DNT. DNT is a synthetic byproduct of TNT and is present in nearly all landmines containing TNT. The vapor pressure of DNT is much higher (about 2 orders of magnitude: 100 ppb) than TNT so although it may consist of only 10% of the explosive component of a buried landmine, it will be the dominate species in the vapor phase. Thus, it is thought to be the chemical which dogs smell when discovering a buried mine. Also, DNT is commercially available so fresh samples of analyte were at our disposal.

In our experiments, we compare the attenuation of the ASE peak to the attenuation of the spontaneous emission peak upon exposure to DNT. Stimulated emission response to DNT exposure was monitored at a constant excitation power as a function of time and at a constant exposure time as a function of excitation power. The former experiments established the minimum measurable responses since quenching

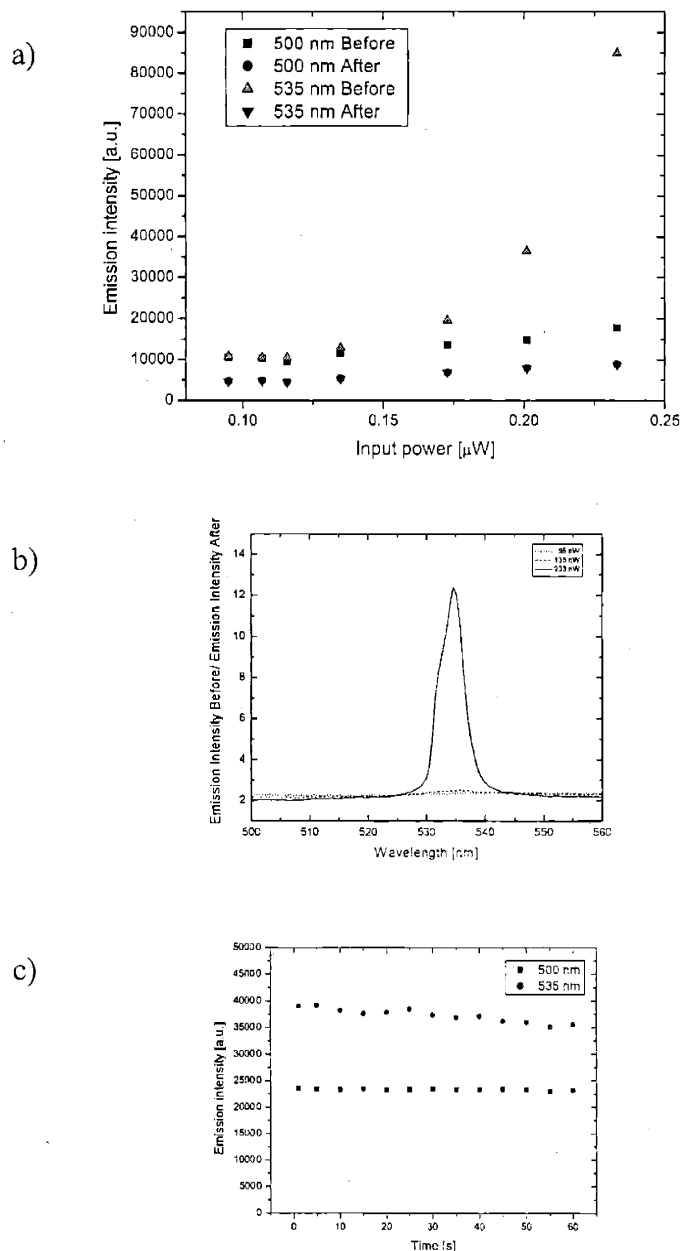


Figure 11. Spectral response of the optically pumped 750 Å of Polymer 1 on parelene coated glass before and after a 2 minute exposure to DNT. (a) Emission intensity as a function of pump input power at 500 nm (corresponding to spontaneous emission) and at 535 nm (corresponding to ASE) before and after the DNT exposure. (b) Emission spectra before exposure divided by emission spectra after exposure at 95, 135 and 223 nW input power. Largest signal is observed at lasing wavelength at highest input power. (c) Control experiment in which film is pumped above threshold in ambient air. No significant signal attenuation is observed indicating quenching in (a) and (b) are due solely to analyte exposure.

occurs rapidly upon exposure while the latter experiments retain the advantage of exposing the polymer film for only short times (less than 1 min) and intermittently to the were performed under identical conditions to assure the signal measured resulted from analyte exposure and not from photobleaching or any artifact of our set-up.

Two minute exposures to saturated DNT vapor significantly decreased both the primary PL emission as well as the ASE observed from the first vibronic transition. This laser beam, minimizing the photobleaching observed with longer exposure times. It is noteworthy to mention that it was not trivial to verify the validity of discounting photobleaching in our measurements. Multiple rigorous controls for each experiment dose is large enough to raise the lasing threshold above the power range of our setup (Fig. 11a). Note that the spontaneous emission peak at 500 nm reduced its emission intensity by a factor of ~ 2 . In contrast, the 535 nm peak reduced its intensity by more than a factor

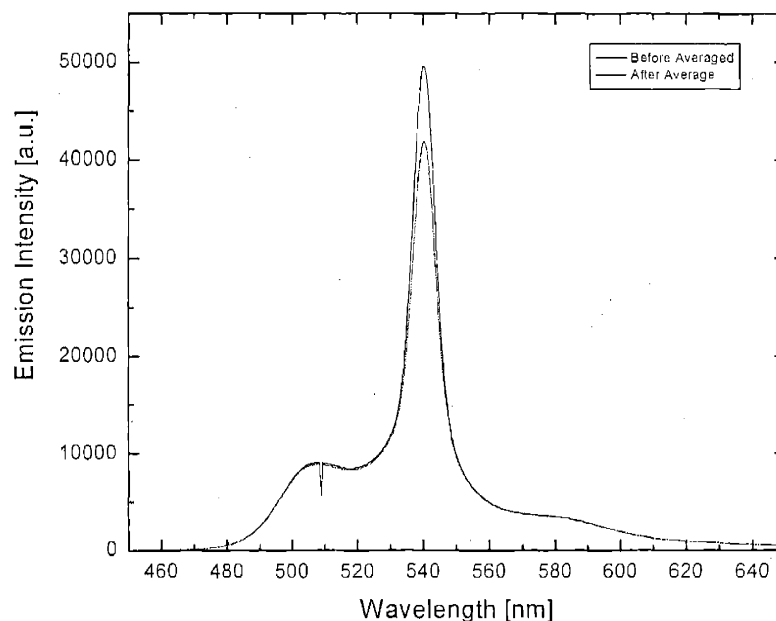


Figure 12. ASE attenuation in the absence of spontaneous attenuation upon 1 s exposure to saturated DNT vapor pressure.

of 10 for pumping power of 230 nW. Depending on the power of the excitation beam, larger differential between exposed and unexposed samples can be registered (Fig. 11b). For more demanding applications, where more material can be sacrificed to photobleaching, one may increase input power to lower the detection limit of these explosives.

The two minute dose of DNT attenuated both spontaneous and stimulated signals significantly. This was an important proof of the heightened sensitivity that lasing can provide. However, we were more interested in proving that lasing can probe the presence of DNT in situations where spontaneous emission cannot. This involves demonstrating no quench in PL concomitant with a significant quench in ASE. Therefore, shorter exposure times were investigated. In these experiments, only one pump energy was probed to eliminate photobleaching. The small reduction in emission can then be assigned entirely to DNT response. Several exposure times between 1 and 30 seconds were interrogated. We found that rapid quenching by DNT demanded the shortest exposure time possible with our set-up (1s) otherwise spontaneous emission is also affected. Several spectra were taken before and after exposure to average out detector jitter, laser power undulations or other sources of noise in our set-up. For one-second exposure times to saturated DNT vapor (100 ppb), significant attenuation in the ASE peak is chronicled with no measurable attenuation in the spontaneous peak (Fig. 12). Since this is still well above the detection limit of our spectrometer, much shorter exposure times would also be effective.

A natural corollary to these experiments is to measure real time quenching, that is signal intensity simultaneous with introduction of analyte. This would define the

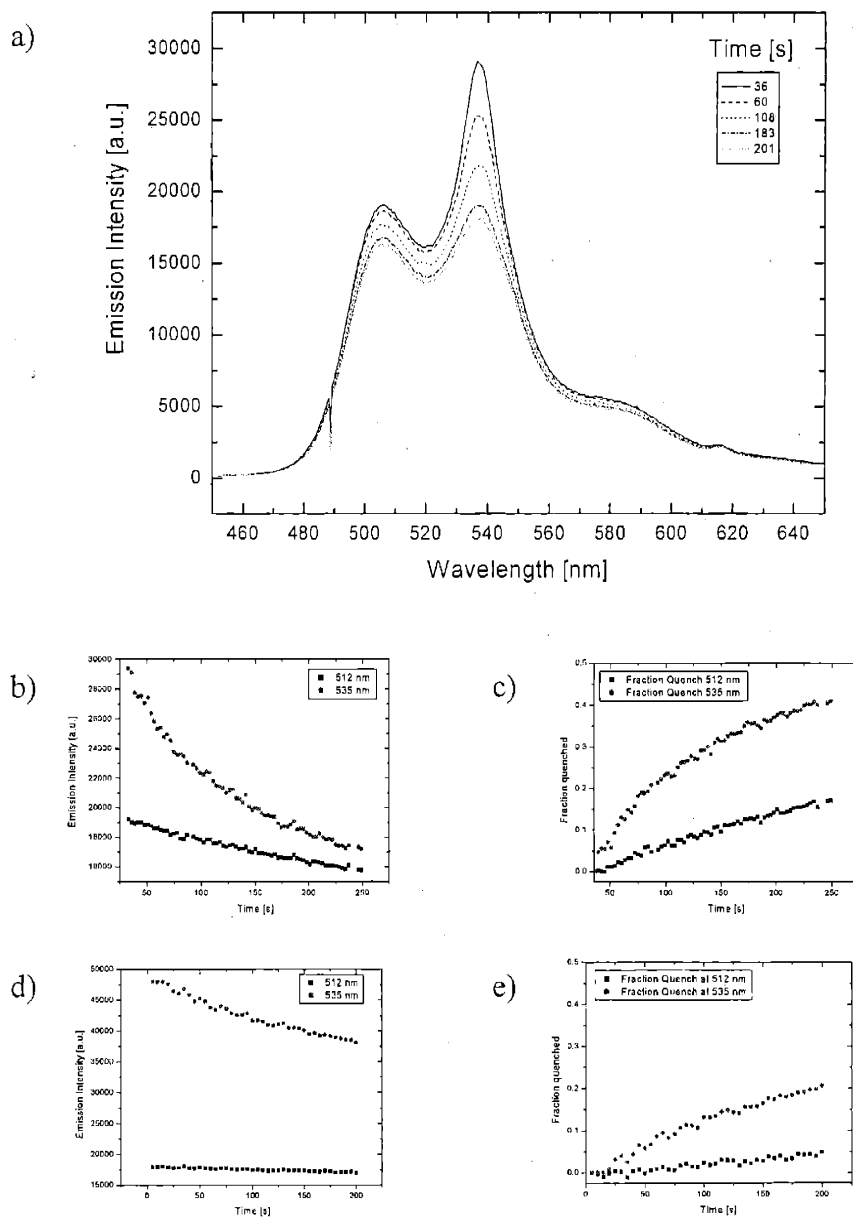


Figure 13. (a) Emission spectra of a thin film of Polymer **38** at various times after the introduction of a saturated atmosphere of DNT. (b) Emission intensity at 512 nm (spontaneous emission) and 535 nm (ASE) of the film as a function of time in a saturated atmosphere of DNT. (c) Calculated fraction of initial emission quenched at 512 nm (spontaneous emission) and 535 nm (ASE) of the film as a function of time in a saturated atmosphere of DNT. (d) Control experiment at same input power (270 nW): emission intensity at 512 nm (spontaneous emission) and 535 nm (ASE) of the film as a function of time in ambient air. (e) Calculated fraction of initial emission quenched at 512 nm (spontaneous emission) and 535 nm (ASE) of the film as a function of time in ambient air.

minimum time necessary to register a measurable response and has obvious implications for in-field devices. Millions of acres of land are littered with landmines, often in the poorest nations. The faster they can be detected, the more area can be cleared for farming and habitation to the benefit of the neediest people in the world. Unfortunately, these measurements proved difficult to perform on our experimental set-up. The challenge lies in chronicling exposure times of less than a second. Detector response to a laser trigger input was not reproducible enough to confidently establish that a constant number of pulses reached the sample per period of integration. This would be easily remedied by a more sophisticated laser system with shorter pulse widths and/or higher rates of repetition. Attempts to use a diode laser with a kilohertz repetition rate were unsuccessful because the power output was not sufficient to pump materials above lasing threshold. We did however manage to procure real-time data for larger time scales where longer integration times could be used to average out differential pulse numbers. This is plotted in Figure 13. The steep initial slope in the stimulated emission decay curve for times less than 100 s suggests shorter time resolution is worth pursuing.

2.4. Distributed-feedback structures

To further lower the ASE threshold and increase the chemical sensitivity, we incorporated the organic material into a distributed feedback (DFB) structure, as shown in Fig. 14c. The period of the in-plane periodic reflection of the DFB matches the wavelength of the emitted light generating lasing emission. The substrates were fabricated by Mr. John Ho, and films were cast as previously described on glass. The lasing threshold is reduced (Fig. 15) as compared to structures with no DFB. However,

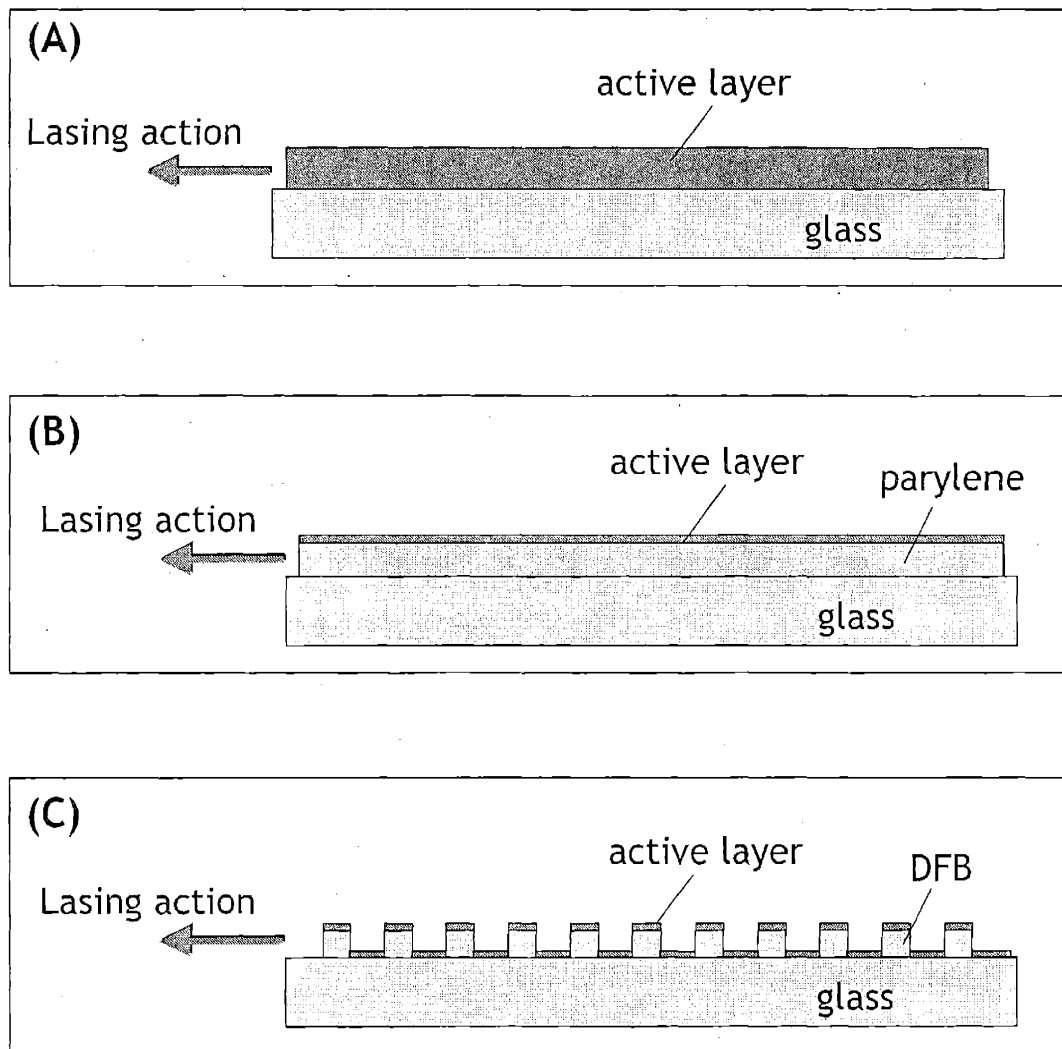


Figure 14. Three renditions of a planar laser structure. (a) Polymer waveguide on glass. (b) Thin active layer on paralene. The combined thickness of polymer and paralene generates waveguide. (c) Thin active layer on distributed feedback (DFB) grating. The DFB reduces lasing threshold.

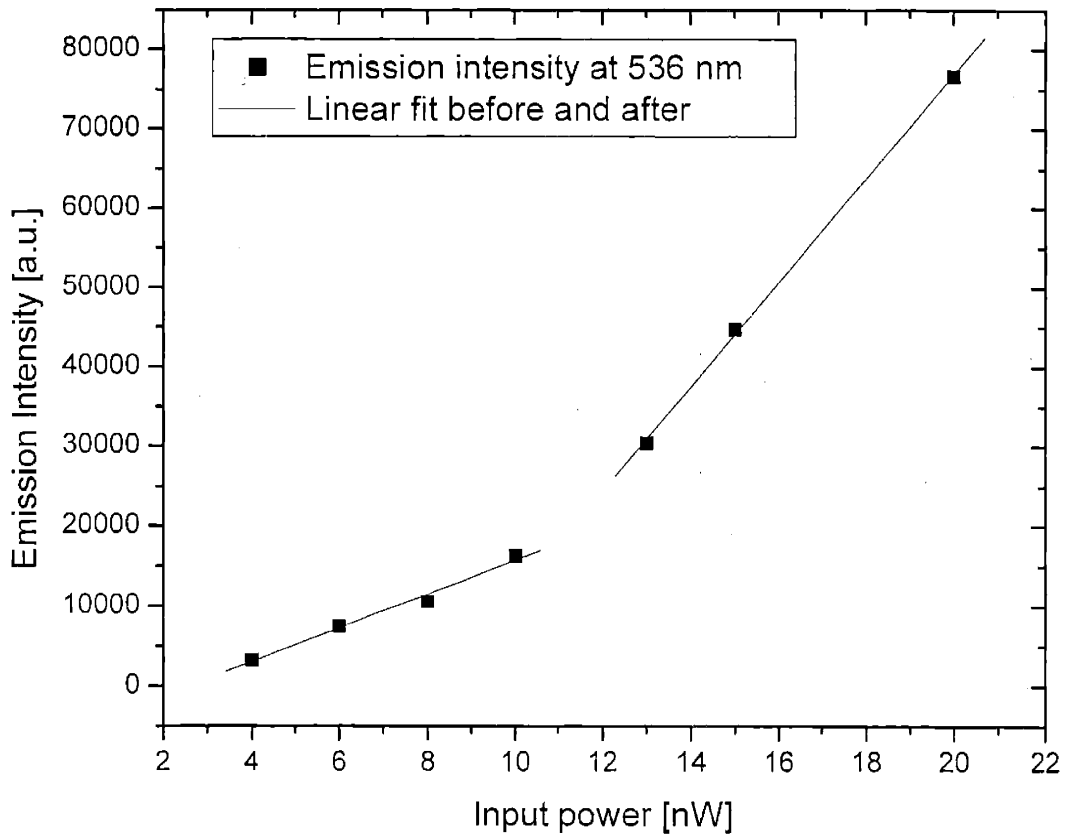


Figure 15. Low lasing threshold of Polymer 38 atop a DFB structure. Emission intensity of stimulated peak (536 nm) as a function of input power. Lasing threshold is approximately at 12 nW with same spot size used on glass and paralene structures.

DFB structures have reduced thresholds by orders of magnitude in small molecule organics. The observed enhancement in our system was not as significant, with threshold reduction only about a factor of 3 compared to a similar film on glass.

Device performance may be improved with a lower DFB surface roughness or a periodicity closer to the natural lasing wavelength of the material. Efforts to improve these characteristics could serve to optimize sensory device performance. Photo-oxidation of the active polymers would be minimized. Furthermore, a very thin active polymer layer would be needed to generate lasing action, which would maximize the polymer sensitivity to the presence of analytes.

3. Conclusions

Asymmetric waveguide structures were constructed with novel CPs developed in our laboratory. Through optical pumping, ASE was readily observed at the lower thresholds than any previously reported. Low thresholds are crucial to preventing photobleaching and hence operating these devices as working sensors in ambient air. Significantly amplified response was measured upon exposure to saturated vapor pressure of DNT. Responses were measured in the lasing peak before any attenuation was observed in the spontaneous peak. Current and future efforts focus on incorporating these novel materials into feedback structure which will allow us to further reduce threshold as well as the thickness of the active layer. We hope these advances in explosive detection will someday serve to save life and limb.

4. References

- ¹ Moses, D. *Appl. Phys. Lett.* **1992**, *60*, 3215.
- ² Hide, F.; Schwartz, B. J.; Díaz-García, M. A.; Heeger, A. J. *Chem. Phys. Lett.* **1996**, *256*, 424.
- ³ Tessler, N., Denton, G. J., Friend, R. H. *Nature* **1996**, *382*, 695.
- ⁴ (a) Kumar, N. D.; Bhawalkar, J. D.; Prasad, P. N.; Karasz, F. E.; Hu, B. *Appl Phys Lett* **1997**, *71*, 999. (b) Henari, F. Z.; Manaa, H.; Kretsch, K. P.; Blau, W. J.; Rost, H.; Pfeiffer, S.; Teuschel, A.; Tillmann, H.; Hörhold, H. H. *Chem Phys Lett* **1999**, *307*, 163. (c) Schwartz, B. J.; Hide, F.; Díaz-García, M. A. Heeger, A. J. *Synth Met* **1997**, *91*, 35.
- ⁵ Scherf, U.; Richel, S.; Lemmer, U.; Mahrt, R.F. *Curr Opin Solid State Mater Sci* **2001**, *5*, 143.
- ⁶(a) Zhou, Q.; Swager, T. M. *J. Am. Chem. Soc.* **1995**, *117*, 7017-8. (b) Zhou, Q.; Swager, T. M. *J. Am. Chem. Soc.* **1995**, *117*, 12593-12602.
- ⁷ (a) Yang, J.-S.; Swager, T. M. *J. Am. Chem. Soc.* **1998**, *120*, 5321. (b) Fisher, M.; Cummings, C. *7th International Symposium on the Analysis and Detection of Explosives*, **2001**, Edinburgh Scotland, UK.
- ⁸ Levitsky, I. A.; Kim, J.; Swager, T. M. *J. Am. Chem. Soc.* **1999**, *121*, 1466.

Chapter 5

Appendix 1

Cylindrical spot size measurement and calculation of flux.

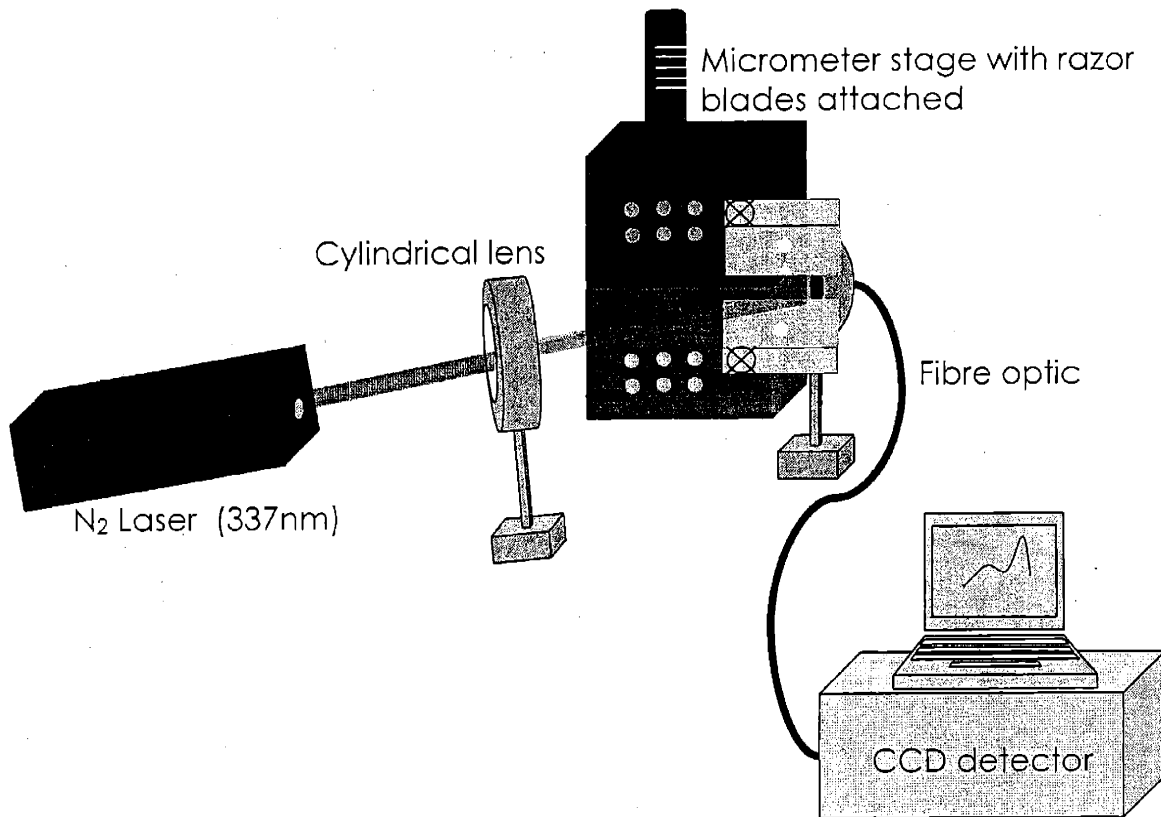


Figure 1a. Experimental setup used to measure spot size of cylindrical beam.

The spot size of the cylindrically focused laser beam is needed to calculate the actual lasing threshold in units of energy per unit area. The width of the beam is large in size and therefore straightforward to measure. The height of the beam is much smaller, 100 μm or less so its measurement can introduce more error. We followed the procedure outlined here. We used a micrometer stage originally configured by Dr. Hans Eisler. One razor blade is affixed to the translatable portion of the stage while the other is affixed to the stationary portion. By rotating the caliber on top of the stage the two blades are moved closer to each other, eventually cutting off the laser beam. Behind the razor blade sits the detector which recorded laser intensity as the stage is moved incrementally. A

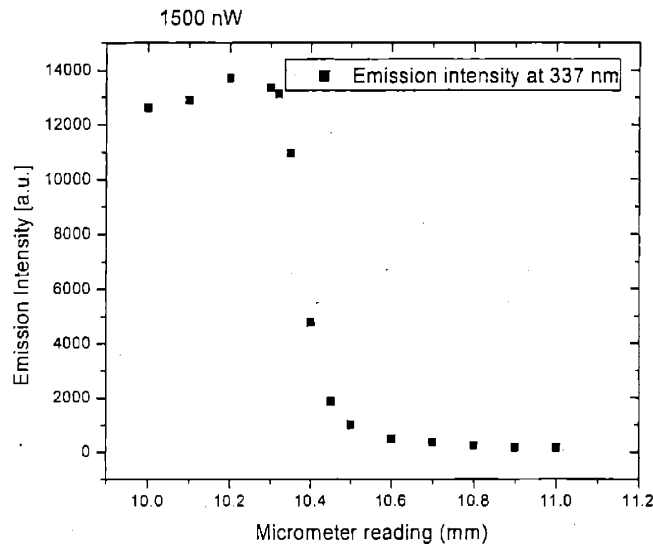


Figure 2a. Beam intensity decrease as it is incrementally clipped by two razor blades.

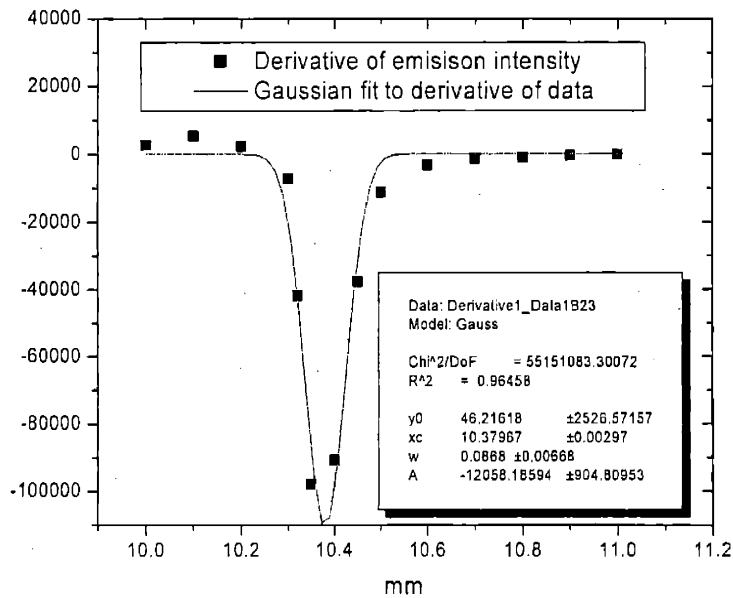


Figure 3a. Gaussian fit to fits derivative of data from Figure 2a.

neutral density filter may be needed if laser beam saturates the detector or one may alternatively measure the second harmonic of the laser. Reading off the caliber, we correlated emission intensity with micrometer reading as we rotated the caliber about 0.1 mm at a time. Figure 2a plots this data for a beam intensity of 1500 nW. We then taking the first derivative of this data and fitting the curve to a Gaussian (Fig. 3a). The full width at half maximum is the beam height. This measurement was repeated many times and with several different input powers. The smallest value measured is commonly thought the most accurate since a slight angle of the blade would result in a measurement too large. In our experiments, beam height was measured to be 90 μm .

With dimensions of the spot in hand, calculation on the threshold is then straightforward. Our observed threshold was 74 nW; our laser puts out 30 pulses/s; and out spot size was measured to be 0.9 cm * 0.009 cm = 0.081 cm^2 .

For our system:

$$74 \frac{\text{nJ}}{\text{s}} * \frac{1\text{s}}{30 \text{ pulses}} * \frac{1}{0.0081 \text{ cm}^2} = 310 \frac{\text{nJ}}{\text{cm}^2}$$

which is much lower to our knowledge than the literature precedent¹ (10 $\mu\text{W}/\text{cm}^2$) for CPs in an asymmetric waveguide architecture or in fact any architecture.²

¹ Xiao, L.; Malinowski, A.; Bradley, D.C.C.; Inbasekaran, M.; Woo, E.P. *Chem. Phys. Lett.*, **1997**, 272, 6.

² Scherf, U.; Richel, S.; Lemmer, U.; Mahrt, R.F. *Curr Opin Solid State Mater Sci* **2001**, 5, 143.

Curriculum Vitae

Aimee Rose

Highlights

- Extensive experience in fluorescence spectroscopy (steady state and time resolved) and instrument maintenance and design.
- Proficient in air sensitive polymerizations and general Schlenk line techniques.
- Research focus on materials design, synthesis, and characterization for electronic and photonic applications.
- Collaborative, multidisciplinary background.

Education

Massachusetts Institute of Technology Cambridge, MA
Candidate for Ph.D. in Physical Chemistry (September 1997 - present)
Thesis: Optimization of sensory response in conjugated polymers through energy migration enhancement.

St. Michael's College Colchester, VT
ACS certified Bachelor of Science, *summa cum laude*, May 1996.
Major in chemistry. GPA 3.94/4.0. Class rank 3/402.

Research Experience

Massachusetts Institute of Technology Cambridge, MA
Department of Chemistry
Advisor: Professor Timothy M. Swager
Position: Research Assistant
Evaluated energy migration processes in conjugated polymers through rational materials design and synthesis and extensive physical characterization. Employed techniques such as Schlenk-line synthesis, fluorescence spectroscopy, transient absorption spectroscopy, and optically pumped stimulated emission measurements. Incorporated unique chromophores to extend excited state lifetimes of conjugated polymers thereby inducing enhanced energy migration and augmenting sensory response to analytes such as TNT. (September 1997 - present)

Pacific Northwest National Laboratory Richland, WA
Division of Materials and Chemical Science
Advisor: Dr. Gregory Exarhos
Position: Associated Western Universities Research Fellow
Explored solution chemistry routes for deposition of transparent, conducting thin films for air purification and electronics applications. Measured and interpreted Raman spectra, ellipsometric spectra, and absorbance and reflection spectra to characterize solid-state electronic structure. (September 1996 - August 1997)

Pacific Northwest National Laboratory

Richland, WA

Advisor: Glen Dunham

Position: U.S. Department of Energy Research Fellow

Developed prototypical sensing apparatus using quartz crystal microbalances coated with thin polymer layers. Programmed vapor generator for sensor calibration. Operated device for real-time, in-field analyses to successfully assess environmental contamination. (*August 1995 - December 1995*)

University of California at Santa Barbara

Santa Barbara, CA

Advisor: Professor Galen Stucky

Position: National Science Foundation Solid State Chemistry and QUEST (Center for the Study of Quantized Electronic Structures) Research Fellow

Studied silica assembly in marine algae for photonic band gap applications. Developed macroscopic growing techniques for algae. Characterized silica framework through AFM, thermogravimetric analysis, quantitative fluorescence, and infrared spectroscopy. (*June 1995 - August 1995*)

Teaching Experience**MIT Department of Chemistry Teaching Assistant**General Chemistry (*September 1998 - December 1998*)Thermodynamics and Chemical Kinetics (*February 1998 - May 1998*)Organic Chemistry (*September 1997 - December 1997*)**St. Michael's College Department of Chemistry Laboratory Assistant**General Chemistry (*September 1993 - May 1996*)**Awards and Honors**Hertz Foundation Scholar *May 1997**Summa cum laude* Bachelor of Science *May 1996*American Institute of Chemists Senior Achievement Award *May 1996*Chemistry Department Honors (St. Michael's College) *May 1996*Sigma Delta Epsilon National Scholastic Honor Society Member *December 1995*Eastern Analytical Symposium Student Achievement Award *November 1995*ACS Award for Outstanding Achievement in Organic Chemistry *May 1995*ACS Award for Outstanding Achievement in Analytical Chemistry *May 1995*CRC Press Freshman Achievement Award *May 1993*Dean's List Scholar *1992-1996***Activities**Co-organizer of MIT Physical Chemistry Graduate Student Seminar Series (*September 1999 - January 2001*)Co-organizer of MIT's Women In Chemistry's 'Careers in Chemistry' Panel Discussion Series (*Fall 2000*)

Member American Chemical Society : Member Materials Research Society

Oral Presentations

"Electronic Polymers for Explosives Detection." A. Rose and T. M. Swager, Aviation Security Technology Symposium, Atlantic City, NJ *November 2001*.

"Triphenylene-based conjugated polymers." A. Rose and T. M. Swager, ACS National Meeting, San Diego, CA *April 2001*.

"Optimization of TNT Sensory Polymers." A. Rose, C. G. Lugmair, V. E. Williams, and T. M. Swager, Aerosense, Orlando, FL *April 2000*.

"Ellipsometric studies of thermally induced transformation phenomena in oxide films." A. Rose and G.J. Exarhos, AVS Annual Meeting, San Diego, CA *April 1997*.

- Poster Presentations** "Triphenylene-based PPEs – Synthesis and Spectroscopy" A. Rose, C. G. Lugmair and T. M. Swager, Materials Research Society Meeting, San Francisco, CA April 2002
- "Dual Quartz Crystal Microbalances- An Integrated In-Field Analysis Technique." A. Rose and G.C. Dunham, ACS Student Research Symposium, Northwestern University, Boston, MA April 1995.
- Publications** "Functionalizable Polycyclic Aromatics through Oxidative Cyclization of Pendant Thiophenes." J.D. Tovar, A. Rose and T. M. Swager, *J. Amer. Chem. Soc.*, **2002**, *124*, 7762.
- "Excited State Lifetime Modulation in Triphenylene-Based Conjugated Polymers." A. Rose, C.G. Lugmair and T. M. Swager, *J. Amer. Chem. Soc.*, **2001**, *123*, 11298.
- "Directing Energy Transfer within Conjugated Polymer Thin Films." D. T. McQuade, J. Kim, A. Rose, Z. Zhu and T. M. Swager, *J. Amer. Chem. Soc.*, **2001**, *123*, 11488.
- "A Rotaxane Exciplex." M. J. MacLachan, A. Rose, and T. M. Swager, *J. Amer. Chem. Soc.* **2001**, *123*, 9180.
- "Optimization of TNT Sensory Polymers." A. Rose, C. G. Lugmair, J. Kim, I. G. Levitsky, Y. J. Miao, V. E. Williams, and T. M. Swager, *Proc SPIE Vol. 4038 Detection and Remediation Technologies for Mines and Minelike Targets V*, A. C. Dubey, J. F. Harvey, J. T. Broach, R. E. Dugan, Eds. **2000**, 512.
- "Localized Deposition of Zinc Oxide Films by Automated Fluid Dispensing Method." K. Domansky, A. Rose, W. H. Grover, and G. J. Exarhos, *Materials Science and Engineering B-Solid State Materials for Advanced Technology* **2000**, *76(2)*, 116.
- "Postdeposition Reduction of Noble Metal Doped ZnO." G. J. Exarhos, A. Rose, L. Q. Wang, and C. F. Windish Jr., *Journal of Vacuum Science and Technology A* **1998**, *16(3)*, 1926.
- "Ellipsometric Studies of Thermally Induced Transformation Phenomena in Oxide Films." A. Rose and G. J. Exarhos, *Thin Solid Films* **1997**, *308-309*, 42.
- "Spectroscopic Characterization of Processing-Induced Property Changes in Doped ZnO Films." G. J. Exarhos, A. Rose, and C. F. Windish Jr., *Thin Solid Films* **1997**, *308-309*, 56.
- "Pulsed Laser Irradiation of Isothermally Heated Titania Films." G. J. Exarhos, A. Rose, and K. P. Shielke, *Proc. SPIE Vol. 3244 Laser-Induced Damage in Optical Materials 1997*, G. J. Exarhos, A. H. Guenther, M. R. Kozłowski, M. J. Soilcau, Eds. **1997**, 458.

Acknowledgements

Foremost, I would like to thank Tim Swager for the years of support. I didn't realize before joining his group that one could be taught creativity but the effusive enthusiasm he conveys when speaking about chemistry and materials is undoubtedly contagious. More importantly, he always encourages exploratory research and independent thinking with the notion that there is more to our education than lab work. It is through this interactive approach to science that the serendipity of collaboration can be born and, in this manner, many of the experiments in this thesis were designed. While I hope that the best years of my research career are not behind me, I suspect it will be difficult to replicate such a dynamic, fulfilling environment. The rare combination of compassion and intelligence with which Tim runs his group inspires awe. From my perspective at MIT, the former is sometimes the most remarkable.

I would also like to extend deep gratitude to my 'second' advisor Vladimir Bulovic, with whom many experiments in Chapter 5 were performed. His expertise in device preparation and optically pumped lasing were invaluable to realizing many important experiments. However, it was his general enthusiasm for science and advising I found most inspiring. I hope we can put our name together 'in lights' someday soon.

Upon joining the Swager group, my synthetic abilities were non-existent. In fact, a rotovap was enough to confuse me. I must therefore thank those who spent their valuable time dispelling my ignorance. Dr. Claus G. Lugmair, my baymate and late-night companion in the lab, taught me almost everything I know about inert atmosphere synthetic techniques. My only reciprocation to his infinite patience was the few chuckles I would supply him as I made yet another mistake. His mentorship afforded me the skills to 'hold my own' in an organic laboratory. As importantly, his triphenylene synthesis was instrumental in initiating the train of thought behind much of this thesis. While the gruesome details were modified slightly, it was entirely Claus' talent that allowed us to first generate triphenylene polymers. Krustav Crawford initially introduced me to Sonogashira polymerizations. I am grateful for his assistance. My next benchmate, Zhengguo Zhu, provided the polymer investigated in Chapter 5 and various monomers. More importantly, he provided an ice skating partner in addition to an indispensable synthetic advisor. I thank him for a fun two years. Dr. Hans Eisler performed the initial ASE measurements described in Chapter 5. I thank him for them along with helpful discussions and good beer.

Additional thanks to Mr. John Ho who provided the DFB structure covered in Chapter 5. Dr. Quin Zhou and Mr. Sean K. McHugh made some model polymers studies in Chapters 3 and 4.

To my coauthors on papers not covered in this thesis, Mark (the Shark) Maclauchlin, D. Tyler McQuade, and Jinsang Kim (the O. G. of L. B.), it was a pleasure working with you all (though to varying degrees ~ just kidding Tyler). With Tyler, I learned to play volleyball which later served other important functions in my life. I hope we have the chance to play doubles together again someday.

To those who joined the group with me, Bruce Yu (the O. G. of G. B.) and J. D. Tovar, I am happy we shared the same lab-philosophies and could collectively improve our surroundings. Bruce: I will never forget the time I beat you in one-on-one basketball nor will most of the world since the score was posted on my website for several months. More seriously, you were a great friend to me through the years especially when I needed you most. I am sorry for the nickname I imparted on you which has followed you around indefinitely but it seems to fit you well. There are a few people you might say without whom you would have never made it through; for me, J. D. Tovar is one of them. His synthetic talent and materials insight contributed significantly to the conclusions of this thesis. More significantly, our shared perspective helped 'keep it real' for me over the years. I learned so much from J. D. and our discussions, which would often spill over till 4am. I have taken great pride in all your accomplishments and expect to be busy doing so for many years to come.

Thanks to my good friend Vikram Sundar, who fearlessly endured relentless teasing from his labmates just for being associated with me. You helped me make many important decisions in my life (what to eat, when to go for a run etc.), and your continued support is deeply appreciated. Our scientific discussions and the ideas for Chapter 5 were also greatly appreciated along with your attempts to mask your condescension. You taught me a lot about preserving a good attitude. I hope the future is rewarding to you and that periodically I am filled in on it.

I would also like to thank Ken Shimizu for all the money he borrowed from me in addition to adjusting my internal clock to Ken time. We have yet to fully explore the phenomena of Keniluminescence; it could prove to open a new field of science someday. I offer many thanks to Michael Hewitt who provided a strong shoulder during some tough times. Thank you to Alex Paraskos who could always be convinced to stay out a bit later. To Michelle Chang, together we were able to conquer the boys and send them running for cover. Thanks to Yutaka Nishiyama for allowing me to elevate him to legendary status in the group.

This thesis wouldn't be complete without a thanks to Charles Reedy, Greg Dudley, Gabriel Mauro, Neil Gupta and Donal Lyle. They know what for.

The bumpy road to a Ph. D. was constantly and instrumentally softened by the support of my family. My mother, to whom I dedicate this thesis, was and continues to be my constant champion. It's a fortunate person whom has such an enthusiastic, yet seasoned, advocate. My sister Stephanie was nearly as patient with my sloppy grad school attire and even sloppier correspondence. My aunt, Katherine Labanaris, actually knows a bit about what I was working on! Her perennial enthusiasm for my achievements inspired me to add to them.

And lastly, I would like to thank Manfred Kraus. Although he was the most recent addition to this list, I hope he will be one of the most enduring.